Studies on Pyridinyl-Based High-Spin Molecules

Kouzou Matsumoto

1998

Department of Chemistry, Graduate School of Science,

Osaka University

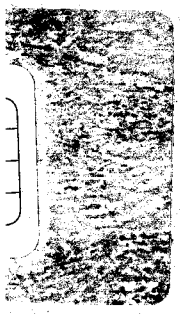

Studies on Pyridinyl-Based High-Spin Molecules

Kouzou Matsumoto

1998

Department of Chemistry, Graduate School of Science,

Osaka University

Contents

1. General Introduction

1-1. Introduction

The chemistry of organic stable radical was initiated in 1900 by Gomberg who reported the isolation of triphenylmethyl radical.[1] After this paper, a number of organic stable radicals have been synthesized. For example, Schlenk's hydrocarbon was prepared in 1915.[2] Tetraphenylallyl radical,[3] diphenylvinyl-9-xanthyl radical,[4] and pentaphenylcyclopentadienyl radical[5] were synthesized in 1922-1925. Among many other moderately stable radicals, diphenylpicrylhydrazyl (DPPH)[6] and galvinoxyl radicals,[7] which are stable under air at room temperature, were isolated in 1924 and 1962, respectively.

The stable pyridinyl radical, 1-ethyl-4-carbomethoxypyridinyl prepared by the reduction of the corresponding pyridinium iodide with zinc or magnesium was reported by Kosower and Poziomek in 1963.[8] They isolated this pyridinyl radical as a free form by distillation under high vacuum. The progress of pyridinyl radical chemistry is summarized in the next section.

During 1900-1965, the isolation of stable radical attracted general interest of many organic chemists, who realized that "radical" is not conceptional idea but a real isolable chemical species. The discovery of ESR by Zaboisky in 1945[9] accelerated the progress of the chemistry of radical species. Although the chemistry of stable radical has been a great topic in organic chemistry, the isolation itself was not enough to lead to the current development of molecular magnetism. An important finding greatly contributed to the progress of today's molecular magnetism. That is a finding of organic high-spin species. Many organic molecules have singlet ground states and organic molecules with high-spin ($S \geq 1$) ground states are rare. Organic high-spin molecule was firstly demonstrated by Dowd.[10] He prepared trimethylenemethane (TMM) by the photolysis of methylenepyrazoline **I** in hexafluorobenzene matrix (eq. 1-1) and demonstrated that TMM has a triplet ground state.

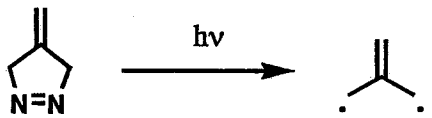

(eq. 1-1)

I TMM

One year later, Itoh demonstrated a quintet biscarbene generated by the photolysis of bisdiazo compound **II** in a benzophenone single crystal (eq. 1-2).[11] In the same year, Wasserman et al., also reported a randomly oriented quintet ESR pattern of a similar biscarbene.[12] Breslow and co-workers demonstrated that cyclopentadienylium is a triplet species.[13] These studies stimulated many organic chemists and very high-spin organic species have been prepared by the collaboration of Iwamura's and Itoh's groups.[14] These high-spin molecules demonstrate that electronic spin can be arranged in parallel and a microscopic magnet in a molecular level can be achieved.

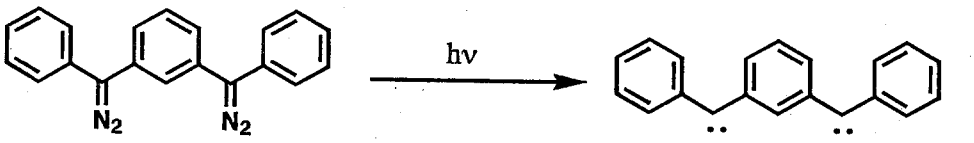

II (eq. 1-2)

Today, molecular magnetism has grown into a central and fascinating area of study in the natural sciences. In this field, synthesis of new materials including organic, inorganic, organometallic compounds, and their composite aimed for molecular devices, and characterization using modern techniques (SQUID, ESR, solid state NMR etc.) have been carried out. Especially, synthesis of new materials is a key to develop this field. Hitherto, several new materials exhibiting unique magnetic properties (for instance high Tc) have been found. However, organic chemists note that these new materials frequently contain a few particular structures of stable radicals, typically nitroxide radicals. To achieve further development of this field, construction of high-spin species with a variety of spin-sources is essential.

This thesis focuses on the pyridinyl radical as a spin-building block of high-spin species. Unique characters expected in the pyridinyl-based high-spin molecules are described in a section of "Purpose of this study and contents of this thesis". Before entering this section, it is useful to introduce 1) the previous studies on the pyridinyl radicals and 2) theory of spin alignment in high-spin molecules.

1-2. Brief review of pyridinyl radicals

N-Substituted-pyridinyl radicals are typically synthesized by the reduction of pyridinium salts with 3 % Na-Hg in acetonitrile (eq. 1-3).[15] N-Hydropyridinyl can be generated by the photoreduction of pyridines in 2-propanol and acetone (eq. 1-4).[16]

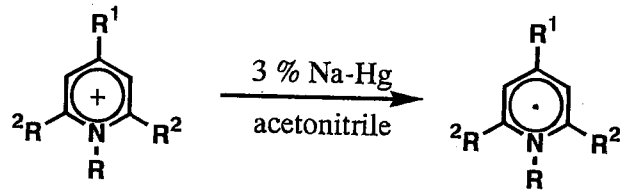

(eq. 1-3)

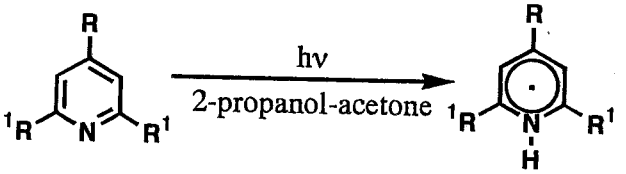

(eq. 1-4)

As described in the preceding section, Kosower et al. isolated 1-ethyl-4-carbomethoxypyridinyl by distillation under high vacuum and clarified the physical and chemical properties of this radical; pure 1-ethyl-4-carbomethoxypyridinyl is an emerald-green oil, $d^{25}_4 = 0.85$, which solidifies to a sapphire-blue solid at ca. -10 °C. It reacts with halocarbons to afford a pyridinium halide and dihydropyridines.[17]

After Kosower's finding, a number of stable pyridinyl radicals have been synthesized and characterized. For example, Dohrmann and Kieslich reported an ESR study of hydropyridinyl derivatives.[18a] Greci et al. also reported a similar study for various N-substituted-pyridinyl derivatives.[18b] The hyperfine splitting constants (hfc) for the 1-ethyl, 1-isopropyl, and 1-*tert*-butyl-

Table 1-1. Hyperfine splitting constants (a in G) for 1-alkyl-4-methoxycarbonyl-pyridinyls in isopentane at r.t.

substituent (R)	CH_3	CH_2CH_3	$CH(CH_3)_2$	$C(CH_3)_3$
Hammett's σ^o	−0.124	−0.131	−0.156	−0.174
$a^H(2)$	4.27	4.20	4.05	3.93
$a^H(6)$	4.35	4.28	4.14	4.00
$a^H(3)$	0.06	0.07	0.08	0.09
$a^H(5)$	0.14	0.15	0.17	0.19
a^N	6.24	6.29	6.46	6.67
$a^H(\beta)$	5.30	3.32	1.50	
$a^H(\gamma)$		0.22	0.20	0.18
$a^H(OCH_3)$	0.78	0.78	0.79	0.78

4-methoxycarbonylpyridinyl radicals were completely assigned by Ikegami et al.[19] The hfcs of the ring nitrogen atom and the protons at the 2 and 6-positions are influenced by the alkyl group attached to the nitrogen atom as shown Table 1-1. They concluded that the difference of hfcs was attributed to the difference of the electron-releasing abilities of the alkyl groups.

Sander and Dohrmann measured the proton and nitrogen hfc of short-lived N-hydropyridinyl radical over the range -80 to 42 °C.[20] As shown in Figure 1-1, the NH proton splitting strongly decreases with increasing temperature and shows a nonlinear temperature dependence above 10 °C. They explained these results by the model of localized out-of-plane vibrations of the protons.

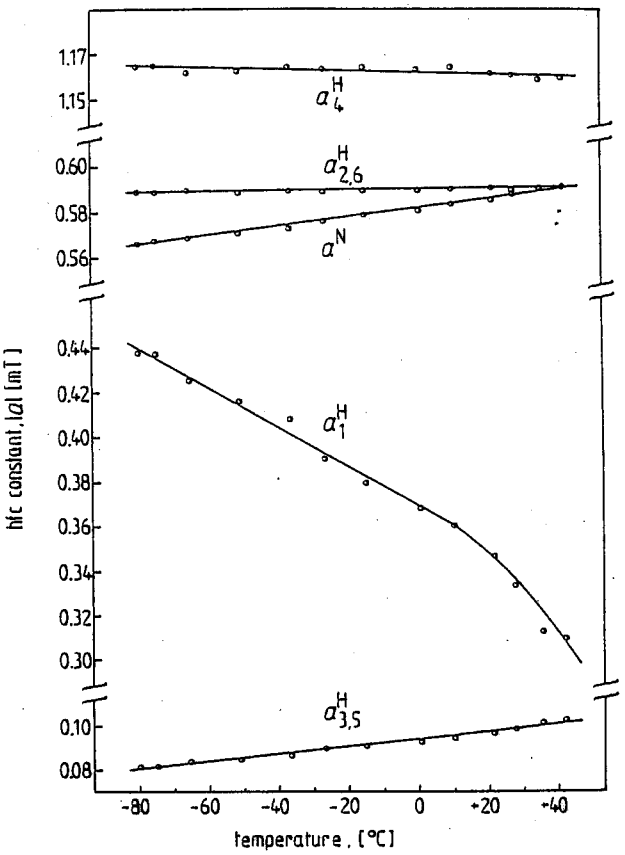

Figure 1-1. Temperature dependence of the hyperfine coupling constants (absolute values) in the N-hydropyridinyl radical.

Ikegami et al. reported the solvent effect on the 1-methyl-4-methoxycarbonylpyridinyl radical.[21] The ESR spectra of this radical were measured in nine solvents (Table 1-2). The hfcs of the protons at the H-2 and H-6 positions, as well as at the H-3 and H-5 positions were unequivalent. The reason for the unequivalence was ascribed to the lack of rotation of the methoxycarbonyl group, which is strongly conjugated with the coplanar pyridinyl ring. It is obvious from Table 1-2 that the solvent effect mainly operates on the hfcs of the ring protons. The hfcs for H-2 and H-6 tend to decrease with increasing solvent polarity while the values for H-3 and H-5 show the reverse tendency. They concluded that the major effect of solvation on the spin distribution is arisen from polarization of the carbonyl group which is strongly conjugated with the coplanar pyridinyl ring. This consideration was supported by theoretical calculations.

Table 1-2. Hyperfine splitting constants (a in G) of 1-methyl-4-methoxycarbonylpyridinyl in various solvent polarity parameters.

solvent	i-C_5H_{12} 1	C_6H_6 2	Et_2O 3	MTHF 4	THF 5	DME 6	Me_2CO 7	DMF 8	MeCN 9
μ, D	0.0	0.0	1.15		1.75	1.71	2.69	3.86	3.92
Z value	60.1	54				62.1	65.7	68.5	71.3
$E_T(30)$	30.9	34.5	34.6		37.4	38.2	42.2	43.8	46.0
$a^H(2)$	4.27	3.78	4.00	3.89	3.75	3.76	3.62	3.49	3.57
$a^H(6)$	4.35	3.89	4.08	3.97	3.84	3.83	3.72	3.61	3.66
$a^H(3,5)$	0.06	0.42	0.32	0.45	0.48	0.51	0.58	0.69	0.68
	0.14	0.48	0.38	0.51	0.54	0.57	0.62	0.75	0.74
a^N	6.24	6.26	6.25	6.28	6.27	6.33	6.30	6.30	6.31
$a^H(NCH_3)$	5.30	5.50	5.47	5.59	5.53	5.54	5.56	5.60	5.60
$a^H(OCH_3)$	0.78	0.85	0.83	0.85	0.85	0.85	0.86	0.89	0.91

Dimerization reaction of pyridinyl radicals is the most typical and the most deeply investigated reactions of pyridinyl radicals. A number of pyridinyl radical dimers have been obtained. Most of them are 2, 2'- or 4, 4'-dimers. Ikegami et al. reported a mechanism of both photodissociation reaction of pyridinyl radical dimers and dimerization reaction of pyridinyl radicals. For example, the 2, 2'-dimer of 1-methyl-4-*tert*-butylpyridinyl radical underwent photolytic cleavage to give a singlet radical pair exhibiting an A/E polarization pattern in the transient ESR spectrum.[22] The similar behavior was observed in the 2, 2'-dimer of 1,4-dimethylpyridinyl[23] and 1-methyl-3-methoxycarbonylpyridinyl radicals.[24] In the case of 1-methyl-2-methoxycarbonylpyridinyl, the mechanism of dimerization reaction was examined.[25] Formation of an intermediate was proposed from a two-step decay of the radical, in which the fast step was reversible second order and the slow step was first order, respectively. They concluded that the 2, 2'-dimer was formed by the fast step followed by the [3,3] sigmatropic reaction to afford the final 4, 4'-dimer (Figure 1-2).

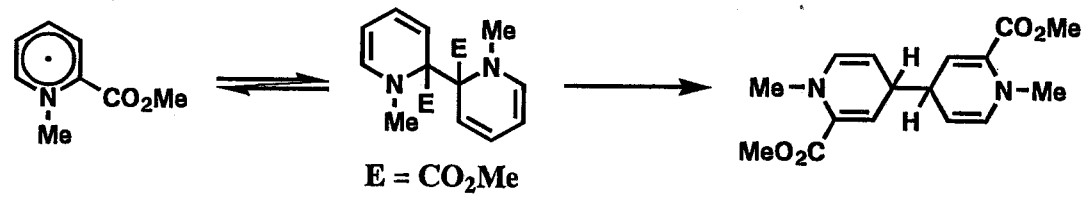

Figure 1-2. Mechanism of dimerization reaction of 1-methyl-2-carbomethoxypyridinyl.

There are a few reports about both intermolecular and intramolecular triplet species based on pyridinyl radicals. Ikegami et al. reported that the dimer of 1-benzyl-4-methoxycarbonylpyridinyl radicals was transformed into the triplet dimer ($D \approx 0.017$ cm^{-1}) by irradiation with 440-470 nm

light.[26] The same phenomenon was observed in the case of 1-alkyl-4-methoxypyridinyl radical[27] and 1-methyl-4-phenylpyridinyl radical.[28] Yamaguchi et al. estimated the effective exchange integrals for three types of sandwich dimer using semiempirical molecular orbital calculations.[29] They concluded that the effective exchange integrals for the free radical dimers were negative in sign in the majority of cases, showing that the singlet state should generally be more stable as compared with the triplet state.

Triplet states of intramolecular bis-pyridinyl radicals linked by polymethylene spacers at 1, 1'-positions (**III**) have also been reported. A triplet ESR spectrum of 1,1'-dimethylenebis(4-carbo-

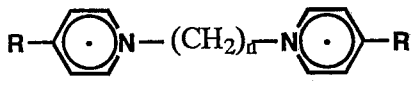

III

methoxypyridinyl) diradical (**III**; R = CO_2Me, n = 2) in MTHF at 77 K was recorded by Kosower.[30] This diradical was shown to be intermolecularly associated at higher concentration to form monoradical-like ESR pattern. Itoh and Kosower also investigated **III** for n = 3, 4, 5; R = CO_2Me.[31] ESR spectra at various concentrations and temperatures showed that the ESR-detected spin concentration divided by the titrated radical concentration varies from 2 % (n = 3) through 20 % (n = 4) to 100 % (n = 5), which suggests the formation of intramolecular dimers (n = 3 and 4). A concentrated solution showed a strong visible absorption which is assigned to be a charge-transfer band between the two pyridinyl radical moieties.

Ikegami et al. studied the reactivity of the bis-pyridinyl radicals **III** (n = 2, 3; R = H, Me, ^{t}Bu, and CO_2Me).[32] Two-electron reduction of the corresponding bispyridinium dibromide with Na-Hg afforded the *meso* and *dl*-cyclomers. The *meso*-isomer was thermally transformed into the *dl*-isomer, whereas the *dl*-isomer was photolytically converted into the *meso*-isomer. They obtained the bis-pyridinyl radicals by photodissociation of the cyclomers and characterized them by ESR spectroscopy at 77 K.

The bis-pyridinyl radicals linked by 1,8-dimethylenebiphenylenediyl **IV** and *o*-xylylene **V**, and their magnesium complexes were synthesized by Kosower and Teuerstein.[33] They studied photochemical behavior of these diradicals and their magnesium complexes. Irradiation of them at the visible

absorption band (620 nm for **IV** and 690 nm for **V**) of these diradicals did not cause photodecomposition; however, irradiation of the first strong absorption band (near 400 nm) was

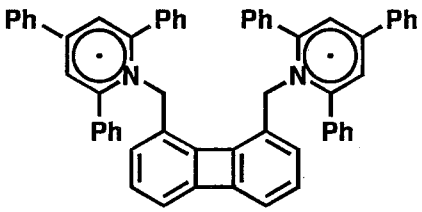

IV

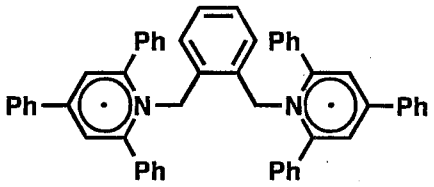

V

effective for photodecomposition and produced methyl isonicotinate and 1,8-dimethylbiphenylene, identified by TLC and UV spectroscopy. Although this photodecomposition seemed to proceed *via* 1,8-dimethylenebiphenylene, they did not try to observe it by ESR spectroscopy. However, more recently, triplet ESR spectra of 1,8-dimethylenenaphthalene and *m*-xylylene have been observed by photodecomposition of the corresponding bis(4-carbobutoxypyridinyl) diradicals (eq. 1-5, 1-6).[34]

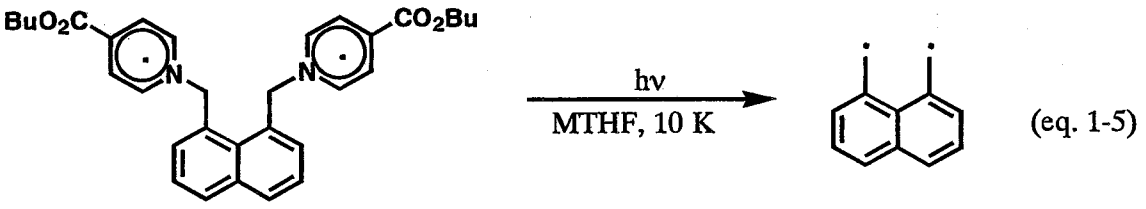

(eq. 1-5)

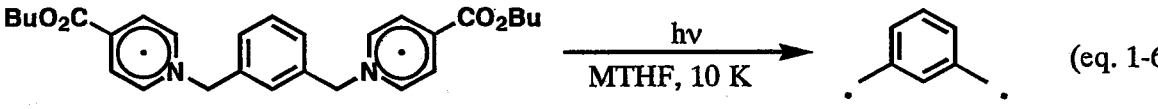

(eq. 1-6)

1-3. Theory of spin alignment in high-spin molecules

Pioneering high-spin studies and many newer experimental and theoretical contributions have improved our understanding of spin alignment in organic (poly)radicals. Today, we have some spin-predicting models, especially for alternant hydrocarbon polyradicals. Among several predicting models, Longuet-Higgins approach (MO method 1), Ovchinikov's approach (VB method), and the joint or nondisjoint approach (MO method 2), and the dynamic spin polarization approach (MO method 3) are easy to handle and the predicting models can be visualized schematically.

1-3-1. Number of unpaired electrons in alternant hydrocarbons by Longuet-Higgins[35] (MO method 1)

According to the resonance theory, *m*-xylylene structure is drawn as **VI**, where a dot represents an unpaired electron. We expect that *m*-xylylene has two unpaired electrons in the ground state. Longuett-Higgins analyzed this idea in terms of the MO theory. They proposed that alternant hydrocarbons must have at least N-2T unpaired electrons in the ground state; N is the number of carbon atoms in the molecule and T is the maximum number of double bonds that may be drawn for the system. In this treatment, the number of unpaired electrons is assumed to be equal to the number of NBMO's.

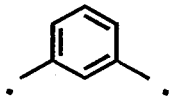

VI

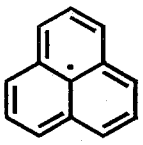

VII

VIII

In many cases, N-2T equals to the number of unpaired electrons or the number of NBMO's. For instance, *m*-xylylene has N = 8, T = 3, then the number of unpaired electrons are 2. Allyl radical has N = 3 and T = 1, then number of unpaired electron (NBMO) is 1. Phenalenyl radical **VII** has N = 13, T = 6, then the number of unpaired electron (NBMO) is 1.

However, cyclobutadiene **VIII** has N = 4, T = 2, then the number of unpaired electrons (NBMO) is 0. But, we know that although the number of unpaired electron is thus calculated to be 0, the number of NBMO's in HMO level is 2. Obviously, the prediction gives the least number.

1-3-2. Spin multiplicity of the ground state of alternant organic molecules by Ovchinikov[36] (VB method)

Ovchinikov described a model for alternant conjugated non-Kekulé molecules that is based upon a reorganization of the Pariser-Parr-Pople Hamiltonian describing electron exchange. In his approach, carbon atoms are divided into alternating α- and β- spin sites in a typical valence bond manner, by designating one spin type as starred, and the other unstarred. Then, the spin number of the molecule can be derived by the equation shown below. The spin multiplicity is given by 2S + 1.

$S = (n^* - n) / 2$ (n^* and n are the number of starred and unstarred carbons, $n^* > n$)

According to this theory, it is obvious that cyclobutadiene has a singlet ground state and *m*-xylylene has a triplet ground state. Furthermore, this theory predicts that Chichibabin's hydrocarbon **IX** ($n^* = n = 19$) has a singlet ground state and its meta-isomer **X** ($n^* = 20$, $n = 18$) a triplet ground state. There is an experimental data which suggests that Schlenk-Brauns hydrocarbon **XI** has a triplet ground state. However, this theory predicts the ground state of **XI** ($n^* = n = 19$) should be a singlet state. According to Ovchinikov, **XI** has a plane of symmetry to which the starred and unstarred carbons are symmetrically arranged and such a molecule always has a singlet ground state.

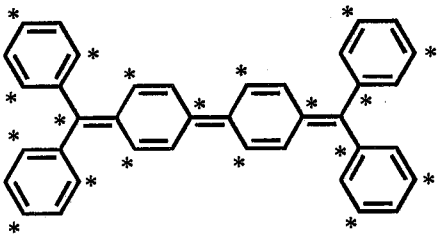

IX

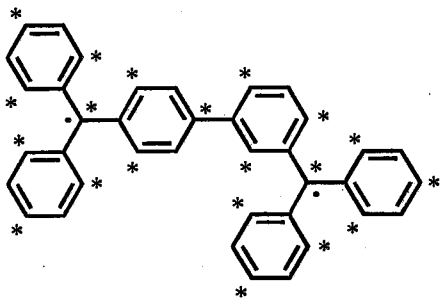

X

Although Ovchinikov stated that this theory can be applied to heteroatom-bridged alternant hydrocarbons, the detailed procedure of counting n^* and n was not described.

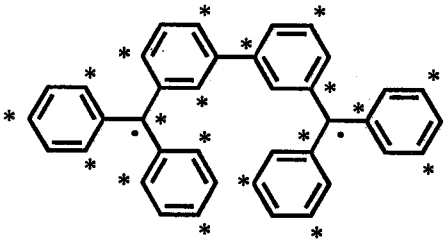

XI

1-3-3. "Disjoint" and "non-disjoint" classifications of hydrocarbon diradicals by Borden and Davidson [37] (MO method 2)

In 1977, Borden and Davidson classified π-conjugated hydrocarbon diradicals into "disjoint" and "non-disjoint" hydrocarbons according to the shape of NBMO's in the Hückel MO. Suppose a molecule with two NBMO's; one NBMO is localized at C1, C2, C3, ..., and Cn carbons, the other

NBMO at Ca, Cb, Cc, ..., and Cm carbons. If there is no a common carbon atom between the two groups, i.e., the carbon atoms are clearly separable into either of the NBMO's, we call such a molecule as "disjoint molecule". If such clear separation is impossible, i.e., there is a common carbon atom(s) between the two sets (C1, C2, ..., Cn carbon and Ca, Cb, ..., Cm carbon), we call such a molecule as "non-disjoint molecule". Borden and Davidson proposed that disjoint hydrocarbons have singlet ground states with a small S-T gap, whereas non-disjoint hydrocarbons have triplet ground states. The proposal is based on *ab initio* SCF and full CI calculation of some model compounds.

For instance, cyclobutadiene has two NBMO's (**VIII**-1 and **VIII**-2). The **VIII**-1 has a large AO coefficient at the C1 and C3, whereas the **VIII**-2 at the C2 and C4. The carbon atoms are clearly separable into the two sets (C1 and C3 for **VIII**-1, C2 and C4 for **VIII**-2) and there is no a common carbon between the two groups; accordingly, cyclobutadiene is a disjoint hydrocarbon and has a singlet ground state.

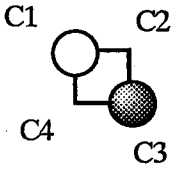

VIII-1

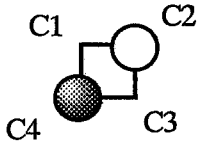

VIII-2

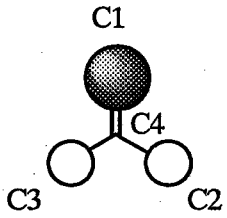

XII-1

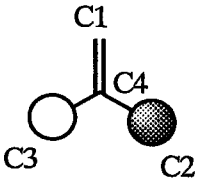

XII-2

Trimethylenemethane has two NBMO's (**XII**-1 and **XII**-2). The NBMO **XII**-1 is localized on the C1, C2, and C3 carbons, whereas **XII**-2 on the C2 and C3 carbons. Since there are common atoms (C2 and C3) between the two groups, trimethylenemethane is a non-disjoint hydrocarbon and has a triplet ground state.

1-3-4. The dynamic spin polarization model[38] (MO model 3)

According to the Pauli principle, two electrons with the same spin do not occupy the same region of space at the same time but no such restriction applies to two electrons with different spins. As a result, the two electrons with the same spin receive smaller electronic repulsion and are in a lower energy state. Thus, for example in *m*-xylylene **VI**, the π-spin (up) at one of the radical centers (the C1 carbon)

attracts the up-spin of the σ-orbital in its vicinity and pushes the down-spin away in the σ-bond. The down-spin in the polarized σ-bond induces the down-spin in the π-orbital on the C2 carbon, leading to a spin alternation (up-down) relation in the π-network. This is dynamic spin polarization effect. Such alternate relation in the π-spin sequence can be achieved in the *m*-xylylene triplet and, therefore, the triplet is stabilized.

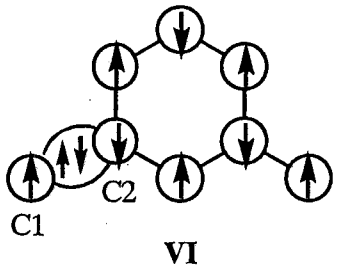

VI

1-3-5. Effect of dihedral angles between the radical moieties and the spacer

Although many diradicals connected by a *m*-phenylene spacer have high-spin ground states, there are some exceptions. Rassat et al. showed that **XIII** has a singlet ground state with ΔE_{S-T} = ca. 150 cal/mol.[39] Iwamura et al. also reported that **XIV** has a singlet ground state.[40] These two bis-nitroxides have large dihedral angles between the *m*-phenylene spacer and the nodal planes of nitroxides.

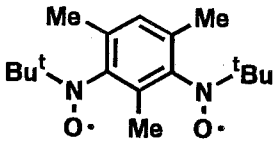

XIII

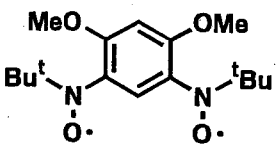

XIV

Borden et al. rationalized these observations by *ab initio* calculation for *m*-phenylene bis-nitroxide.[41] The reason for the singlet state was attributed to the large dihedral angle which induces the orbital interaction between two NBMO's through the σ-bond of *m*-phenylene linker. Low-spin molecules with *m*-phenylene and related spacers so far reported are shown below.

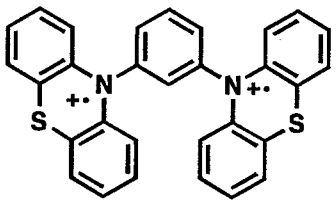

XV; singlet[42]

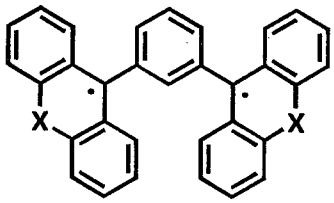

XVI (X = O); singlet
XVII (X = S); triplet[43]

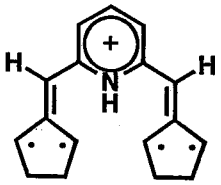

XVIII; triplet[44]

1-4. Purpose of this study and contents of this thesis

High-spin compounds using pyridinyl radical as a spin building block involve the following interesting aspects. Firstly, relatively little study has been made on pyridinyl poly- or diradicals. Studies so far reported are concerned with bis-pyridinyl radicals linked by dimethylene and trimethylene chains as described in the previous section (1-2). These polymethylene linked diradicals have been studied in relation to monomer-dimer equilibrium, π-mer formation, or the photoreactivity of their cyclomers. Although their ESR spectra and zero-field splitting (zfs) parameters have been analyzed, there is no description for the determination of the ground state of these compounds. The exchange interaction of polymethylene or alkanediyl-linked 2,4,6-triphenylpyridinyl radicals will be described in Chapter 4. Several pyridinyl di- or triradicals linked by π-conjugated systems are described in Chapters 2 and 3.

Secondly, pyridinyl-based high-spin species are expected to have considerably different properties when compared with hydrocarbon-based high-spin molecules. As shown in the previous section (1-3), there are several theoretical models to predict the ground state of alternant hydrocarbon high-spin molecules. Are these models also applicable for pyridinyl-based high-spin system ? Experimental approaches to answer this question are described in Chapters 2 and 3. Before discussing them, it seems to be useful to consider the difference between hydrocarbon system and this pyridinyl system in well understandable bases (VB and HMO approaches). The analysis will be made in the following two simple cases.

1-4-1. Spin distribution of pentadienyl radical and pyridinyl radical

Pentadienyl radicals **XIX** are alternant hydrocarbons and their spin distribution patterns may be expressed using a series of canonical VB structures **XIX**-1, **XIX**-2, and **XIX**-3. Therefore, the carbons at the 1,3,5-positions are in the high spin density. The conceivable ionic spin structure **XIX**-4, where the C-2 has a high spin density, is not important, since such an ionic structure would be unstable in the all carbon system (homoatomic system). As a whole, the up-down spin relation (dynamic spin polarization relation) can be hold in the cyclopentadienyl radical.

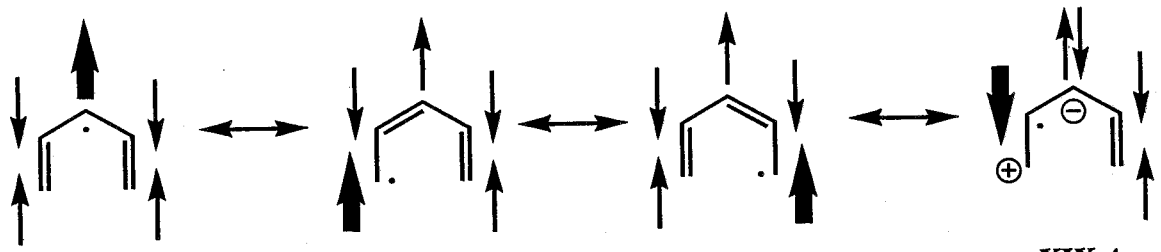

XIX-1 **XIX**-2 **XIX**-3 **XIX**-4

However, pyridinyl radical (nitrogen bridged pentadienyl radical) may be expressed using several extra contributions (**XX**-1~**XX**-6). If the pyridinyl radical has main spin structures of cyclopentadienyl (**XX**-1~**XX**-3) plus lone pair electrons on the nitrogen atom, the nitrogen atom has both up and down spins (no net spin). However, as shown in the previous section (1-2), we know that the nitrogen has the largest spin density. The appearance of the up spin on the nitrogen atom can be easily shown by the delocalization of the down spin on the nitrogen atom leading to the structures of **XX**-4~**XX**-6. The spin canonical structures **XX**-4~**XX**-6 are ionic structures. Such ionic structures in the heteroatomic system may not have a high energy because of the electron donating ability of the nitrogen atom with lone pair electrons. When the electron donating alkyl group is substituted on the nitrogen atom, the delocalization of the lone pair electrons can be assisted. Thus, the electron donating substituent on the nitrogen atom will decrease the net spin densities of the carbon atoms at the 2,4, and 6-positions. These considerations are in well accordance with the experiments (section 1-2). Provided that the above analysis is correct, the pyridinyl radical has a non-alternant spin relation (i. e., up-up relation) between

the nitrogen and the adjacent carbon atom spins as shown in **XX**-4~**XX**-6. Thus, these spin structures, which are characteristic for pyridinyl radicals, break the "up-down" spin alternation relation that is a basis of theoretical model of spin alignment in the high-spin molecules.

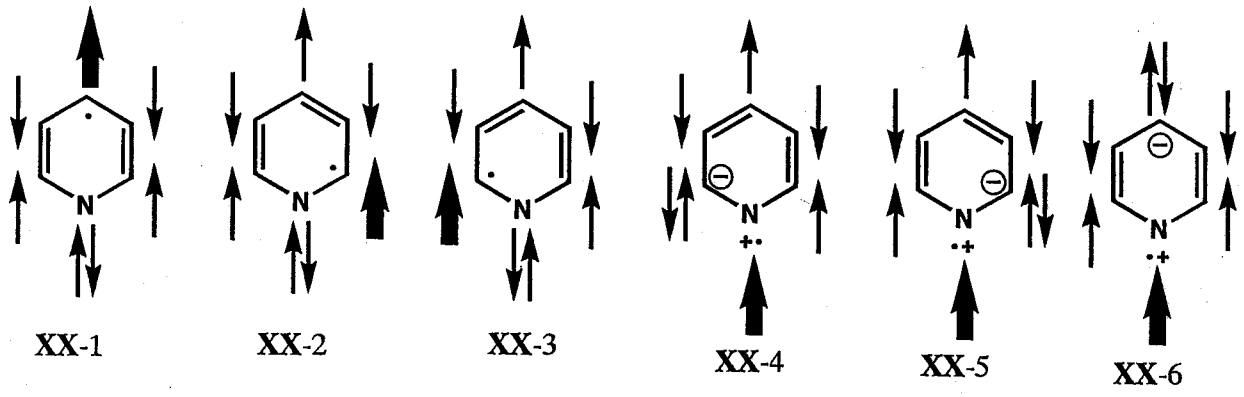

1-4-2. Pyridinyl-based high-spin molecule with m-phenylene or p-phenylene linkage

We consider two hypothetical diradicals **1m** and **7m** (m for the model compounds). Although *m*-phenylene-linked hydrocarbon diradicals usually give stable triplet states, the prediction of the ground state for **1m** is not easy because of the following reasons. The spin structure **1m**-1 shows a triplet structure which has lone pair electrons on the nitrogen atoms. The delocalization of one of the lone pair electrons to the adjacent carbon leads to another triplet spin structure of **1m**-2, which has energetically high up-up spin relation between the nitrogen and the adjacent carbon atom. Such a spin structure would decrease the triplet stabilization. Furthermore, there is a singlet stabilizing spin structure like **1m**-3 where the up-down spin relation can be hold (except for the relation involving lone pair electrons). For these reasons, the energy difference between the triplet and singlet states is small. Similar consideration can be drawn by the MO calculation (ΔE by Hückel MO with the nitrogen parameter of 0.89 for the resonance integral and 1.37 for the coulombic integral).[45] The diradical **1m**-1 has nondegenerate HOMO and LUMO (the energy difference, $\Delta E = 0.06\ \beta$), whereas **XXI** has degenerate HOMO and LUMO. Obviously, introduction of nitrogen lone pair electrons disturbs the degeneracy of the two orbitals. Therefore, the prediction of the ground state is not easy for this diradical.

Similar analysis can be extended to the *p*-phenylene-linked bis-pyridinyl radical **7m**. When two hydrocarbon spins are separated by *p*-phenylene, the diradicals has usually have a singlet ground state.

However, the spins of the diradical **7m** are separated by *p*-phenylene and two nitrogen atoms which have no net spin. Therefore, the triplet and singlet states of this diradical may have similar energies (see section 3-1-2 for more detailed discussion). The HMO calculation of the diradical **7m** indicates a relatively small energy gap ($\Delta E = 0.16\ \beta$) between HOMO and LUMO, compared to that of *p*-xylylene ($\Delta E = 0.62\ \beta$) and Thiele's hydrocarbon ($\Delta E = 0.31\ \beta$).

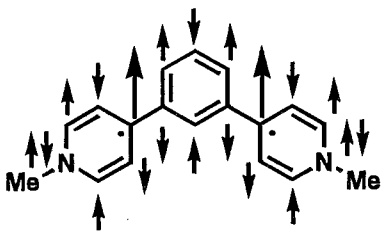

1m-1

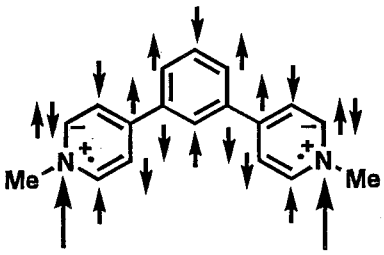

1m-2

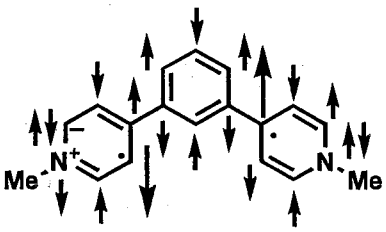

1m-3

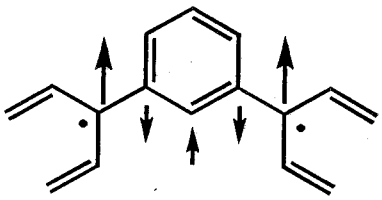

XXI

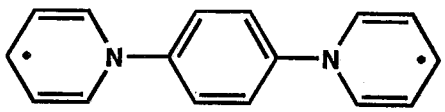

7m

In general, the spin-predicting theoretical model can be successfully applied only to the alternant hydrocarbon high-spin molecules. Application of spin-prediction models to heteroatomic systems may not be valid. *The main purpose of this thesis is to obtain an experimental answer of this ambiguity on the heteroatomic systems using some pyridinyl-based high-spin molecules.*

1-4-3. Contents of this thesis

In Chapter 2, various bis-pyridinyl or tris-pyridinyl radicals **1-5** were prepared and their spin-spin interactions were studied.

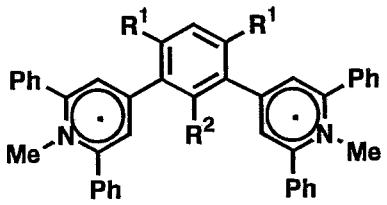

1 ($R^1 = R^2 = H$)
3 ($R^1 = H$, $R^2 = Me$)
4 ($R^1 = Me$, $R^2 = H$)

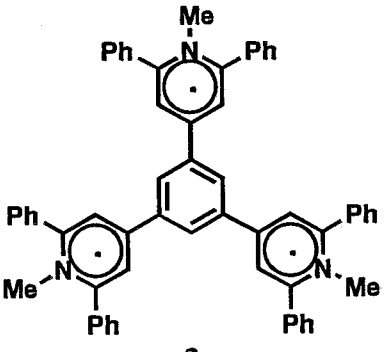

2

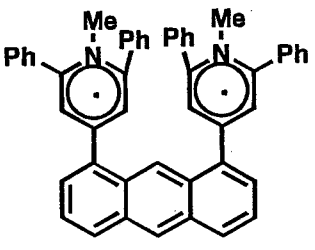

5

Chapter 3 describes the preparation and exchange interaction of **6**, **7** and **8**.

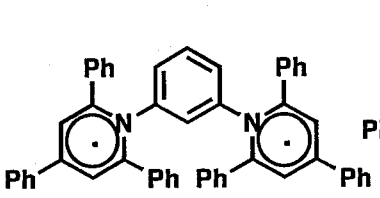

6

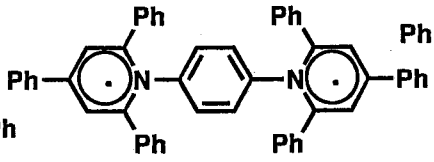

7

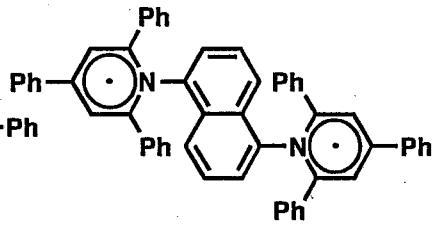

8

Final Chapter 4 provides the exchange interaction of alkanediyl-spaced bis-pyridinyl diradicals **9**-**15**.

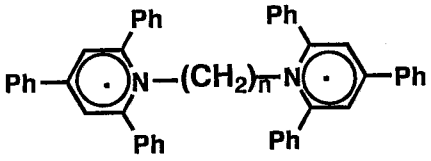

9 (n = 2), **10** (n = 3), **11** (n = 4),
12 (n = 5), **13** (n = 6), **14** (n = 8)

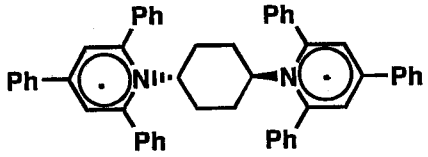

15

1-5. References

[1] a) M. Gomberg, *J. Am. Chem. Soc.*, **22**, 757 (1900).

b) M. Gomberg, *Chem. Ber.*, **33**, 3150 (1900).

[2] W. Schrenk and M. Brauns, *Chem. Ber.*, **48**, 661 (1915).

[3] K. Zieglar and C. Ochs, Chem. Ber., **55**, 2257 (1922).

[4] K. Zieglar, G. Bremer, F. Thiel and F. Thielmann, *Justus Liebigs Ann.*, **434**, 34 (1923).

[5] K. Zieglar and B. Schnell, *Justus Liebigs Ann.*, **445**, 266 (1925).

[6] S. Goldschmidt and K. Eular, *Justus liebigs Ann.*, **437**, 194 (1924).

[7] G. M. Coppinger, *J. Am. Chem. Soc.*, **79**, 501 (1957).

[8] a) E. M. Kosower and E. J. Poziomek, *J. Am. Chem. Soc.*, **85**, 2035 (1963).

b) E. M. Kosower and E. J. Poziomek, *J. Am. Chem. Soc.*, **86**, 5515 (1964).

[9] E. Zavoisky, *J. Phys. (USSR)*, **9**, 211, 245 (1945).

[10] a) P. Dowd, *J. Am. Chem. Soc.*, **88**, 2587 (1966).

b) P. Dowd and K. Sachdev, *J. Am. Chem. Soc.*, **89**, 715 (1967).

c) P. Dowd and M. Chow, *Tetrahedron*, **38**, 799 (1982).

[11] K. Itoh, *Chem. Phys. Letters 1*, **1967**, 235.

[12] E. Wassermann, R. W. Murray, W. A. Yager, A. M. Trozzolo, and G. Smolinsky, *J. Am. Chem. Soc.*, **89**, 5076 (1967).

[13] R. Breslow, H. W. Chang, R. Hill, and E. Wassermann, *J. Am. Chem. Soc.*, **89**, 1112 (1967).

[14] a) I. Fujita, Y. Teki, T. Takui, T. Kinoshita, K. Itoh, F. MIno, Y. Sewaki, H. Iwamura, A. Izuoka, T. Sugawara, *J. Am. Chem. Soc.*, **112**, 4074 (1990).

b) N. Nakagawa, K. Inoue, and H. Iwamura, *Angew. Chem. Int. Ed. Engl.*, **32**, 872 (1993).

[15] a) J. Hermolin, M. Levin and E. M. Kosower, *J. Am. Chem. Soc.*, **103**, 4808 (1981).

b) K. Akiyama, S. T. Kubota, Y. Ikegami, and T. Ikenoue, *J. Phys. Chem.*, **89**, 339 (1985).

[16] a) T. Rakowsky and J. K. Dohrmann, *Ber. Bunsenges. Phys. Chem.*, **79**, 18 (1975).

b) H. Zeldes and R. Livingston, *J. Phys. Chem.*, **76**, 3348 (1972).

c) J. K. Dohrmann and R. Becker, *J. Magn. Reson.*, **27**, 371 (1977).

[17] E. M. Kosower and I. Schwager, *J. Am. Chem. Soc.*, **86**, 5528 (1964).

[18] a) J. K. Dohrmann and W. Kieslich, *J. Magn. Reson.*, **32**, 353 (1978).

b) L. Greci, A. Alberti, I. Carelli, A. Trazza, and A. Casini, *J. Chem. Soc., Perkin Trans. 2*, **1984**, 2013.

[19] K. Akiyama, S. Kubota, and Y. Ikegami, *J. Phys. Chem.*, **85**, 120 (1981).

[20] U. Sander and J. K. Dohrmann, *Ber. Bunsenges. Phys. Chem.*, **83**, 1258 (1979).

[21] S. Kubota and Y. Ikegami, *J. Phys. Chem.*, **82**, 2739 (1978).

[22] K. Akiyama, S. T.-Kubota, Y. Ikegami, and T. Ikenoue, *J. Phys. Chem.*, **89**, 339 (1985).

[23] a) K. Akiyama, S. T.-Kubota, Y. Ikegami, and T. Ikenoue, *J. Am. Chem. Soc.*, **106**, 8322 (1984).

b) K. Akiyama, S. T.-Kubota, T. Ikenoue, and Y. Ikegami, *Chem. Lett.*, **1984**, 903.

[24] K. Akiyama and Y. Ikegami, *Chem. Lett.*, **1988**, 255.

[25] a) S. T.-Kubota, Y. Sano, and Y. Ikegami, *J. Am. Chem. Soc.*, **104**, 3711 (1982).

b) H. Shimoishi, S. T.-Kubota, and Y. Ikegami, *Bull. Chem. Soc. Jpn.*, **58**, 553 (1985).

[26] Y. Ikegami, S. Kubota, and H. Watanabe, *Bull. Chem. Soc. Jpn.*, **52**, 1563 (1979).

[27] a) Y. Ikegami, H. Watanabe, and S. Seto, *J. Am. Chem. Soc.*, **94**, 3274 (1972).

b) Y. Ikegami and S. Seto, *J. Am. Chem. Soc.*, **96**, 7811 (1974).

[28] K. Akiyama, S. Kubota, and Y. Ikegami, *Chem. Lett.*, **1981**, 469.

[29] K. Yamaguchi, T. Fueno, K. Nakasuji, and I. Murata, *Chem. Lett.*, **1986**, 629.

[30] E. M. Kosower and Y. Ikegami, *J. Am. Chem. Soc.*, **89**, 461 (1967).

[31] a) M. Itoh and E. M. Kosower, *J. Am. Chem. Soc.*, **90**, 1843 (1968).

b) M. Itoh, *Bull. Chem. Soc. Jpn.*, **46**, 821 (1973).

[32] a) T. Muramatsu, K. Hanaya, and Y. Ikegami, *Chem. Lett.*, **1986**, 2139.

b) T. Muramatsu, K. Hanaya, S. Onodera, and Y. Ikegami, *Chem. Lett.*, **1987**, 1683.

c) Y. Ikegami, T. Muramatsu, and K. Hanaya, *J. Am. Chem. Soc.*, **111**, 5782 (1989).

d) T. Muramatsu, K. Hanaya, and Y. Ikegami, *Bull. Chem. Soc. Jpn.*, **63**, 1413 (1990).

[33] a) E. M. Kosower and A. Teuerstein, *J. Am. Chem. Soc.*, **100**, 1182 (1978).

b) E. M. Kosower, *ACS Symp. Ser.*, **69** (Org. Free Radicals), 447 (1978).

[34] K. Okada, H.Mori, M. Kozaki, K. Sato, and T. Takui, *Tetrahedron Lett.*, **39**, 6315 (1998).

[35] H. C. Longuet-Higgins, *J. Chem. Phy.*, **18**, 265 (1950).

[36] W. T. Borden and E. R. Davidson, *J. Am. Chem. Soc.*, **99**, 4587 (1977).

[37] A. A. Ovchinikov, *Theoret. Chim. Acta (Berg)*, **47**, 297 (1987).

[38] W. T. Borden, In *Diradicals*; W. T. Borden, Ed.; Wiely-Interscience; New York, 1982; pp 1-72.

[39] M. Dvolaitzky, R. Chiarelli, and A. Rassat, *Angew. Chem., Int. Ed. Engl.*, **31**, 180 (1992).

[40] F. Kanno, K. Inoue, N. Koga, and H. Iwamura, *J. Am. Chem. Soc.*, **115**, 847 (1993).

[41] S. Fang, M.-S. Lee, D. A. Hrovat, and W. T. Borden, *J. Am. Chem. Soc.*, **117**, 6727 (1995).

[42] K. Okada, T. Imakura, M. Oda, H. Murai, and M. Baumgarten, *J. Am. Chem. Soc.*, **118**, 3047 (1996).

[43] K. Okada, T. Imakura, M. Oda, A. Kajiwara, M. Kamachi, and M. Yamaguchi, *J. Am. Chem. Soc.*, **119**, 5740 (1997).

[44] A. P. West Jr, S. K. Silverman, and D. A. Dougherty, *J. Am. Chem. Soc.*, **118**, 1452 (1996).

[45] F. A. Van-Catledge, *J. Org. Chem.*, **45**, 4801 (1980).

Chapter 2. Preparations and properties of 1,3-bis(1-methyl-2,6-diphenyl-pyridinyl-4-yl)benzene, 1,3,5-tris(1-methyl-2,6-diphenylpyridinyl-4-yl) benzene, and their analogues

2-1. Introduction

As described in section 1-2, only a little study of bis-pyridinyl radicals has been reported. Especially, there is no report for the poly-pyridinyl radicals linked by π-spacers. The best precursors of pyridinyl radicals are obviously pyridinium ions. In order to achieve an efficient synthesis of the pyridinium ions $\mathbf{1}^{2+}$ and $\mathbf{2}^{3+}$, the choice of synthetic methodologies is important.

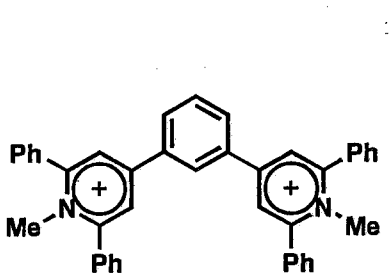

$\mathbf{1}^{2+}$

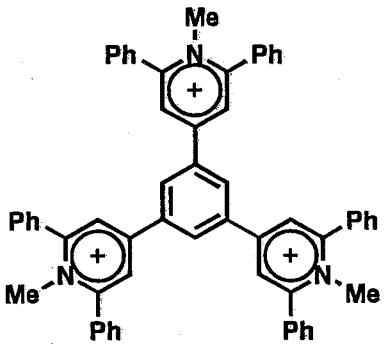

$\mathbf{2}^{3+}$

There are two strategies for the synthesis of bispyridinium ion $\mathbf{1}^{2+}$(Scheme 2-1). One is a method using a cross-coupling reaction of dihalobenzene with 4-metalo-2,6-diphenylpyridine followed by N,N'-dimethylation (eq. 2-1). The other involves the reaction of bispyrylium ion with methylamine. Bispyrylium ion would be obtained from isophthalaldehyde in three steps (eq. 2-2).

The former method will be effective when the corresponding polyaldehyde, for example 1,8-naphthalenedialdehyde, cannot be easily obtained. 4-Bromo-2,6-diphenylpyridine can be synthesized by the Jones method.[46] The coupling reaction would be accomplished using the Stille or the Suzuki reaction. Moreover, N-methylation of 2,6-diphenylpyridine would also be accomplished by the Hünig's procedure.[47] However, the route of eq. 2-1 was abandoned because preliminary experiments showed that the double N-methylation was not successful even under severe conditions.[48] On the other hand, the latter method was shown to be effective for the preparation of

2,4,6-triphenylpyrylium salts from benzaldehyde in three steps and the reaction of pyrylium salts with amines smoothly proceeded.[49] Before the synthesis of the bispyridinium ion $\mathbf{1}^{2+}$ and trispyridinium ion $\mathbf{2}^{3+}$, 1-methyl-2,4,6-triphenylpyridinyl radical (**16**) were prepared in order to know its stability.

Scheme 2-1

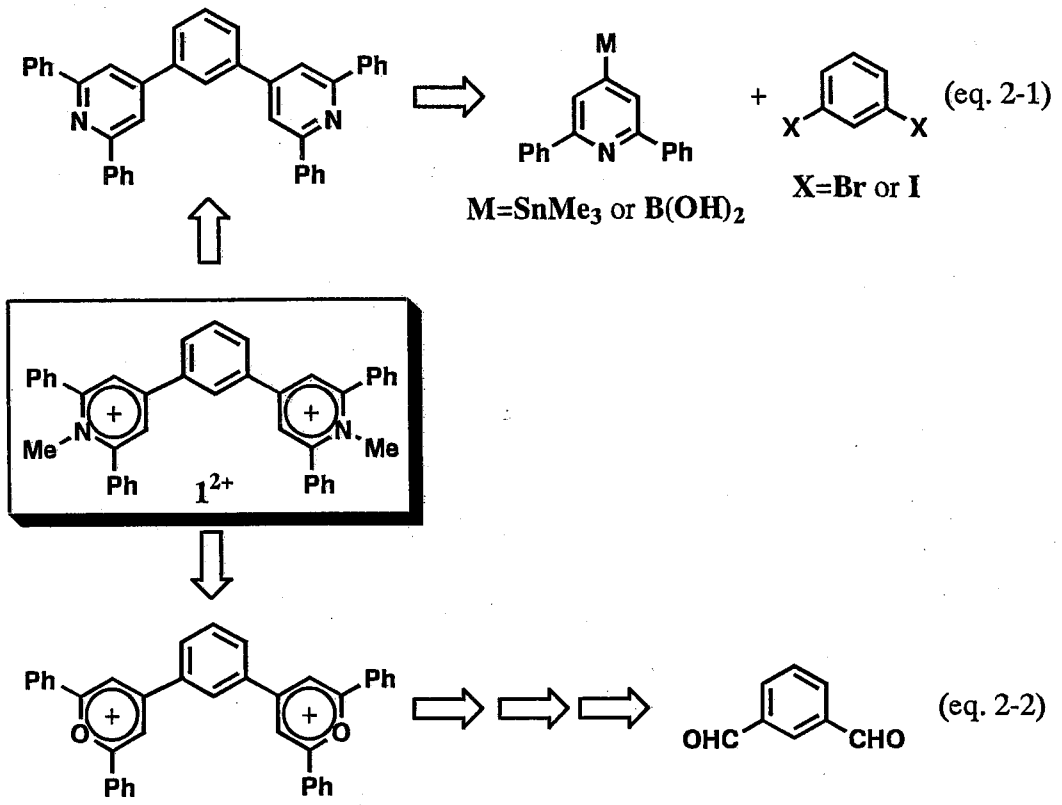

2-2. Preparation and characterization of 1-methyl-2,4,6-triphenylpyridinyl radical (16)

Although the synthesis and ESR spectrum of **16** were reported by Yampol'skii et al.,[50] the study on its stability remains to be investigated (Figure 2-1). Herein we synthesized **16** by the method described by Katritzky et al.[49d] and investigated its structural features.

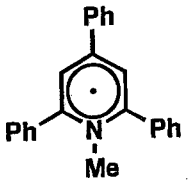

16

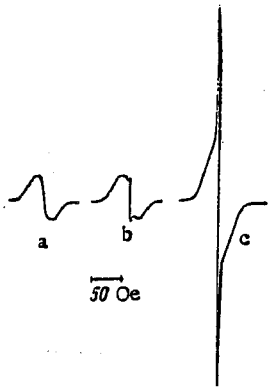

Figure 2-1. ESR spectrum of 1-methyl-2,4,6-triphenylpyridinyl radical (**16**) in benzonitrile reported by Yampol'skii: a) with removal of oxygen; b) without removal of oxygen; c) after heating of the sample to 240 K.

2-2-1. Synthesis of 1-methyl-2,4,6-triphenylpyridinium tetrafluoroborate [16$^+$•(BF_4^-)]

Scheme 2-2

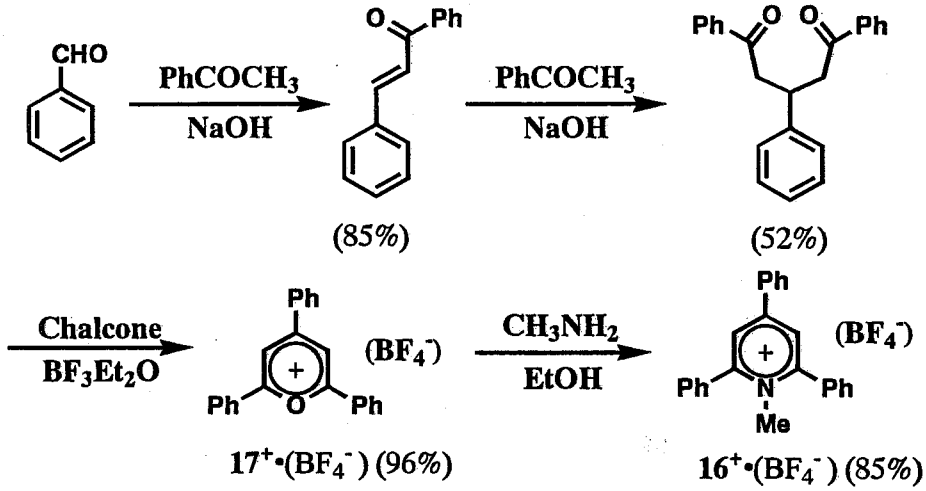

The pyridinium ion **16**$^+$ was synthesized according to the reported procedures.[51] Scheme 2-2 shows the synthetic path. Fairly good total yield of 35% indicates the synthetic applicability of this procedure.

2-2-2. Preparation and characterization of 1-methyl-2,4,6-triphenylpyridinyl radical (16)

Reduction of **16**$^+$ with 3% Na-Hg in acetonitrile was monitored by the measurement of UV-vis spectra at room temperature. Since the reduction must be performed under oxygen free conditions, an

apparatus shown in Figure 2-2 was used for the measurement of the UV-vis spectra. The procedures of the reduction were as follows: about 1.5 mg of pyridinium salt was charged in the vessel B and about 300 mg of 3% Na-Hg was placed in the vessel C. The system was degassed after the point D was sealed. About 5 ml of a well degassed solvent [acetonitrile or 2-methyltetrahydrofuran (MTHF)-acetonitrile (1:1 v/v)] was transferred into the B from the vessel K, and the point F was sealed. A solution of pyridinium salt in the B was transferred into the UV cell A (d=1 mm) and UV-vis spectrum of the solution of pyridinium salt was measured. The solution was transferred into the C. After shaking with 3% Na-Hg for a suitable time, the solution was filtered through the glass filter E. The UV-vis spectrum of this partially reduced solution was measured. The UV-vis spectral change was measured by the repetition of this procedure. The solution was separated from 3% Na-Hg during the measurement of UV-vis spectrum. Each spectrum was recorded as a function of the time contact.

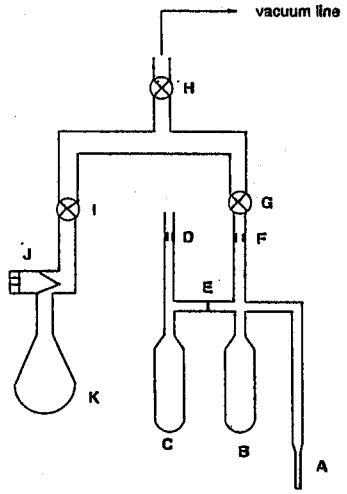

Figure 2-2. Apparatus for measurement of UV-vis spectra of pyridinyl radicals.

Figure 2-3 shows the UV-vis spectral change thus obtained. As the reduction proceeded, the solution turned blue and new absorptions appeared at 353 nm and 579 nm while the intensity of the absorption at 302 nm due to **16**$^+$ decreased. The isosbestic points were observed at about 270 nm and 320 nm. This blue (579 nm) species was assigned as 1-methyl-2,4,6-triphenylpyridinyl radical **16**. This assignment is reasonable in comparison with the known absorption (530 nm) of 1-methyl-4-phenylpyridinyl radical.[52] Reportedly, 1-methyl-4-phenylpyridinyl radical showed the absorption at 390 nm due to a pyridinyl radical dimer even at 20 °C and the radical absorption (530 nm) completely disappeared below -40 °C because of the dimerization. In contrast, the radical **16** did not show the absorption around 390 nm even at -30 °C. Furthermore, the intensity of the absorptions at 353 nm and 579 nm did not decrease by lowering the temperature. This experiment shows that **16** exists as a monomer in a wide range of temperature.

The radical **16** is stable at room temperature at least for 1 day under an inert atmosphere. But when aerated, the solution immediately turned pale yellow. Interestingly, the absorption of 302 nm due to the

starting pyridinium ion was observed by 80% of the original intensity (Figure 2-4). This finding shows that the pyridinyl radical **16** was generated at least in 80% yield by the reduction of $\mathbf{16}^+$. The regeneration of $\mathbf{16}^+$ is ascribed to the oxidation of **16** by molecular oxygen to give $\mathbf{16}^+$ and $O_2^{\bullet -}$. The similar behavior was observed by Kosower et al. in the reaction of 4-carbomethoxy-1-ethylpyridinyl radical with oxygen [8b].

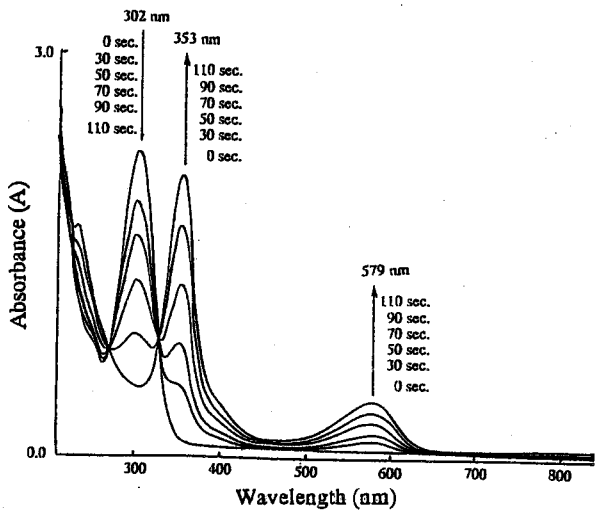

Figure 2-3. UV-vis spectral change upon reduction of $\mathbf{16}^{+\bullet}(BF_4^-)$ to form pyridinyl radical **16**.

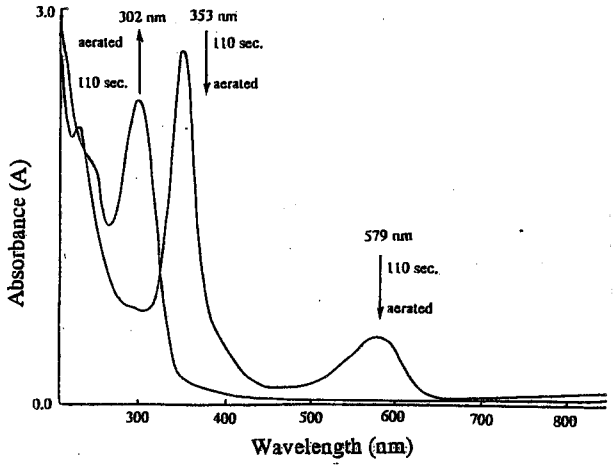

Figure 2-4. UV-vis spectral change when the solution of pyridinyl radical **16** was aerated.

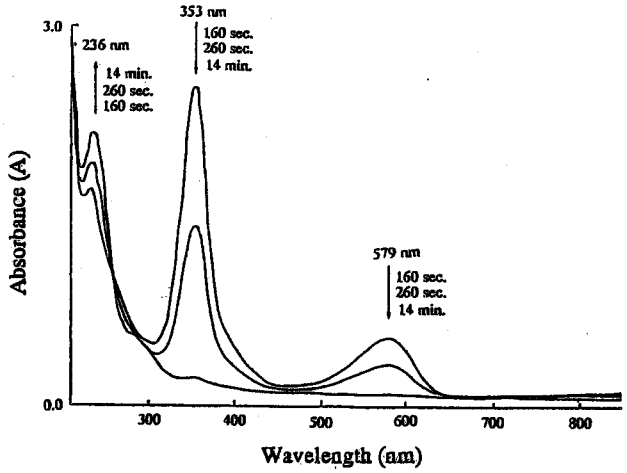

Figure 2-5. UV-vis spectral change when the solution of pyridinyl radical **16** was treated with 3% Na-Hg.

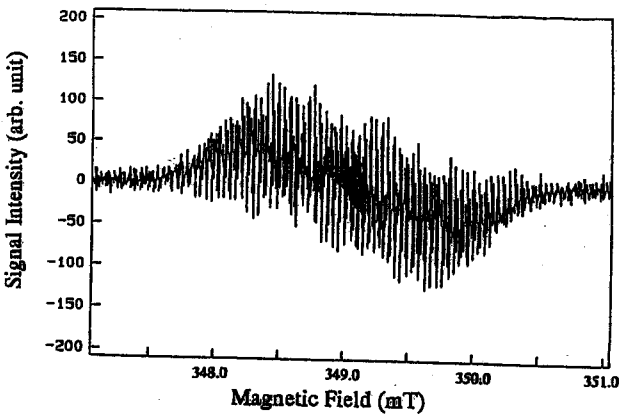

Figure 2-6. ESR spectrum of **16** in acetonitrile at room temperature.

Further contact of the blue species with 3% Na-Hg under degassed conditions decreased the radical absorption (Figure 2-5). This process should involve the formation of the pyridinyl anion $\mathbf{12}^-$.

However, no absorption for $\mathbf{1}^{2-}$ was not observed in the visible region. Since $\mathbf{1}^{2-}$ has an 8π-electrons and would be unstable, the observed spectrum would be due to a decomposed or protonated species. The exposure of the $\mathbf{1}^{2-}$ to air did not reproduce the starting cation.

ESR spectrum of **16** in acetonitrile at room temperature is shown in Figure 2-6. It is a well-resolved spectrum, compared to that obtained by Yampol'skii (Figure 2-1). Simulation for the determination of the hyperfine splitting constants was not achieved because of many protons involved.

2-3. Preparation and characterization of 1,3-bis(1-methyl-2,6-diphenylpyridinyl-4-yl)benzene (1) and 1,3,5-tris(1-methyl-2,6-diphenylpyridinyl-4-yl)benzene (2)

As described in the preceding section, the radical **16** was shown to be stable under an inert atmosphere. These results suggest that **16** can be used as a spin source for high-spin molecules. In this section, the preparation and characterization of the titled high-spin molecules are described.

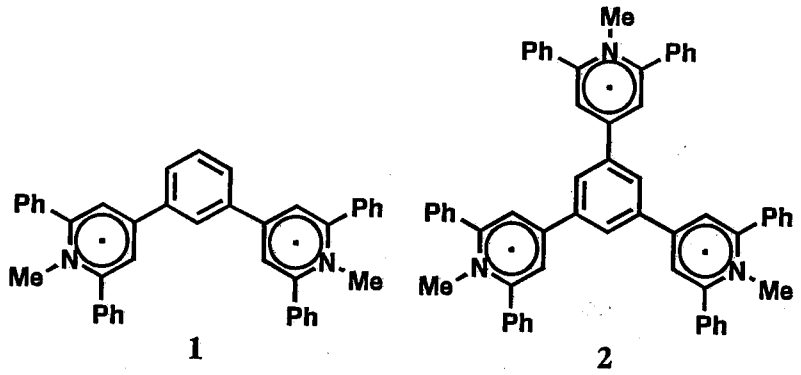

2-3-1. Synthesis of bispyridinium salt $\mathbf{1}^{2+}$•2(BF_4^-)

The synthesis of 1,3-bis(1-methyl-2,6-diphenylpyridinium-4-yl)benzene $\mathbf{1}^{2+}$ is illustrated in Scheme 2-3. In order to synthesize 1,3-bis(2-benzoylethenyl)benzene (**18**), isophthalaldehyde was at first tried to be condensed with acetophenone. However, a complex mixture was obtained and **18** could not be obtained. Compound **18** could be successfully obtained by the Wittig reaction in a good yield. Isophthalaldehyde was treated with 2.2 equivalents of phosphonium ylide obtained from

benzoylmethyltriphenylphosphonium bromide and potassium *tert*-butoxide in DMSO to give the dienone **18** in 75% yield. The conversion of **18** into **19** was achieved in 42% yield using excess amounts of acetophenone in the presence of potassium *tert*-butoxide in THF-*tert*-butanol (3:2 v/v). The bispyrylium ion $\mathbf{20}^{2+}$ was obtained in 76% yield by the reaction of **19** with 2.0 equivalents of chalcone and excess amounts of boron trifluoride etherate. The target dication, bispyridinium ion $\mathbf{1}^{2+}$, was obtained in 72% yield by the reaction of $\mathbf{20}^{2+}$ with methylamine in acetonitrile at room temperature. The reaction in ethanol resulted in a low yield of 57%.

Scheme 2-3

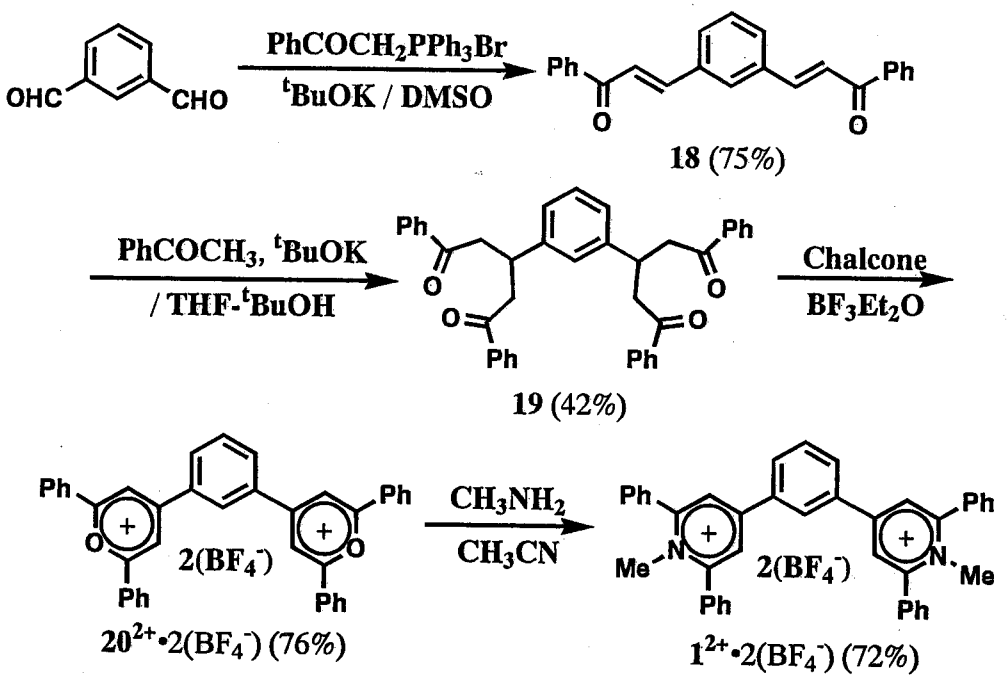

2-3-2. Synthesis of trispyridinium salt 2^{3+}*•3(*BF_4^-*)*

The synthesis of 1,3,5-tris(1-methyl-2,6-diphenylpyridinium-4-yl)benzene $\mathbf{2}^{3+}$ is shown in Scheme 2-4. The procedure for the synthesis of $\mathbf{2}^{3+}$ are essentially similar to that for $\mathbf{1}^{2+}$. 1,3,5-Triformyl-benzene was heated with 3.3 equivalents of benzoylmethyltriphenylphosphonium bromide and 3.3 equivalents of potassium *tert*-butoxide in DMSO at 80 °C for four hours to afford **21** in 78% yield. Then, **21** was treated with excess amounts of acetophenone in the presence of potassium *tert*-butoxide in THF-*tert*-butanol (3:2 v/v) for two hours at room temperature to give the hexaketone **22** in 39% yield. Heating of **22** with 3.0 equivalents of chalcone and excess amounts of boron trifluoride etherate

for five hours at 100 °C afforded the trispyrylium ion $\mathbf{23^{3+}}$, which was converted into the trispyridinium ion $\mathbf{2^{3+}}$ on treatment with 6.0 equivalents of methylamine in acetonitrile at room temperature overnight. For purification of $\mathbf{2^{3+}}$, a special procedure was necessary (see the experimental section).

Scheme 2-4

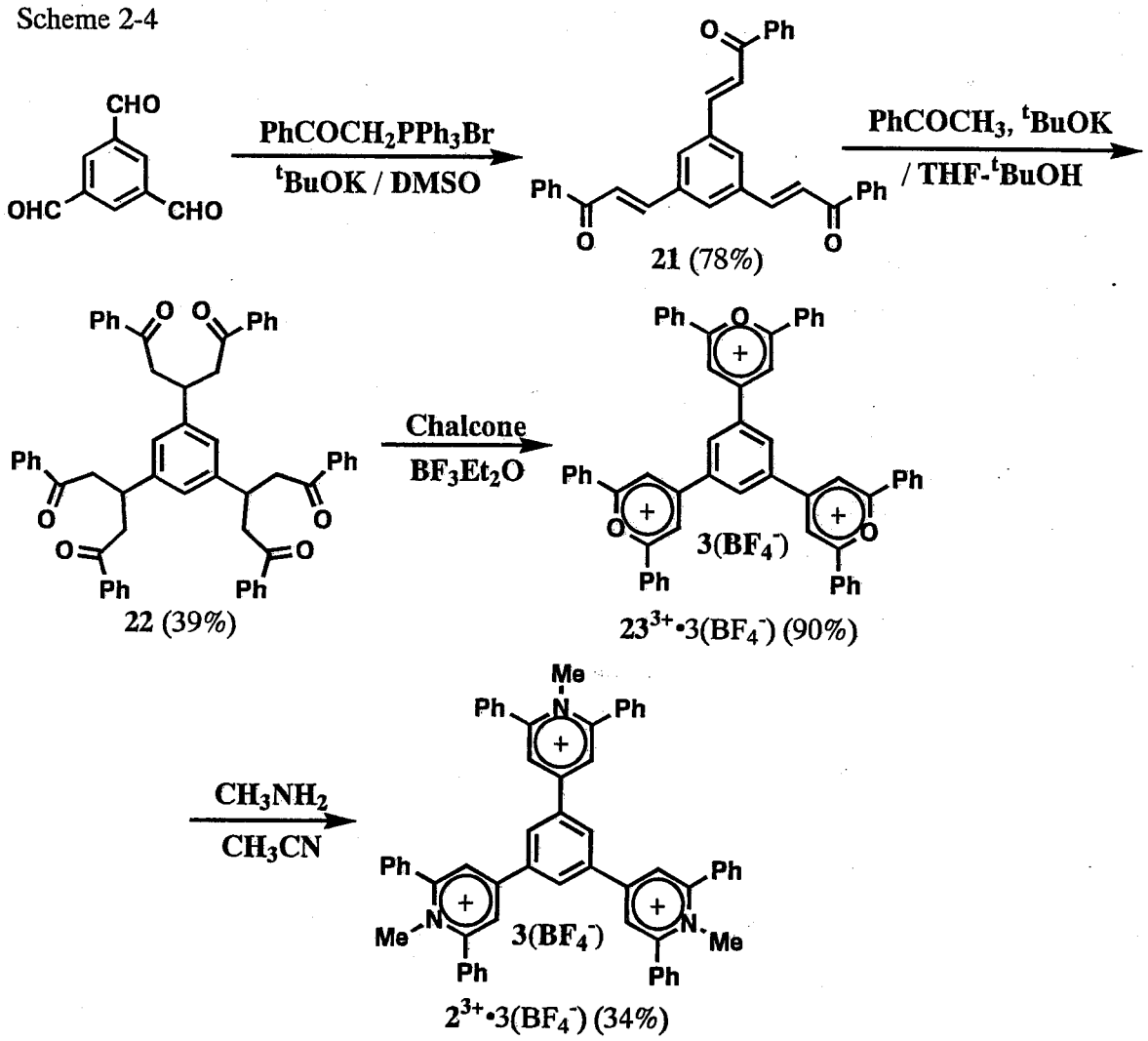

2-3-3. ^{1}H and ^{13}C chemical shifts of bispyridinium salt $\mathbf{1^{2+}}$•2(BF_4^-) and trispyridinium salt $\mathbf{2^{3+}}$•3(BF_4^-)

Figure 2-7 summarizes ^{1}H and ^{13}C chemical shifts of the pyridinium ion $\mathbf{16^{+}}$, bispyridinium ion $\mathbf{1^{2+}}$, and trispyridinium ion $\mathbf{2^{3+}}$. The bold letters are for ^{13}C chemical shifts and plain letters for ^{1}H chemical shifts. Assignments were performed using C-H cosy and long range C-H cosy spectra for

1^{2+} and 2^{3+}. In these cations, the H-3(5) protons in the pyridinium ring and the H-2(6) proton of the central benzene ring appear as a singlet signal in the 4:1 integrated ratio for 1^{2+}; and the 2:1 ratio for 2^{3+}. The other proton assignments were made started from these assignments.

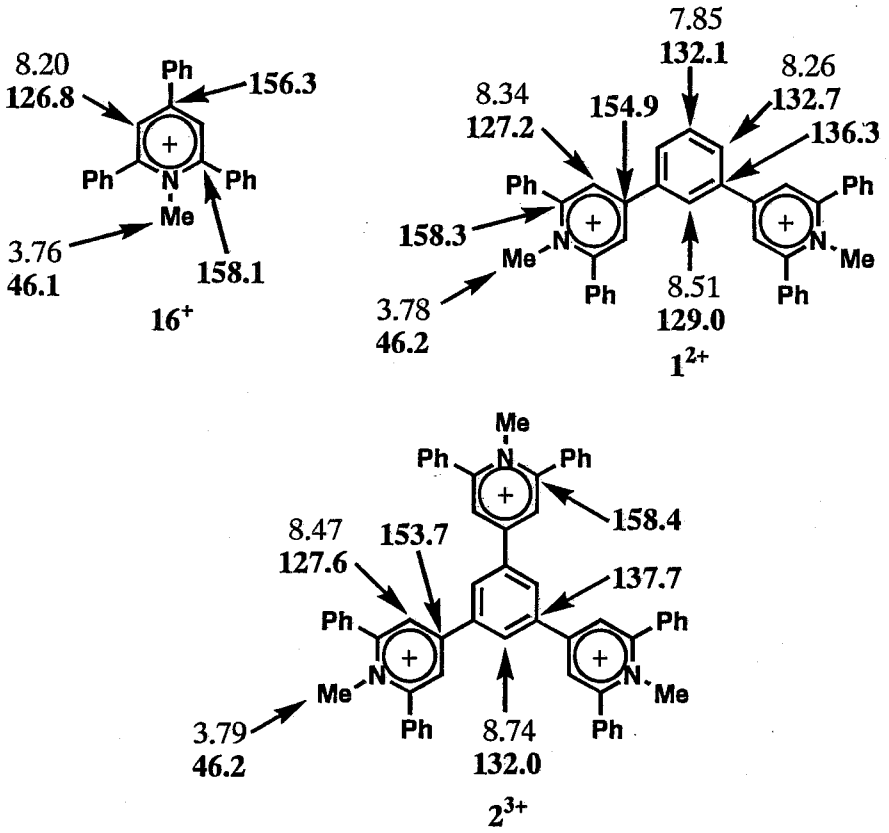

Figure 2-7. ^{1}H and ^{13}C chemical shifts of pyridinium ions 16^{+}, 1^{2+}, and 2^{3+} (in CD_3CN).

^{13}C chemical shifts of the C-2(6) and C-4-positions in the pyridinium ring are particularly large (153.7-158.4 ppm) in both the dication 1^{2+} and the trication 2^{3+}. The difference of the chemical shifts for these carbons between 1^{2+} and 2^{3+} are small; the signal of the C-4 in 1^{2+} appears at a little lower field than that in 2^{3+}. The signal of the protons and carbons of 2(6)-phenyl groups on the pyridinium ring in both 1^{2+} and 2^{3+} appear in the range of 7.74-7.67 ppm and 130.1-133.9 ppm, respectively. Furthermore, the protons of the central benzene ring appear at lower field than those of phenyl groups in both 1^{2+} and 2^{3+}. The N-methyl-proton [3.78(9) ppm] and N-methyl-carbon (46.2 ppm) of 1^{2+} and 2^{3+} appear at almost the same positions.

2-3-4. Reduction potentials and absorption maximum in electronic spectra of bispyridinium salt $1^{2+}\bullet 2(BF_4^-)$ and trispyridinium salt $2^{3+}\bullet 3(BF_4^-)$

Table 2-1 shows the reduction potentials (cyclic voltammetry: CV) and the absorption maximum in the electronic spectra of the pyridinium ion $\mathbf{16}^+$, bispyridinium ion $\mathbf{1}^{2+}$, and trispyridinium ion $\mathbf{2}^{3+}$. The pyridinium ion $\mathbf{16}^+$ showed two reversible reduction waves at -1.20 V and -1.65 V which would correspond to the reduction processes of cation ↔ radical and radical ↔ anion, respectively. The reversibility accords with the fact that **16** is stable at room temperature for 1 day. The bispyridinium ion $\mathbf{1}^{2+}$ showed four reversible reduction waves at -1.10 V, -1.23 V, -1.66 V, and -1.77 V. These reduction potentials correspond to the redox processes of dication ↔ cation radical, cation radical ↔ diradical, diradical ↔ anion radical, and anion radical ↔ dianion, respectively. This suggests that the bis-pyridinyl radical **1** is fairly stable.

Table 2-1. Reduction potentials [a, b] and absorption maximum of the pyridinium salts $\mathbf{16}^+\bullet(BF_4^-)$, $\mathbf{1}^{2+}\bullet 2(BF_4^-)$, and $\mathbf{2}^{3+}\bullet 3(BF_4^-)$.[b]

	E_1 / V	E_2 / V	E_3 / V	E_4 / V	λ_{max} / nm (ε x 10^{-4})
$\mathbf{16}^+\bullet(BF_4^-)$	-1.20		-1.65		302 (3.16)
$\mathbf{1}^{2+}\bullet 2(BF_4^-)$	-1.10	-1.23	-1.66	-1.77	298 (5.94)
$\mathbf{2}^{3+}\bullet 3(BF_4^-)$	-1.02	-1.12	-1.27[c]		296 (8.14)

a) supporting electrolyte, 0.1 M tetrabutylammonium tetrafluoroborate; indicating electrode, glassy carbon; reference electrode, S. C. E.; scan rate, 100 mV / sec
b) in acetonitrile c) peak potential

In contrast to these cations, the trispyridinium ion $\mathbf{2}^{3+}$ showed two reversible reduction waves at -1.02 V and -1.12 V, the third irreversible reduction wave at -1.27 V. The fourth reduction potentials could not be determined because the reduction wave was so broad. These observations suggest that tris(pyridinyl radical) **2** is too unstable to cleanly prepare. Interestingly, when the sweep width in CV of $\mathbf{2}^{3+}$ was set to +0.73 V ~ -1.27 V, the latter being the peak potential for the triradical, a new irreversible oxidation wave appeared at about +0.3 V. A similar behavior has been reported for 1-benzyl-2,4,6-trimethylpyridinium ion and 1-(*p*-cyanobenzyl)-4-methylpyridinium ion (0.19 V and 0.21 V, respectively) by Pragst et al.[53] They attributed these oxidation waves to the oxidation of the

pyridinyl dimers. These findings may suggest the formation of dimers, oligomers, or intramolecular dimers for the reduction of $\mathbf{2}^{3+}$.

The absorption maximum in the electronic spectra of both $\mathbf{1}^{2+}$ and $\mathbf{2}^{3+}$ is similar, although a little blue shift is observed in $\mathbf{2}^{3+}$. The molar absorptivity of the bispyridinium ion $\mathbf{1}^{2+}$ and trispyridinium ion $\mathbf{2}^{3+}$ are 1.9 and 2.6 times larger than that of $\mathbf{16}^{+}$, in consonant with *m*-substituted dication and trication structures.

2-3-5. Electronic spectra obtained by reduction of bispyridinium salt $\mathbf{1}^{2+}\bullet 2(BF_4^-)$ and trispyridinium salt $\mathbf{2}^{3+}\bullet 3(BF_4^-)$

In the preceding section, it was suggested that the diradical **1** is stable and cleanly prepared by the reduction of $\mathbf{1}^{2+}$ whereas the triradical **2** is unstable. In this section, the reduction of $\mathbf{1}^{2+}$ and $\mathbf{2}^{3+}$ was investigated under similar conditions for $\mathbf{16}^{+}$.

Figure 2-8 shows UV-vis spectral change upon the reduction of $\mathbf{1}^{2+}$ with 3% Na-Hg in acetonitrile at room temperature. As observed in the reduction of the pyridinium ion $\mathbf{16}^{+}$, the colorless solution turned blue and new absorptions (358 nm and 588 nm) appeared. Two isosbestic points were observed at about 270 nm and 330 nm.

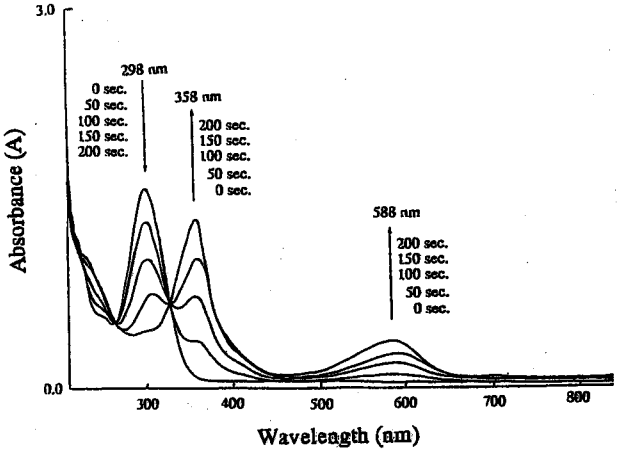

Figure 2-8. UV-vis spectral change upon reduction of $\mathbf{1}^{2+}\bullet 2(BF_4^-)$ with 3% Na-Hg to form diradical **1**.

Because of the nature of *m*-disubstituted benzenes, diradical **1** would have absorption maxima at similar wavelength with the pyridinyl monoradical **16**, and cation radical $\mathbf{1}^{+\bullet}$ would have superposed the absorptions of $\mathbf{16}^{+}$ and **16**. So, when the absorption at 298 nm due to the pyridinium ion moiety completely disappeared, the diradical **1** would be exclusively formed. For this reason the species produced after 200 sec. (contact time) was assigned to be **1**. As recognized from comparison between Figure 2-3 and Figure 2-8, the intensity ratios of [ca. 300 nm at contact time 0] / [ca. 580 nm of the (di)radical absorption at the final contact time] are keeping in almost constant, 5 (Figure 2-8) ~ 6

(Figure 2-3). Since the molar absorptivity of $\mathbf{1}^{2+}$ is twice larger than that of $\mathbf{16}^{+}$, the above finding indicates that the molar absorptivity of **1** is twice larger than that of **16**, indicating that **1** is a diradical. The diradical solution can be stored for a few hours under an inert atmosphere at room temperature. However, the solution slowly faded after longer standing at room temperature (Figure 2-9). The decrease of the absorption may be due to reactions with some impurities involved in the solvent or may be due to slow intramolecular reaction such as C-N bond cleavage (see chapter 4). The possibility of slow dimerization may also not be excluded.

When the diradical solution was aerated, the absorption of pyridinium moiety was recovered in 65% of the original intensity (Figure 2-10) as observed for $\mathbf{16}^{+}$. On the other hand, further reduction of the diradical solution gave a pale yellow solution. In this case, the absorption due to the starting pyridinium ion was not recovered upon aeration.

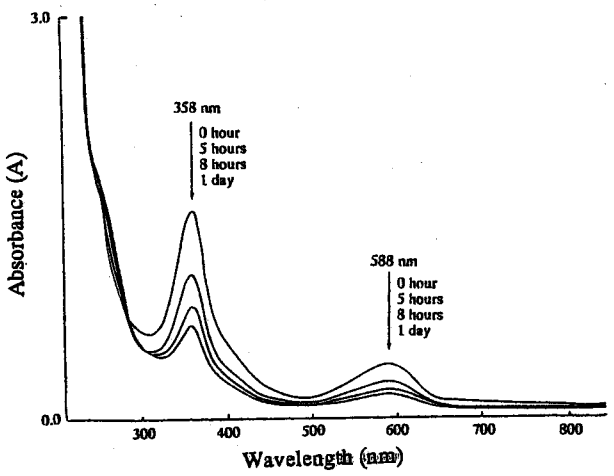

Figure 2-9. Stability of diradical **1**.

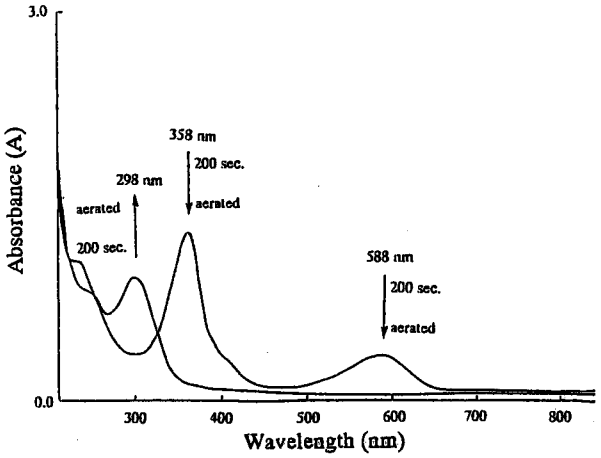

Figure 2-10. UV-vis spectral change when the solution of diradical **1** was aerated.

Figure 2-11 shows UV-vis spectral change upon the reduction of $\mathbf{2}^{3+}$ with 3% Na-Hg in acetonitrile at room temperature. The colorless solution of $\mathbf{2}^{3+}$ turned blue-green and then dark green as the reduction proceeded. Though the absorptions due to pyridinyl radical moiety were observed at 363 nm and 591 nm, a new absorption at 676 nm, which grew during the reduction, was observed. Further reduction decreased all these absorptions (Figure 2-12) and the resulting solution turned dark yellow. The assignment of the absorption at 676 nm is not clear at present, although pyridinyl dimers, oligomers, or intramolecular dimers etc. are suggested in the CV section (2-3-4).

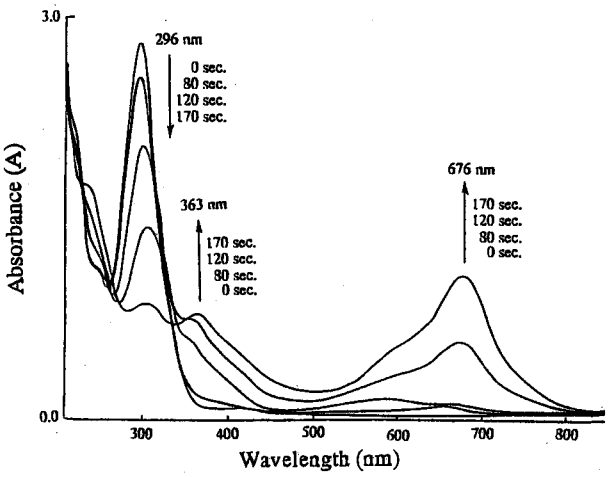

Figure 2-11. UV-vis spectral change upon reduction of $2^{3+}\cdot 3(BF_4^-)$.

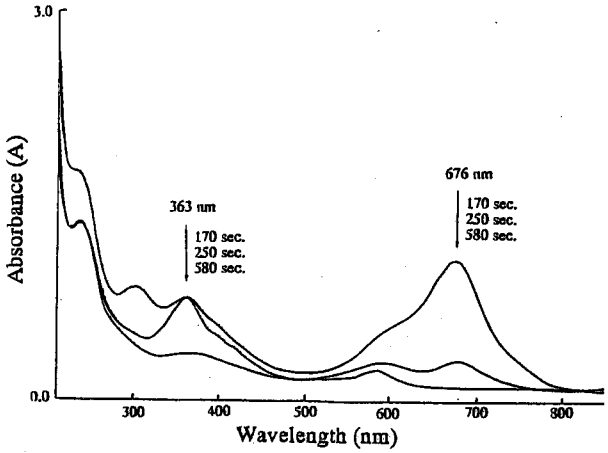

Figure 2-12. UV-vis spectral change obtained by further reduction of the solution shown in Figure 2-11.

2-3-6. ESR spectra obtained by reduction of bispyridinium salt $1^{2+}\cdot 2(BF_4^-)$ *and trispyridinium salt* $2^{3+}\cdot 3(BF_4^-)$

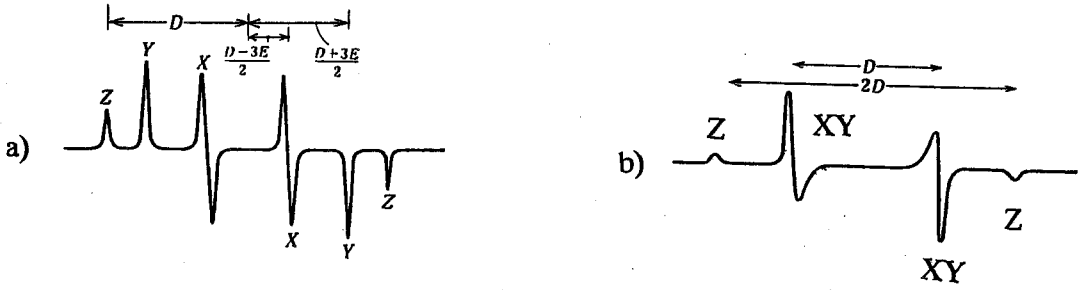

Figure 2-13. Typical ESR spectra of randomly oriented triplet species: a) E≠0; b) E=0.

For characterization of high-spin molecules, ESR spectroscopy is useful. Unique ESR split patterns based on the dipole-dipole interaction between electron spins can be observed in solid states. Typical ESR patterns of randomly oriented triplet species are shown in Figure 2-13. These patterns are well characterized by two parameters *D* and *E*, which are called as zero-field splitting parameters. These triplet patterns usually have a large split ($D \geq 5.0$ mT) and a large half-width (> 1.0 mT). The small hyperfine splitting constants (hfc) are frequently not observed. Triplet species usually show a weak signal due to forbidden $\Delta Ms = \pm 2$ transition in g = 4 region. Detection of the weak $\Delta Ms = \pm 2$ transition signal can be used as a piece of evidence of triplet species.

Temperature dependence of these ESR signal intensity provides an important information whether the observed triplet is at a ground state or not. Curie plots are frequently used for the determination of spin multiplicity of the ground state. In general, when a triplet state is a ground state or degenerated with a singlet state, the signal intensity is proportional to the reciprocal of temperature. On the other hand, when a singlet state is a ground state, the signal intensity (I) is represented by an equation of $I = C [\exp (-\Delta E_{S-T} / RT)] / T [1+3 \exp (-\Delta E_{S-T} / RT)]$, where C is a constant, ΔE_{S-T} is an energy gap between the singlet and triplet states, and R is the gas constant.

2-3-6-1. ESR spectrum of diradical ***1***

Preparation of the ESR samples were carried out using an apparatus (Figure 2-14) which is similar to that depicted in Figure 2-2, except for attachment of an ESR tube (L). Reduction of the pyridinium salt **1** was already described in the section 2-3-5 [MTHF-acetonitrile (1:1 v/v) was used as solvent]. When the intensity of the absorption (558 nm) of the pyridinyl radical **1** started to decrease, the reduction was stopped. The reduced solution was transferred to L up to 2-3 cm height and the tube was sealed at M. The blue species obtained in the reduction of $\mathbf{1}^{2+}$ showed an ESR spectrum in a frozen MTHF-acetonitrile (1:1 v/v) at -150 °C (Figure 2-15).

The strong centered lines [split into three lines by a nitrogen 14 nucleus (I = 1)] are due to a monoradical impurity. Since the transition probability of doublet species (monoradical) is generally high, the central signals are always observed in this type of experiments, even if monoradical concentration is small. The small and broad peaks beside the monoradical signals is assignable to the triplet species. The observed spectrum has a rather peculiar triplet pattern and does not look like the above mentioned typical triplet patterns. However, the triplet nature of these signals were supported by the observation of the forbidden $\Delta Ms = \pm 2$ transition signal around g = 4 region.

The ESR spectrum [Figure 2-15 (a)] can be simulated using the zero-field splitting parameters of D = 4.0 mT and E = 1.2 mT. The peculiar pattern is ascribable to the large E value. The D value corresponds to 8.9 Å as an averaged distance between two radical centers by the point dipole approximation. This calculated distance is longer than the distance (ca. 5 Å) between the C-4 and C-4' carbons of the pyridinyl rings but rather close to the distance (ca. 10 Å) between the two nitrogen

atoms. This consideration suggests that the radical center of the pyridinyl ring is approximated at a closer position to the nitrogen atom rather than the C-4 position. The large E value suggests that the conformation of this radical has a low symmetry.

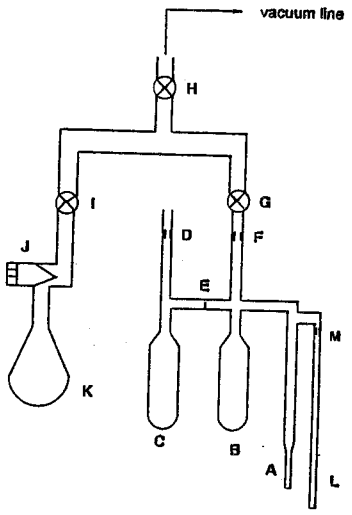

Figure 2-14. Apparatus for measurement of ESR spectra of pyridinyl radicals.

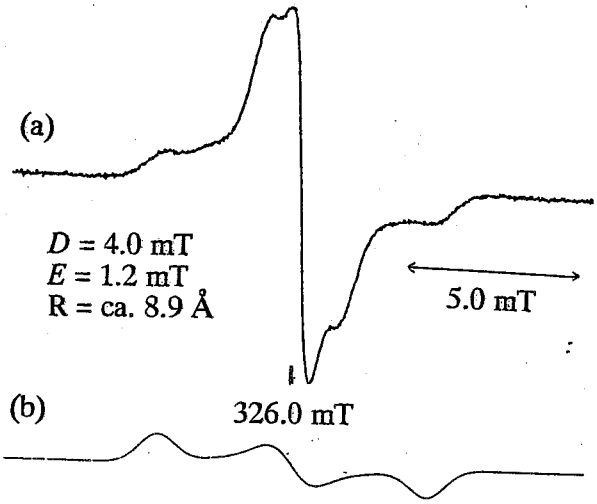

Figure 2-15. (a) ESR spectrum of diradical **1** at -150 °C in MTHF-acetonitrile. (b) simulated spectrum.

Figure 2-16 shows temperature dependence of the signal intensity of $\Delta Ms = \pm 2$ transition. The signal intensity proportionally increased to the reciprocal of temperature. This relation indicates that the bis-pyridinyl radical **1** has a triplet ground state or a singlet ground state with $\Delta E_{S-T} \approx 0$ cal/mol.

This result is compatible with the consideration of the VB structures of **1m**-1~**1m**-3 and the small HOMO-LUMO gap (0.06 β by HMO) (section 1-4-2).

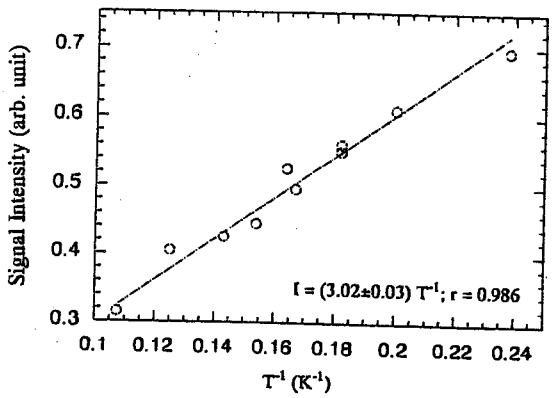

Figure 2-16. Temperature dependence of the signal intensity of $\Delta Ms = \pm 2$ transition of **1**.

2-3-6-2. ESR spectrum of the species obtained by reduction of trispyridinium salt 2^{3+}•3(BF_4^-)

Figure 2-17 shows an ESR spectrum of the species (676 nm) obtained by the reduction of trispyridinium ion $\mathbf{2}^{3+}$. The observed spectrum is similar to that in Figure 2-15 (a). The split width of the outermost signals is also similar (ca. 8.0 mT). The similarity suggests that the observed species would be an ionic diradical **2A**. Evidence of the quartet species has not been obtained.

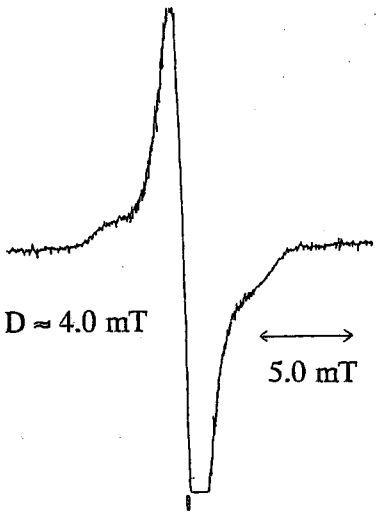

Figure 2-17. ESR spectrum of the species obtained by reduction of $\mathbf{2}^{3+}$•3(BF_4^-).

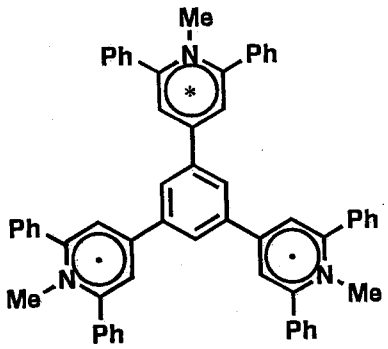

2A (* would be + or -.)

2-3-7. Summary

1) 1-Methyl-2,4,6-triphenylpyridinyl radical (**16**) was stable in acetonitrile at room temperature for one day under degassed conditions. This result suggests that 1-methyl-2,4,6-triphenylpyridinyl radical can be used as a spin source of organic high-spin molecules.

2) 1,3-Bis(1-methyl-2,6-diphenylpyridinyl-4-yl)benzene (**1**) was prepared by the reduction of $\mathbf{1}^{2+}$ with 3% Na-Hg. The ESR spectrum of **1** was characterized as a triplet pattern with zfs; D = 4.0 mT, E = 1.2 mT. The diradical **1** was shown to have a triplet ground state or a singlet ground state with $\Delta E_{S\text{-}T} \approx 0$ cal/mol, based on the temperature dependence of the signal intensity.

3) For the reduction of 2^{3+}, a triplet species was observed. The triplet species was assigned as **2A**. No evidence for the expected quartet species was obtained as suggested from the CV data.

2-4. Preparations and characterization of 1,4-bis(1-methyl-2,6-diphenylpyridinyl-4-yl)benzene (24)

m-Phenylene linked diradical **1** was found to have either a triplet ground state or a singlet ground state with small S-T gap in the preceding section. This result may be compatible with the consideration for the model compound **1m** (1-4-2) which has nondegenerate but nearly degenerate two NBMO's (HMO). The energy difference between the two NBMO's is small (0.06 β). This section describes the electronic nature of the titled *p*-phenylene linked species **24**.

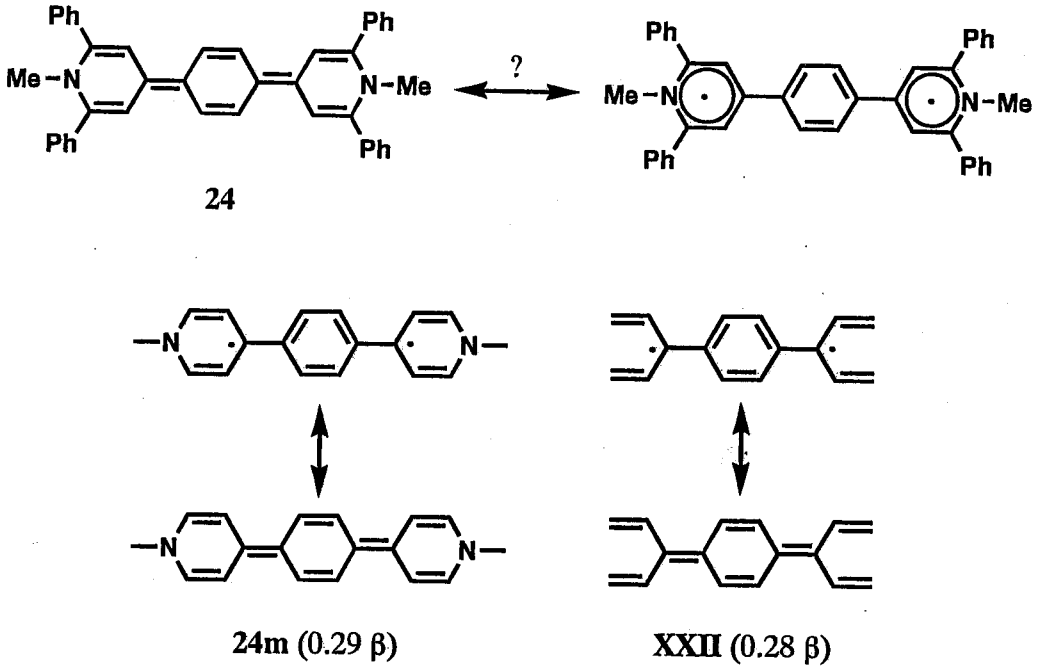

Figure 2-18. Energy gap between HOMO and LUMO by the calculation of HMO.

To compare the electronic nature of **24** with that of *m*-phenylene linked diradical **1**, HMO calculation of the model compound **24m** is meaningful.[45] In order to gain an insight into the delocalization effect of the lone pair electrons, 3,3'-(*p*-phenylene)bis(pentadienyl) **XXII** was also calculated. The

calculated energy gap is considerably large (0.28 ~ 0.29 β) in both cases (Figure 2-18). The results on **24** will be compared to those on **7** (nitrogen substituted *p*-phenylene derivative).

2-4-1. Synthesis of bispyridinium salt $\mathbf{24}^{2+}\bullet 2(BF_4^-)$

The synthesis of 1,4-bis(1-methyl-2,6-diphenylpyridinium-4-yl)benzene $\mathbf{24}^{2+}$ is illustrated in Scheme 2-5. Terephthalaldehyde was treated with 2.2 equivalents of benzoylmethyltriphenyl-phosphonium bromide and 2.2 equivalents of potassium *tert*-butoxide in DMSO at 80 °C for 6 hours. Diketone **25** was obtained in 78% yield. The conversion of **25** to **26** was achieved using excess amounts of acetophenone in the presence of potassium *tert*-butoxide in THF-*tert*-butanol (3:2 v/v) in 85% yield. The bispyrylium ion $\mathbf{27}^{2+}$ was obtained in 99% yield by the reaction of **26** with 2.0 equivalents of chalcone and excess amounts of boron trifluoride etherate at 110 °C for three hours. Finally, the bispyridinium ion $\mathbf{24}^{2+}$ was obtained in 77% yield by the reaction of $\mathbf{27}^{2+}$ with methylamine in acetonitrile at room temperature.

Scheme 2-5

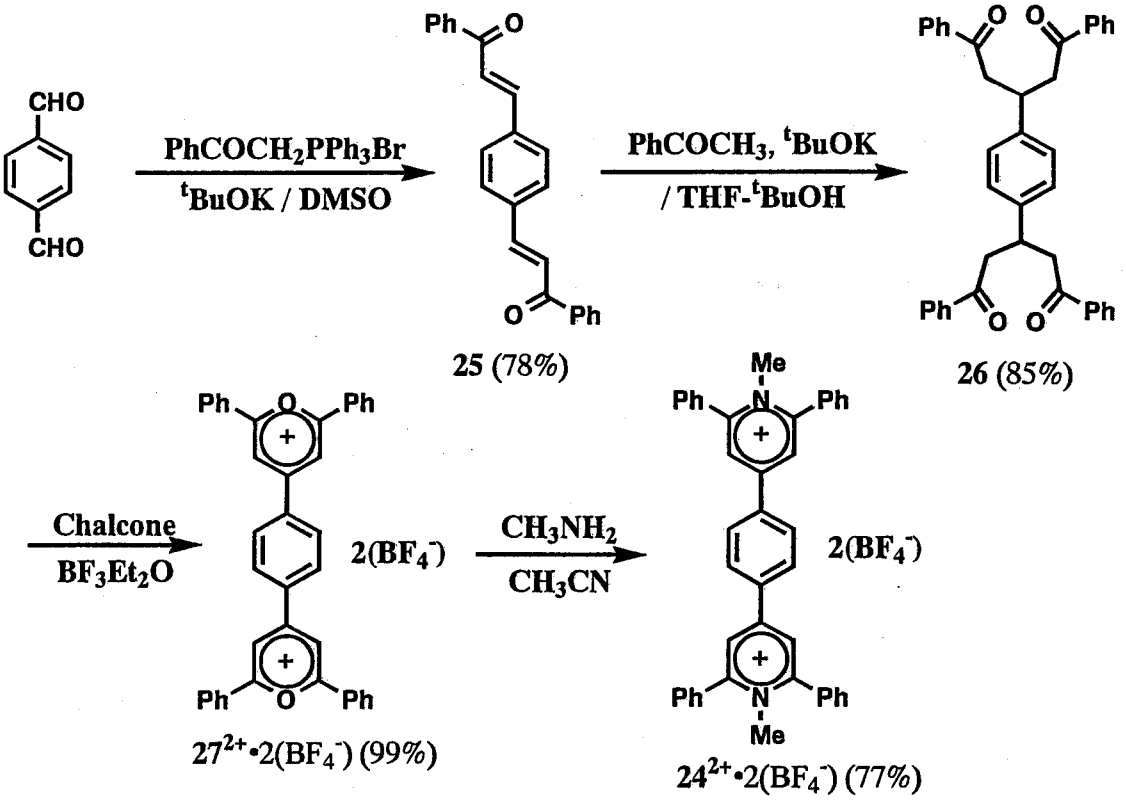

2-4-2. Reduction potentials and absorption maximum in electronic spectrum of bispyridinium salt $\mathbf{24}^{2+}\bullet 2(BF_4^-)$

The bispyridinium ion $\mathbf{24}^{2+}$ showed a reversible reduction wave at -0.82 V and an irreversible reduction wave at -2.02 V. Since the bispyridinium ion $\mathbf{1}^{2+}$ showed four reversible reduction potentials at -1.10 V, -1.23 V, -1.66 V, and -1.77 V, the reduction at -0.82 V would be a two-electron transfer corresponding to the reduction process of dication ↔ quinoid structure like *p*-quinodimethane. The reduction at -2.02 V may correspond to the reduction process of quinoid ↔ quinoid anions. The first reduction potential of $\mathbf{24}^{2+}$ appears in more positive region than that of $\mathbf{1}^{2+}$ and the second reduction potential of $\mathbf{24}^{2+}$ appears in more negative region than that of $\mathbf{1}^{2+}$. These results suggest that the quinoid **24** has a highly negative reduction potential but has a very low oxidation potential (-0.82 V). Since the oxidation potential of **24** is more negative than the reduction potential of molecular oxygen (-0.75 V), this compound cannot be isolated under aerated conditions.

2-4-3. Electronic spectra obtained by reduction of bispyridinium salt $\mathbf{24}^{2+}\bullet 2(BF_4^-)$

The UV-vis spectral change of $\mathbf{24}^{2+}$ upon reduction can be clearly separated into two successive stages (stage I and stage II). Figure 2-19 shows the stage I. The colorless solution of $\mathbf{24}^{2+}$ turned orange and the absorptions appeared at 521 nm and 481 nm as the reduction proceeded. Interestingly, further reduction of the orange solution gave a blue solution and a broad absorption appeared at 647 nm (stage II in Figure 2-20). This suggests that the orange species is the cation radical $\mathbf{24}^{+}$ and the blue species is quinoid **24**. This assignment can be supported by the following considerations; the species $\mathbf{24}^{+}$ has an absorption at 328 nm with the half of the original intensity of $\mathbf{24}^{2+}$, which indicates that $\mathbf{24}^{+}$ has a pyridinium ion structure. Furthermore, $\mathbf{24}^{+}$ has also an absorption at 521 nm which is close to the absorption of the pyridinyl radical. Quinoid **24** has totally different absorptions in comparison with the pyridinyl radical absorptions. This new absorption instantaneously disappeared when aerated. This is in agreement with the CV-prediction that **24** has a more negative oxidation potential than the reduction potential of molecular oxygen.

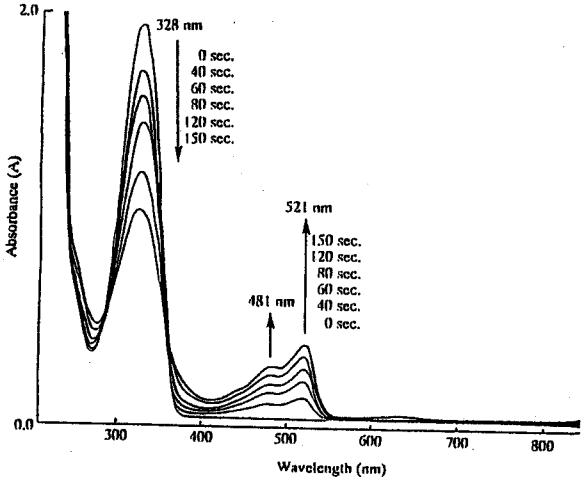

Figure 2-19. Stage I in the UV-vis spectral change upon reduction of $\mathbf{24}^{2+}\bullet 2(BF_4^-)$ in MTHF-acetonitrile (1:1 v/v) at room temperature.

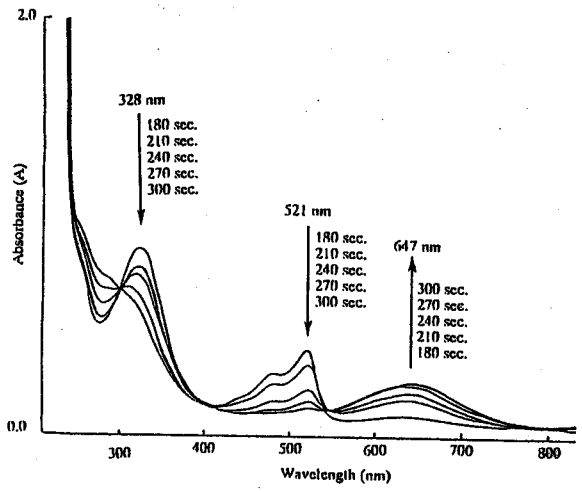

Figure 2-20. Stage II in the UV-vis spectral change upon reduction of $\mathbf{24}^{2+}\bullet 2(BF_4^-)$ in MTHF-acetonitrile (1:1 v/v) at room temperature.

2-4-4. ESR spectra obtained by reduction of bispyridinium salt $\mathbf{24}^{2+}\bullet 2(BF_4^-)$

Figure 2-21 shows a ESR spectrum of the blue species (647 nm) obtained by the reduction of $\mathbf{24}^{2+}$. The signal was very weak and no signal due to triplet species was observed. This suggests that the two-electrons reduction product **24** is not in a diradical structure but in a diamagnetic quinoid structure. The observed weak ESR spectrum would be due to the very amount of $\mathbf{24}^{+}$.

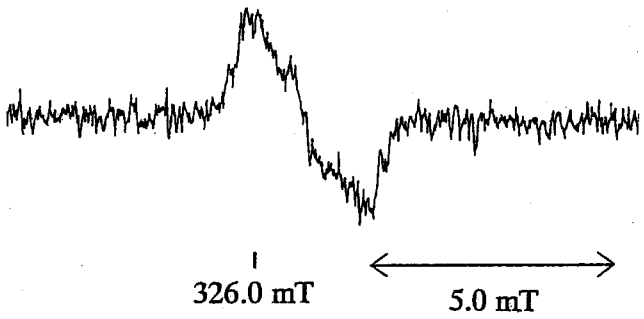

Figure 2-21. ESR spectrum of the species obtained by reduction of $\mathbf{24}^{2+}\bullet 2(BF_4^-)$.

2-5. Preparations and characterization of bis-pyridinyl radicals linked with methyl substituted benzene

In the section 2-3, the ESR spectrum of **1** was characterized by the relatively small *D* value (4.0 mT). The small *D* value corresponds to 8.9 Å as an averaged distance between the radical centers by the point dipole approximation. The estimated distance is obviously longer than the distance (ca. 5.0 Å) between the C-4 and the C'-4 carbons of the pyridinyl ring and is close to the distance (ca. 7.5 Å) between the centers of pyridinyl rings or the distance (ca. 10 Å) between the nitrogen atoms of the pyridinyl rings. This hypothesis is quite reasonable at present and can be rationalized by the spin distribution pattern of the pyridinyl radicals; large spin densities at the nitrogen and the two ortho- and one para-carbons. However, at the time when ESR of **1** was measured, an alternative explanation for the small *D* of **1** was considered; the spectrum in Figure 2-15 (a) may be originated by an intermolecularly associated dimer **XXIII** or **XXIV** which would show small *D* values (Figure 2-22).

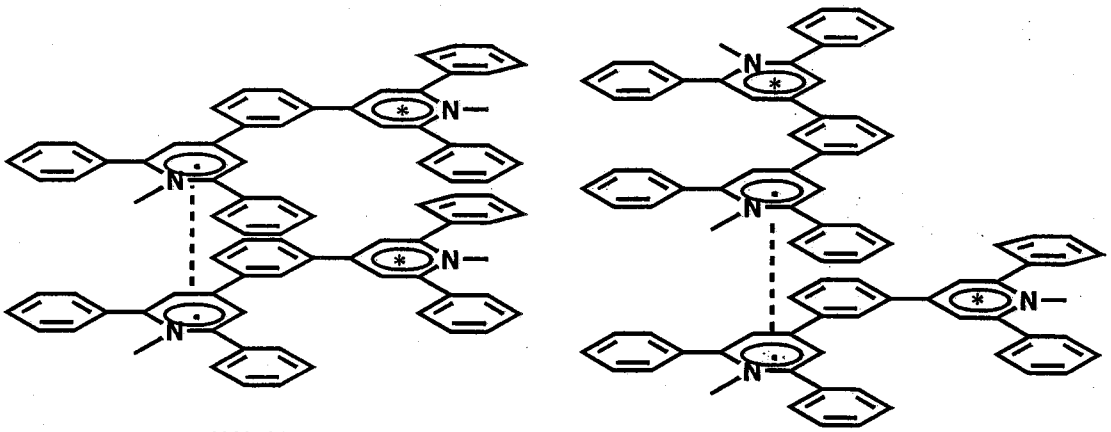

XXIII **XXIV**

Figure 2-22. Alternative structures for the triplet spectrum in Figure 2-15 (a).

In Figure 2-22, a dot (•) shows an unpaired electron and a star (*) shows a charge (+ or -) or an unpaired electron. There may be a weak bond between two stars or between inter-dimer's stars. When the star is an unpaired electron, the assumption of the selective formation of such dimers without detection of the intramolecular diradical **1** may be unreasonable. When the star is a cationic charge (a dimer of cation radical), the formation of such a dimer may be likely. If there is a weak bond between

the stars, or inter-dimer's stars, such possibility may not be excluded. The value of zero-field splitting parameters and the detection of $\Delta Ms = \pm 2$ signals gives no answer. Only the electronic spectrum, which showed the absence of cationic absorption and the presence of two pyridinyl radicals moieties per molecule, is against to these possibilities. However, taking into consideration that 1) the electronic spectrum was measured at room temperature, 2) the ESR measurement was carried out at 77 K, and 3) the bond formation may be likely at lower temperature, these possibilities cannot be excluded.

The formation of the above intermolecular dimers is based on the instability of the intramolecular diradical. These instabilities may also relate to the dihedral angle (ca. 20-25° by analogy of biphenyl) between the pyridinyl ring and the central benzene ring. When methyl group(s) are introduced in 2, 4, and 6-positions of the central benzene ring, the dihedral angle will increase up to ca. 90°. Such geometrical change would kinetically stabilizes intramolecular diradical and would destabilize the dimer structure by steric hindrance. In this section, the bis-pyridinyl radicals **3** and **4**, which have methyl group(s) for increase of steric interaction, were prepared and their ESR spectra were studied. If these diradicals have similar *D* values with that (4.0 mT) of **1**, then the previous assignment for **1** should be correct.

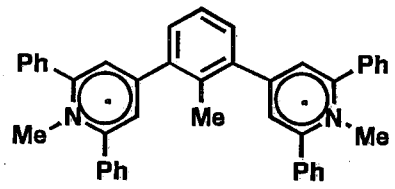

3

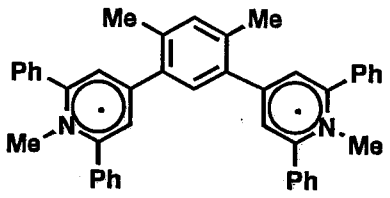

4

2-5-1. Syntheses of 2-methyl-1,3-bis(1-methyl-2,6-diphenylpyridinium-4-yl)benzene bis(tetrafluoroborate) [3^{2+}•2(BF_4^-)] and 2,4-dimethyl-1,5-bis(1-methyl-2,6-diphenylpyridinium-4-yl)benzene bis(tetrafluoroborate) [4^{2+}•2(BF_4^-)]

2-5-1-1. Synthesis of bispyridinium salt [3^{2+}•2(BF_4^-)]

The synthesis of the bispyridinium ion 3^{2+} is shown in Scheme 2-6. The synthetic strategy is essentially the same with those in the previous sections. The procedure and yields are summarized as

follows: 2-methyl-1,3-dicarboxyaldehyde, obtained from 2,6-dichlorotoluene by two steps[54], was treated with 2.4 equivalents of benzoylmethyltriphenylphosphonium bromide and 2.4 equivalents of potassium *tert*-butoxide in DMSO at 80 °C for three hours to give diketone **28** in 73% yield. When **28** was treated with excess amounts of acetophenone in the presence of potassium *tert*-butoxide in THF-*tert*-butanol (3:2 v/v), tetraketone **29** was obtained in 97% yield. Treatment of **29** with excess amounts of boron trifluoride etherate and 2.0 equivalents of chalcone gave the bispyrylium ion $\mathbf{30}^{2+}$ in 68% yield which was converted into the bispyridinium ion $\mathbf{3}^{2+}$ on treatment with 3.0 equivalents of methylamine in acetonitrile at room temperature overnight.

Scheme 2-6

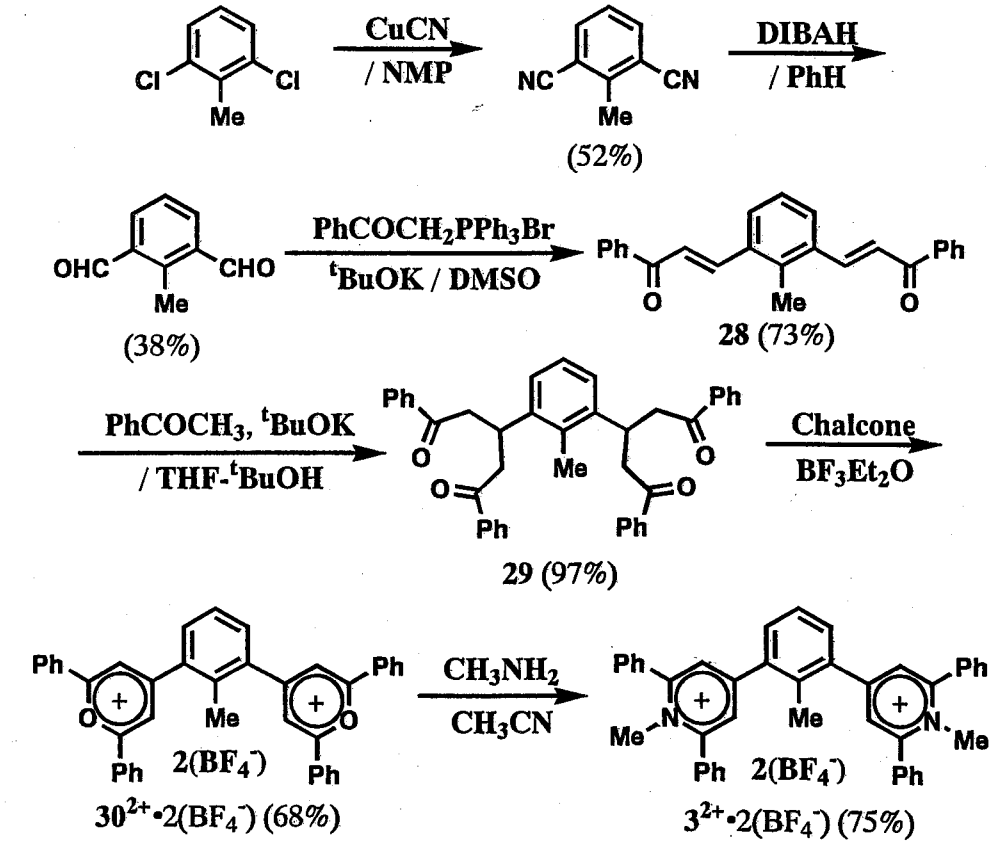

2-5-1-2. Synthesis of bispyridinium salt [$\mathbf{4}^{2+}$•2(BF_4^-)]

The bispyridinium ion $\mathbf{4}^{2+}$ was synthesized in the same way for $\mathbf{3}^{2+}$ (Scheme 2-7). 2,4-Methyl-1,5-dicarboxyaldehyde, obtained from *m*-xylene by dibromination and diformylation, was heated with 2.4 equivalents of benzoylmethyltriphenylphosphonium bromide and 2.4 equivalents of potassium *tert*-

butoxide in DMSO at 80 °C for three hours to give diketone **31** in 55% yield. The yield was somewhat poorer than other Wittig reactions described in this thesis probably because of the steric effect. Then, **31** was treated with excess amounts of acetophenone in the presence of potassium *tert*-butoxide in THF-*tert*-butanol (3:2 v/v), and the tetraketone **32** was obtained in 99% yield. The yields of Michael addition of the diketone **28** and **31** were much higher than other Michael additions and this might be also explained by the favorable effect of methyl groups on the central benzene rings by preventing diketones from side reaction. Treatment of **32** with excess amounts of boron trifluoride etherate and 2.0 equivalents of chalcone gave the bispyrylium ion $\mathbf{33}^{2+}$ in 60% yield which was converted into the bispyridinium ion $\mathbf{4}^{2+}$ by treatment with 3.0 equivalents of methylamine in acetonitrile at room temperature overnight.

Scheme 2-7

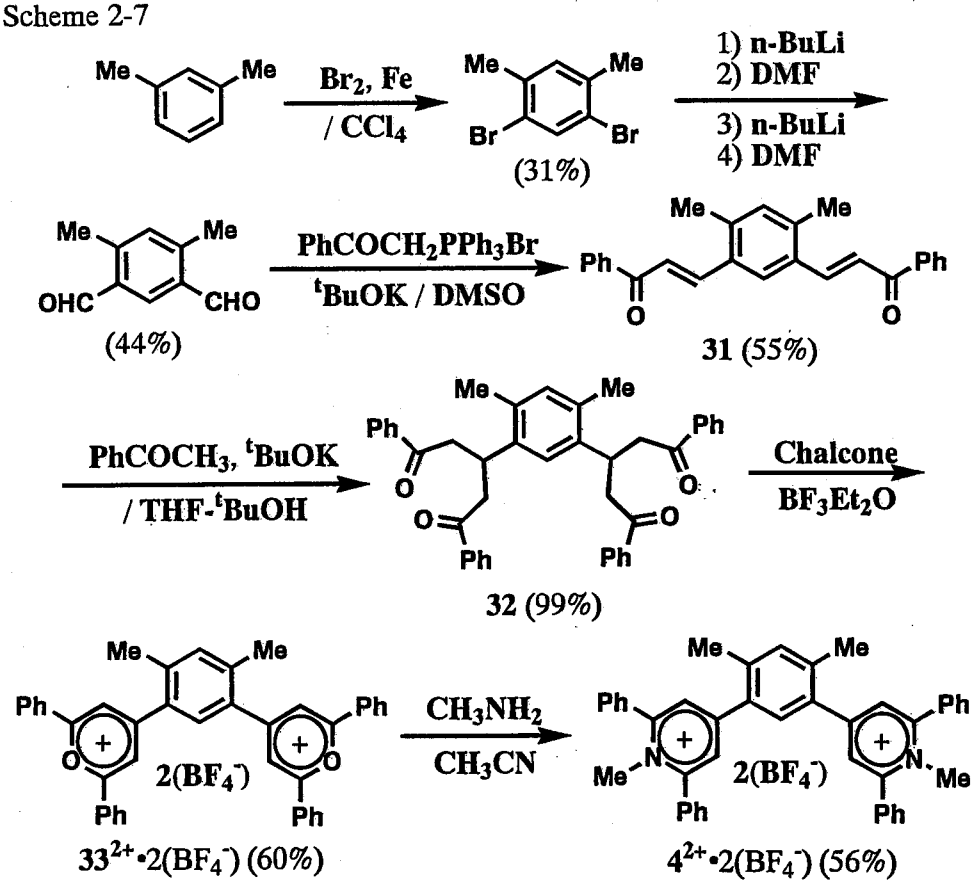

2-5-2. ^1H and ^{13}C chemical shifts of bispyridinium salts $3^{2+}\cdot 2(BF_4^-)$ and $4^{2+}\cdot 2(BF_4^-)$

The ^1H and ^{13}C chemical shifts of the bispyridinium ions $\mathbf{3}^{2+}$ and $\mathbf{4}^{2+}$ in CD_3CN are summarized in Figure 2-23. The bold letters show ^{13}C chemical shifts and plain letters show ^1H chemical shifts. These chemical shifts were determined from C-H cosy and long range C-H cosy spectra. When these values are compared with those of $\mathbf{1}^{2+}$ (Figure 2-7), small but some important differences may be noticed; 1) the C-4 carbon (pyridinium ring) of $\mathbf{3}^{2+}$ and $\mathbf{4}^{2+}$ appears in lower field than that of $\mathbf{1}^{2+}$, and 2) the 2(6) or 4-proton of the central benzene ring appear in higher field than those of $\mathbf{1}^{2+}$. These results are explicable by higher positive charge due to poorer conjugation with the central benzene ring, and anisotropic effect of the pyridinium ring at the perpendicular geometry, respectively.

Other minor features on the chemical shifts can be summarized as follows; the carbons of the central benzene on which methyl group was attached are also observed at lower field, and on the other hand, ^1H and ^{13}C chemical shifts of the phenyl groups at 2 and 6-positions of pyridinium ring is the range of 7.75-7.59 ppm and 130.1-133.8 ppm, respectively, which are almost the same with those in $\mathbf{1}^{2+}$ and $\mathbf{2}^{3+}$. The chemical shifts of the methyl groups on pyridinium ring are also almost the same values with those of $\mathbf{1}^{2+}$.

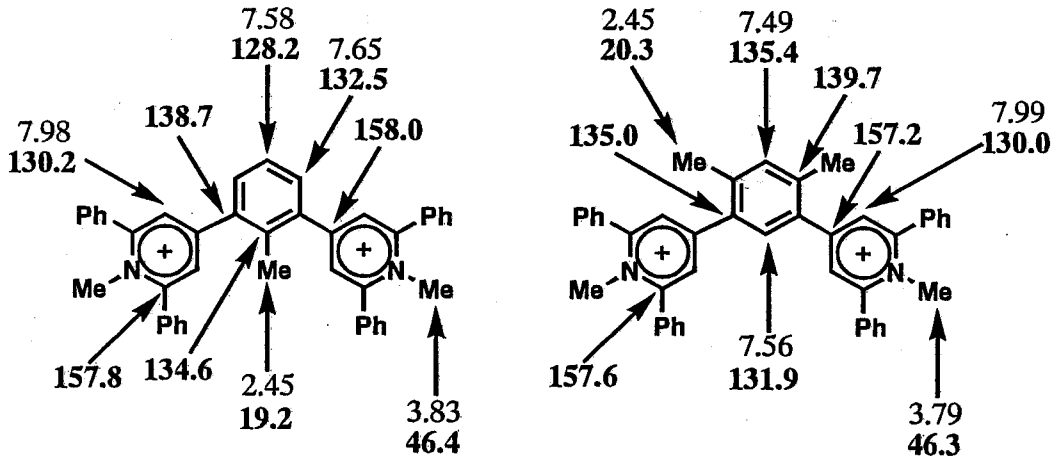

Figure 2-23. ^1H and ^{13}C chemical shifts of $\mathbf{3}^{2+}$ and $\mathbf{4}^{2+}$ (in CD_3CN).

2-5-3. Reduction potentials and absorption maximum in electronic spectra of bispyridinium salts 3^{2+}•2(BF_4^-) and 4^{2+}•2(BF_4^-)

Table 2-2. Reduction potentials [a, b] and absorption maximum of the pyridinium salts 3^{2+}•2(BF_4^-), 4^{2+}•2(BF_4^-), and 1^{2+}•2(BF_4^-).[b]

	E_1 / V	E_2 / V	E_3 / V	E_4 / V	λ_{max} / nm (ε x 10^{-4})
3^{2+}•2(BF_4^-)	-1.20	-1.29	-1.70	-1.79	300 (4.27)
4^{2+}•2(BF_4^-)	-1.23	-1.30	-1.70	-1.77	303 (4.07)
1^{2+}•2(BF_4^-)	-1.10	-1.23	-1.66	-1.77	298 (5.94)

a) supporting electrolyte, 0.1 M tetrabutylammonium tetrafluoroborate; indicating electrode, glassy carbon; reference electrode, S. C. E.; scan rate, 100 mV / sec
b) in acetonitrile

Table 2-2 summarizes the reduction potentials and absorption maximum in electronic spectra of the bispyridinium ions 3^{2+} and 4^{2+} together with that of 1^{2+}. All reduction waves were reversible, which suggests that these bis-pyridinyl radicals **3** and **4** are stable. The reduction potentials of 3^{2+} and 4^{2+} are similar. Compared with 1^{2+}, the following differences are noticed; 1) the first reduction potentials (E_1) of 3^{2+} and 4^{2+} appear in more negative region than that of 1^{2+}, 2) the differences between the reduction potentials ($\Delta E_a = E_1-E_2$, $\Delta E_b = E_3-E_4$) of 3^{2+} and 4^{2+} are smaller than those of 1^{2+}. These results suggest weaker interactions between the pyridinium rings for 3^{2+} and 4^{2+} than that for 1^{2+}. The smaller interaction in 3^{2+} and 4^{2+} are explicable by their near perpendicular geometry.

The absorption maxima of the dications 3^{2+}, 4^{2+}, and 1^{2+} appear at ca. 300 ± 3 nm, although a little longer absorption maximum was observed for 3^{2+} and 4^{2+}. Interestingly, the molar absorptivity of 3^{2+} and 4^{2+} was much smaller than that of 1^{2+}. In general, hypochromic effect is observed when conjugated polyenes cannot be planar.[55] This hypochromic effect most strongly speak the steric effect of the methyl groups on the central benzene ring.

2-5-4. Electronic spectra obtained by reduction of bispyridinium salts $3^{2+}\cdot 2(BF_4^-)$ and $4^{2+}\cdot 2(BF_4^-)$

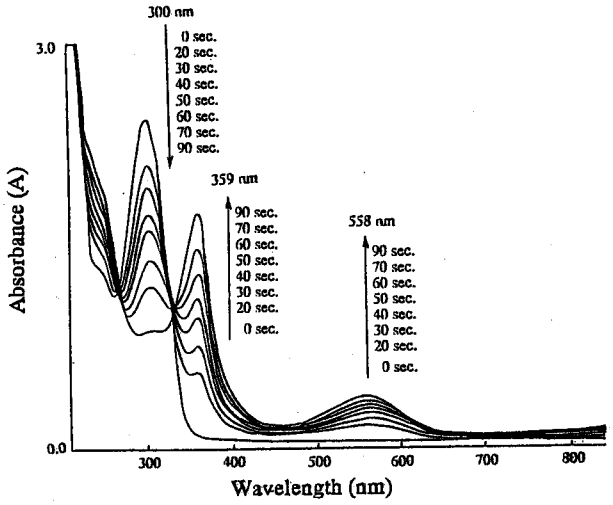

Figure 2-24. UV-vis spectral change upon reduction of $3^{2+}\cdot 2(BF_4^-)$ to form diradical **3**.

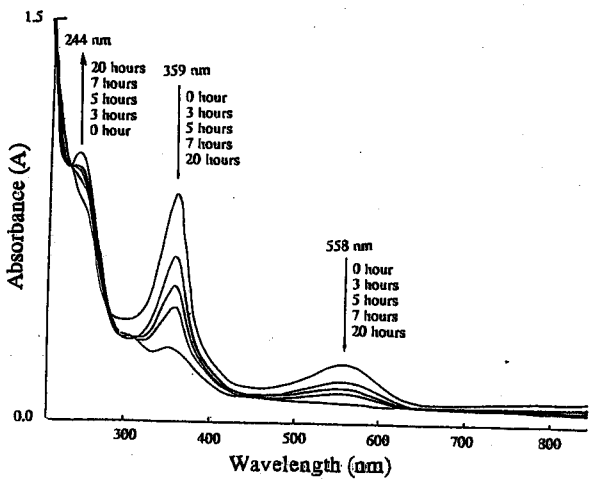

Figure 2-25. UV-vis spectral change when the solution of diradical **3** was stood at room temperature.

When 3^{2+} was treated with 3% Na-Hg in acetonitrile at room temperature under degassed conditions, the colorless solution turned purple and the absorptions at 359 nm and 558 nm increased while the intensity at 300 nm decreased (Figure 2-24). Two isosbestic points were observed at about 270 nm and 330 nm. Since an increase of 558 nm absorption reached maximal intensity (after 90 sec.); similar to the case of **1**, the purple species was assigned to be diradical **3**. The absorption maximum of **3** appears at 558 nm which is 30 nm shorter than the absorption maximum of **1**. This blue shift may be due to the large dihedral angle between the pyridinium rings and the central benzene ring. When this diradical solution was aerated, the absorption at 300 nm was recovered by 56% of the original intensity. When the purple solution was stood in inert atmosphere at room temperature, the intensity of the absorptions due to diradical gradually decreased (Figure 2-25) as observed in the case of **1** (Figure 2-9). The intensity of the absorptions of **3** also decreased by further reduction with 3% Na-Hg.

Similar UV-vis spectral change in electronic spectra was observed in the reduction of 4^{2+} (Figure 2-26). As the reduction proceeded, the colorless solution of 4^{2+} turned reddish purple and the absorptions at 360 nm and 560 nm increased. Two isosbestic points were observed at about 270 nm and 330 nm. After contact time of 120 sec., the increase of the 560 nm absorption saturated, and the

spectrum was assigned to belong to **4**. When the diradical solution was aerated, the absorption at 303 nm was recovered by 57% of the original intensity. The diradical color slowly faded (Figure 2-27). The intensity of the absorptions of **4** also decreased by further reduction with 3% Na-Hg.

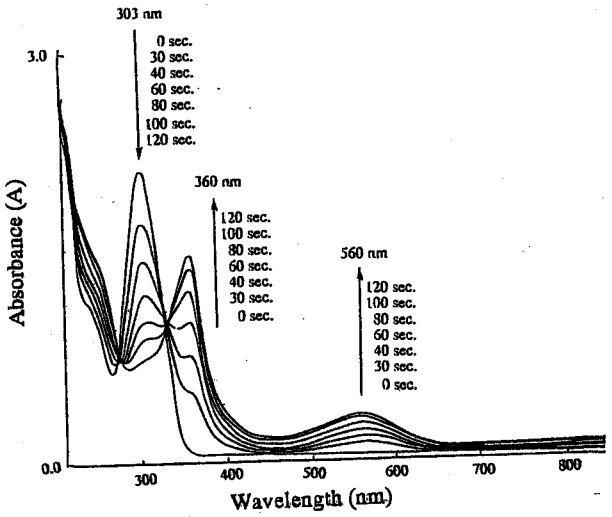

Figure 2-26. UV-vis spectral change upon reduction of $4^{2+}\cdot 2(BF_4^-)$ to form diradical **4**.

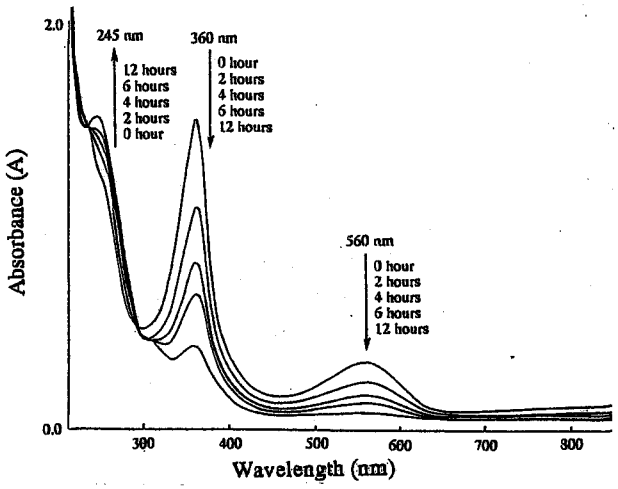

Figure 2-27. UV-vis spectral change when the solution of diradical **4** was stood at room temperature.

2-5-5. ESR spectra of diradicals 3 and 4

In the preceding section, the diradicals **3** and **4** were generated by the reduction of $\mathbf{3}^{2+}$ and $\mathbf{4}^{2+}$. In this section, their ESR spectra were studied. If the triplet species observed in Figure 2-15 (a) are the intermolecularly interacted pyridinyl radical dimers, the ESR spectra of the diradicals **3** and **4** would be quite different from that of **1** and the *D* values of **3** and **4** would be quite larger than **1**. On the other hand, if the ESR spectra of **3** and **4** are similar to that shown in Figure 2-15 (a), the triplet species shown in Figure 2-15 (a) would be the intramolecular triplet diradical having the structure of **1**.

Figure 2-28 shows the ESR spectrum of **3** in MTHF-acetonitrile (1:1 v/v) measured at -150 °C. Four signals are observed beside the central signal due to a monoradical. This spectrum has a typical pattern of triplet species. The *D* value is determined as 4.4 mT and the distance between the radical centers is estimated as ca. 8.6 Å by the point dipole approximation. A quite similar spectrum was obtained for the diradical **4** (*D* = 4.6 mT, R = ca. 8.5 Å, Figure 2-29). These *D* values are close to that

of diradical **1**. These results establish that the triplet species shown in Figure 2-15 (a) is assignable to the intramolecular triplet bis-pyridinyl radical **1**.

These small *D* values indicate that the center of the pyridinyl radical is approximately located at the closer center to the nitrogen atom in the pyridinyl ring. This is compatible with the spin distribution pattern in the pyridinyl ring.

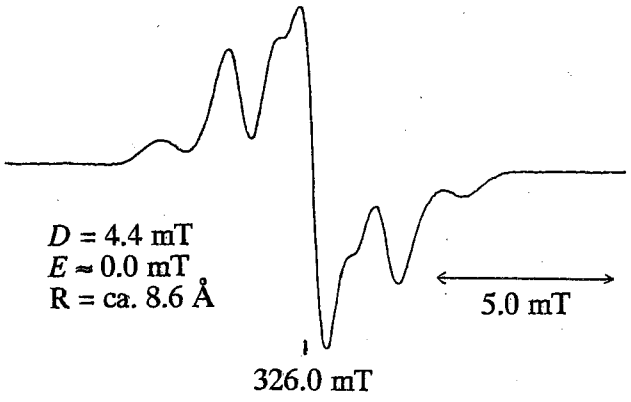

Figure 2-28. ESR spectrum of diradical **3** at -150 °C in MTHF-acetonitrile.

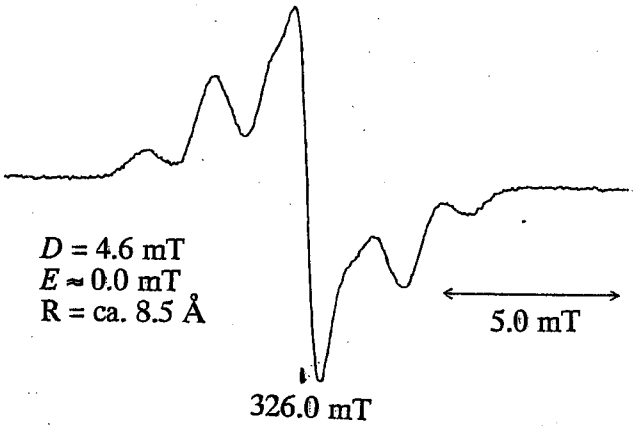

Figure 2-29. ESR spectrum of diradical **4** at -150 °C in MTHF-acetonitrile.

2-5-6. Summary

1) The methyl substituted dications $\mathbf{3}^{2+}$ and $\mathbf{4}^{2+}$ were synthesized in relation to the assignment of the triplet species **1** (Figure 2-15). It was expected that these diradicals **3** and **4** have large dihedral angles between the central benzene ring and the pyridinyl rings and therefore these diradicals would not intermolecularly associate. The large dihedral angles expected for these dications and diradicals were experimentally supported by their electronic spectra, ^{1}H and ^{13}C NMR spectra, and CV.

2) The ESR spectra of diradicals **3** and **4** showed a typical randomly oriented triplet pattern in both cases. The *D* value of diradicals **3** and **4** are similar to that of diradical **1**. Therefore, the triplet species shown in Figure 2-15 (a) are concluded to be intramolecularly interacted bis-pyridinyl radical represented by the structure **1**.

2-6. Preparation and characterization of 1,8-bis(1-methyl-2,6-diphenylpyridinyl-4-yl) anthracene

In the previous sections, the bis-pyridinyl radicals **1**, **3**, and **4** were shown to have relatively small *D* values (4.0 ~ 4.6 mT). The origin of the small *D* value is considered to be relative large spin densities of the nitrogen and the ortho carbons in the pyridinyl rings, so that the small *D* value is a characteristic feature of the bis-pyridinyl radicals linked by *m*-phenylene at the C-4 and C-4' positions.

If different type of linkers were used, this situation will be altered. Anthracene-1,8-diyl seems to be an interesting linker, because the σ-bonds at 1,8-positions of anthracene is arranged in parallel. Introduction of the pyridinyl ring would place the two pyridinyl rings in face to face relation. In such a geometry, the distance between the averaged positions of the unpaired electrons in the pyridinyl rings may be approximated by the distance between the two pyridinyl planes and would be rather insensitive to the positions of the unpaired electrons in the pyridinyl rings. The distance between the two planes is estimated to be ca. 5 Å according to the study of 1,8-diphenylanthracene reported by House et al.[56]

Although anthracene-1,8-diyl can be thought as a ferromagnetic linker by the dynamic spin polarization model, the radical moiety introduced at 1,8-positions may be oriented in face to face relation which may suggest an antiferromagnetic interaction in through-space manner. Experimental approach to high-spin compounds using anthracene-1,8-diyl linker has not been reported. Only notable examples which incorporate anthracenediyl have rather special structures of **34** (quintet ground state) and **35** (singlet ground state) reported by Berson et al.[57]

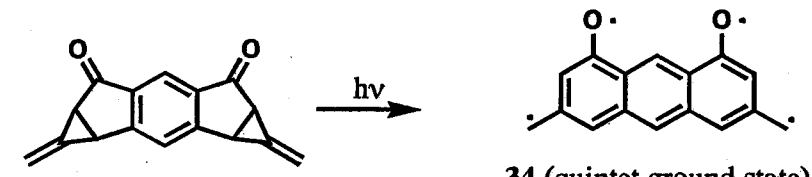

34 (quintet ground state)

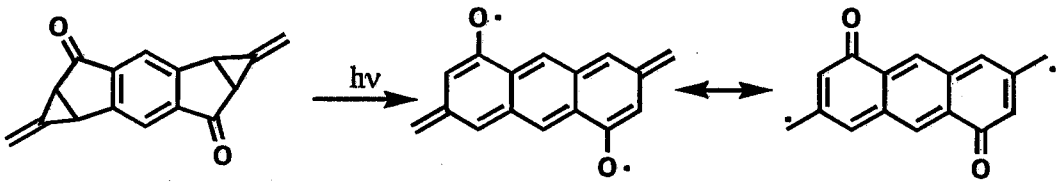

35 (singlet ground state)

This section describes the preparation and the determination of the ground state of **5**.

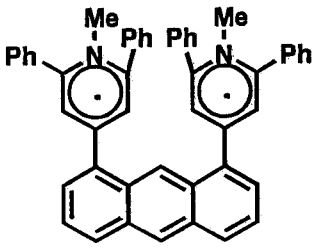

5

2-6-1. Synthesis of 1,8-bis(1-methyl-2,6-diphenylpyridinium-4-yl)anthracene bis(tetrafluoroborate) [5^{2+}•2(BF_4^-)]

Scheme 2-8

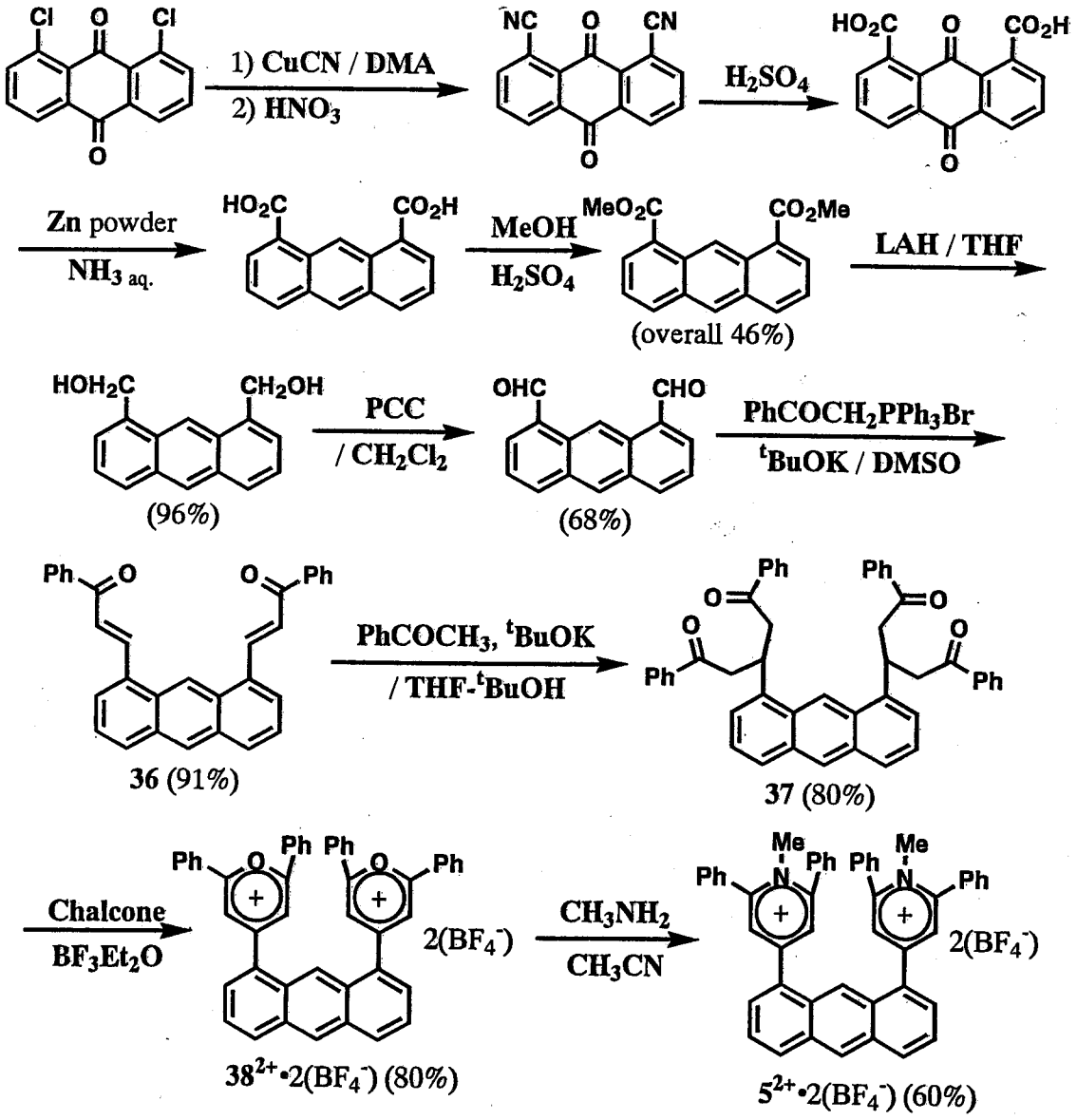

Scheme 2-8 illustrates the synthesis of the bispyridinium ion 5^{2+}. Synthesis of 1,8-bis(methoxycarbonyl)anthracene was carried out essentially according to the literature.[58] At first, 1,8-dichloroanthraquinone was heated to reflux with 2.8 equivalents of copper (I) cyanide in N,N-dimethylacetamide (DMA) for three hours. The obtained copper complex of 1,8-dicyanoanthraquinone was treated with 3 N nitric acid for four hours at 60 °C to give copper free 1,8-dicyanoanthraquinone, which was hydrolyzed by treatment with 70% aqueous solution of sulfuric acid under reflux for one hour to give 1,8-anthraquinonedicarboxylic acid as brown precipitates. The dicarboxylic acid was then heated to reflux with zinc powder in 20% aqueous solution of ammonia for four hours to afford 1,8-anthracenedicarboxylic acid, which was converted to 1,8-bis(methoxycarbonyl)anthracene by heating to reflux in methanol in the presence of concentrated sulfuric acid for 16 hours. The overall yield from 1,8-dichloroanthraquinone was 46%. 1,8-Bis(methoxycarbonyl)anthracene was reduced with 2.0 equivalents of lithium aluminum hydride (LAH) at 0 °C. The obtained aluminum complex of 1,8-bis(hydroxymethyl)anthracene was treated with 6 N hydrochloric acid to give aluminum free 1,8-bis(hydroxymethyl)anthracene as pale yellow precipitates. Oxidation of 1,8-bis(hydroxymethyl) anthracene with PCC in methylene chloride gave 1,8-diformylanthracene in 68% yield. The desired bispyridinium ion 5^{2+} was synthesized from 1,8-diformylanthracene through the similar procedures for the previous pyridinium ions.

2-6-2. Reduction potentials and absorption maxima in electronic spectrum of bispyridinium salt [5^{2+}•2(BF_4^-)]

The reduction potentials and absorption maxima in the electronic spectrum of 5^{2+} are summarized in Table 2-3. The observed two reduction waves at -1.09 V and -1.59 V *vs.* SCE are both reversible. They are assignable to two two-electron reduction processes of dication ↔ diradical and diradical ↔ dianion, in the light of the potential values of the previously assigned pyridinium salts (Table 2-1, 2-2). Two two-electron reduction processes for 5^{2+} suggest that the two pyridinium ions spaced by anthracene-1,8-diyl behave like two independent pyridinium ions, which is compatible with the perpendicular geometry between the pyridinium ring and the spacer plane.

Assuming the perpendicular geometry, the electronic spectrum of 5^{2+} may be explained by the overlap of anthracene moiety and pyridinium ion moieties. Then, the shoulder around 300 nm may be due to pyridinium absorption. However, the absorption of 411 nm has no vibrational structures and does not seem to be anthracene absorption although the molar absorptivity is similar to that of anthracene. This band may be a charge transfer band between anthracene moiety and pyridinium ring, although evidence for this assignment has not been pursued.

Table 2-3. Reduction potentials [a, b] and absorption maxima of $5^{2+}\cdot 2(BF_4^-)$.[b]

	E_1 / V	E_2 / V	λ_{max} / nm (log ε)
$5^{2+}\cdot 2(BF_4^-)$	-1.09	-1.59	249 (4.79) ca. 300 (sh) 411 (3.91)

a) supporting electrolyte, 0.1 M tetrabutylammonium tetrafluoroborate; indicating electrode, glassy carbon; reference electrode, S. C. E.; scan rate, 100 mV / sec
b) in acetonitrile

2-6-3. Electronic spectrum obtained by reduction of bispyridinium salt [$5^{2+}\cdot 2(BF_4^-)$]

In contrast to the reduction of the previous bispyridinium ions 1^{2+}, 3^{2+}, and 4^{2+}, diradical **5** was unstable at room temperature under degassed conditions. At room temperature, the generated red color by the reduction with Na-Hg was immediately decolorized. Fortunately, however, when 5^{2+} was reduced with Na-Hg at -30 ~ -40 °C under the similar conditions, the absorptions at 362 nm and 539 nm increased. The increase of these absorptions saturated after ca. 360 sec. (contact time with Na-Hg). The

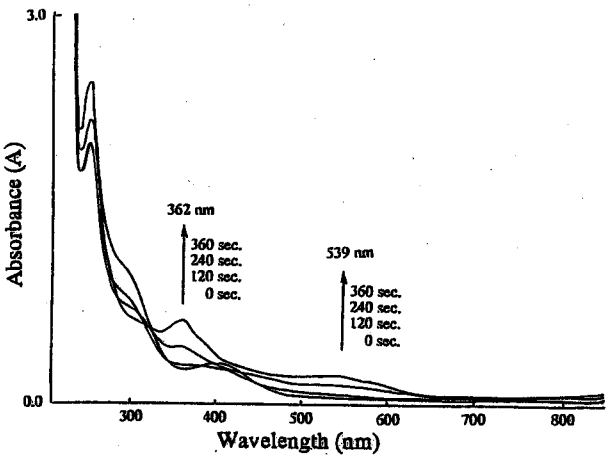

Figure 2-30. UV-vis spectral change upon reduction of $5^{2+}\cdot 2(BF_4^-)$ with 3% Na-Hg in MTHF-acetonitrile at the range of -30 °C to -40 °C.

absorption of 539 nm was then assigned to be diradical **5**. As considered in the previous section (2-5-4), the absorptions of the bis-pyridinyl radicals seem to be considerably dependent on the dihedral angle between the pyridinyl ring and the spacer; **1** has an absorption maximum at 588 nm, **3** at 558 nm, and **4** at 560 nm. This consideration rationalizes the assignment for **5**, although the overall spectral change in Figure 2-30 is not clean.

2-6-4. ESR spectrum of diradical 5

The ESR spectrum of the red species (539 nm) showed a typical randomly oriented triplet species (Figure 2-31). The zero-field splitting parameters were determined to be D = 8.0 mT and $E \simeq 0$ mT. The D value is almost twice as large as that of **1**, **3**, or **4**, and corresponds to 7.1 Å as an averaged distance between the radical centers. This distance is somewhat larger than the expected distance (5 Å) for 1,8-diphenylanthracene. According to a molecular model, the two pyridinyl rings in face to face relation at 1,8-positions receive considerable steric repulsion which enlarges the distance between the edges (the nitrogen positions) of the pyridinyl rings. The observed D value may be rationalized partly by this geometrical change and partly by the poor approximation of the point dipole method.

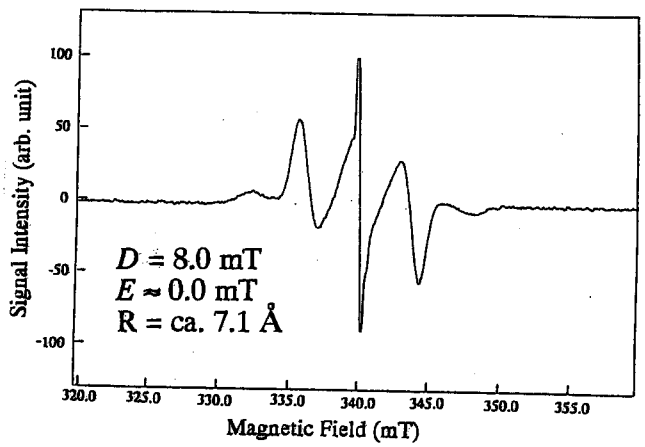

Figure 2-31. ESR spectrum of diradical **5** in MTHF-acetonitrile at 20 K.

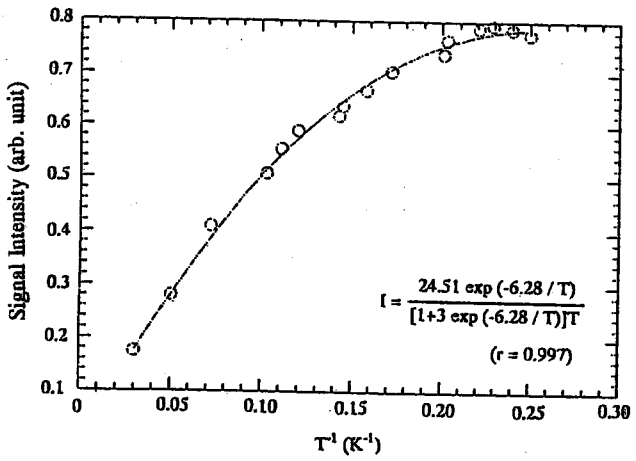

Figure 2-32. Temperature dependence of the signal intensity of ΔMs = ± 2 transition of diradical **5**.

In addition to these ΔMs = ± 1 transition signals, a weak signal due to ΔMs = ± 2 transition was observed in the half magnetic field region. Temperature dependence of the signal intensity of ΔMs = ± 2 transition was investigated (Figure 2-32). The signal intensity increased linearly with reciprocal of

temperature at the range of 50 K to 10 K, but slowly curved at the lower temperature. This thermal behavior shows that the diradical **5** has a singlet ground state. The energy difference between the singlet and triplet states was estimated to be 13 cal/mol using an equation (S-T model) shown in the figure.

The low-spin nature is probably due to the antiferromagnetic through-space interaction between the two pyridinyl groups in face to face relation. In order to obtain an insight for the through-space interaction, semiempirical calculation (AM1-CI) for the model compounds (0, 0)-**XXIII** and (90, 90)-**XXIII** was carried out.[59] The model compound (0, 0)-**XXIII** has a planar geometry, whereas (90, 90)-**XXIII** has a perpendicular geometry between the methylene at 1(8)-position and the anthracene ring. In both compounds, the bond distance of C(methylene carbon)-C(anthracene carbon) is fixed (1.41 Å). The ground state of (0. 0)-**XXIII** was calculated to be triplet with singlet-triplet energy gap ($\Delta E_{S\text{-}T}$) of +4.8 kcal/mol. On the other hand, the singlet and triplet energies at (90, 90)-**XXIII** geometry was identical ($\Delta E_{S\text{-}T}$ = 0 kcal/mol). Since the present calculation is not high level, the absolute prediction on the ground state may be difficult. However, it is clear that the large stabilization of triplet state is obtained in planar geometry and almost no stabilization of triplet in perpendicular geometry. Thus, this calculation is compatible with the experimental value of $\Delta E_{S\text{-}T}$ (13 cal/mol for **5**) which is very small for the kcal scale argument.

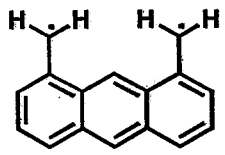

(0, 0)-**XXIII**

triplet ground state

$\Delta E_{S\text{-}T}$ = 4.8 kcal/mol

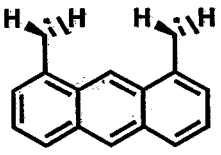

(90, 90)-**XXIII**

singlet and triplet state are nearly degenerate

2-6-5. Summary

1) The bispyridinium ion $\mathbf{5}^{2+}$ was synthesized and characterized (NMR, UV, and CV).

2) The preparation of the diradical **5** was achieved by the reduction at low temperature (-30 ~ -40 °C). The diradical **5** has an absorption at 539 nm, which is compatible with perpendicular geometry of **5**.

3) The triplet state of the diradical **5** was characterized by ESR (D = 8.0 mT, $E \approx 0$ mT). The D value suggests that the two pyridinyl groups at 1,8-position are repulsively interact to enlarge the distance between their edges of the pyridinyl rings.

4) The ground state of diradical **5** was determined as having a singlet ground state. The energy gap between the ground singlet state and the thermally excited triplet state was calculated to be 13 cal/mol. The singlet nature of **5** was rationalized by the antiferromagnetic through space interaction between the pyridinyl rings which would orient in face to face relation. These results are qualitatively compatible with the theoretical study of the model compounds (0, 0)-**XXIII** and (90, 90)-**XXIII** by AM1-CI, which shows that the large stabilization of the triplet state in the planer geometry disappears in the perpendicular geometry.

2-7. Experimental section

General Remarks:

In this study, the following physical properties were measured by the instruments shown below. (This applies to the following Chapters in the same way.)

Melting point; Yanaco NP500D, uncorrected

Mass spectra; JEOL JMS-SX102 and JEOL D-300

NMR spectra; JEOL EX-270, JEOL GSX-400, JEOL LA-300, and JEOL GX-400 (All chemical shifts were referenced to tetramethylsilane ($\delta_{TMS} = 0.00$) as an internal standard.)

Cyclic voltammetric spectra; Yanaco P1100 spectrometer (Cyclic voltammograms of the pyridinium salts were recorded with glassy carbon working electrode and Pt counter electrode in acetonitrile or dimethylformamide (DMF) containing 0.1 M n-Bu_4NClO_4 as the supporting electrolyte. The experiments employed a SCE reference electrode. Electrochemical experiments were performed under a nitrogen atmosphere at 20 °C.)

Electronic spectra; Hitachi U-3400 and Hitachi U-3210

IR spectra; Perkin Elmer 1650

Elemental analyses; I requested the analysis for elemental analysis laboratory, Faculty of Science, Osaka University and Osaka City University.

ESR spectra; JEOL FE-2XG and Bruker ESP-300

Column chromatography was carried out by use of Merck Art. 7734 Kieselgel 60, 70-230 mesh ASTM, or neutral alumina Merck Art. 1097 Aluminiumoxid 90, activity II-III, 70-230 mesh ASTM. Analytical TLC was performed by using plate (0.25 mm) prepared from Merck Art. GF-254.

Materials and Solvents:

Chalcone,[51a] 1-methyl-2,4,6-triphenylpyridinium tetrafluoroborate,[49d] benzoylmethyltriphenyl-phosphonium bromide,[60] 3% Na-Hg,[61] and pyridinium chlorochromate (PCC)[62] were prepared as described in the literature. Acetophenone and boron trifluoride etherate were distilled under reduced

pressure. Isophthalaldehyde, potassium *tert*-butoxide, methylamine (24.3% ethanol solution), iron powder, bromine, and LAH were commercially available and used without further purification. n-Butyllithium in hexane (1.6 M, Mitsuwa Pure Chemicals, Inc.) was purchased and used as it is. Dimethylsulfoxide (DMSO) was dried and distilled from calcium hydride under reduced pressure. Tetrahydrofuran and ether were distilled from potassium hydroxide and then from sodium benzophenone ketyl. *tert*-Butanol was distilled from magnesium-iodine. Acetonitrile was distilled from calcium hydride. MTHF was distilled from potassium hydroxide and then from Na-K alloy. DMF was distilled under reduced pressure from calcium hydride. Carbon tetrachloride was distilled before use. All other solvents were distilled before use.

m- Bis(2-benzoylethenyl)benzene (**18**)

A solution of of isophthalaldehyde (1.0 g, 7.5 mmol) in DMSO (10 ml) was added to a solution of benzoylmethyltriphenylphosphonium bromide (8.6 g, 19 mmol) and potassium *tert*-butoxide (2.1 g, 19 mmol) in DMSO (50 ml) under nitrogen. The reaction mixture was stirred and heated at 80 °C for four hours. After cooling, water (100 ml) and 6 N hydrochloric acid (30 ml) were added, the reaction mixture was extracted with benzene-ethyl acetate (1:1 v/v). The extracts were combined, washed with water and brine, and dried over anhydrous sodium sulfate. After concentration, the residue was purified by column chromatography on silica gel using benzene-ethyl acetate (10:1 v/v). **18** (1.9 g, 75%) was obtained.

18: pale yellow needles (from C_2H_5OH); mp 145-146 °C; EI MS *m/z* 338 (M^+), 233 (M^+-C_6H_5CO); ^{1}H-NMR (270 MHz, $CDCl_3$) δ 8.03 (dt, 4H, *J* = 7.3 Hz, 1.6 Hz), 7.87 (s, 1H), 7.81 (d, 2H, *J* = 15.8 Hz), 7.67 (dd, 2H, *J* = 7.3 Hz, 1.6 Hz), 7.62-7.44 (m, 9H); ^{13}C-NMR (67.8 MHz, $CDCl_3$) δ 189.8, 143.6, 138.0, 35.7, 132.8, 129.9, 129.5, 128.6, 128.5, 128.1, 123.0; IR (KBr) 3060 (w), 1661 (s), 1605 (s), 1446 (m), 1318 (s), 1278 (s), 1210 (s), 1170 (m), 1034 (m), 1019 (s), 972 (s), 852 (m), 804 (w), 767 (s), 704 (m), 684 (s), 658 (s), 578 (m) cm^{-1}; Anal. Calcd for $C_{24}H_{18}O_2$: C, 85.18 ; H, 5.36. Found: C, 84.97 ; H, 5.29.

m-Bis(1,3-dibenzoyl-2-propyl)benzene (**19**)

Potassium *tert*-butoxide (100 mg, 0.9 mmol) was added to a solution of **18** (1.0 g, 3.0 mmol) and acetophenone (5 ml, 40 mmol) in THF (60 ml) and *tert*-butanol (40 ml). The reaction mixture was stirred at room temperature for three hours, then water (50 ml) and 6 N hydrochloric acid (30 ml) were added to the brown solution. The aqueous layer was extracted with benzene-ethyl acetate (1:1 v/v). The organic layers were combined, washed with water and brine, and dried over anhydrous magnesium sulfate. After concentration, the residue was purified by column chromatography on silica gel using benzene to remove acetophenone and then benzene-ethyl acetate (15:1 v/v). **19** (720 mg, 42%) was obtained as pale yellow needles.

19: pale yellow needles (from C_2H_5OH); mp 93-94 °C; FAB MS *m/z* 579 (M^++1), 459 (M^++1-$C_6H_5COCH_2$), 339 [M^++1-2($C_6H_5COCH_2$)]; ^{1}H-NMR (270 MHz, $CDCl_3$) δ 7.88 (d, 8H, *J* = 7.2 Hz), 7.50 (tt, 4H, *J* = 7.2 Hz, 1.7 Hz), 7.39 (t, 8H, *J* = 7.2 Hz), 7.34 (s, 1H), 7.20-7.10 (m, 3H), 7.08 (t, 1H, *J* = 2.0 Hz), 4.01 (quintet, 2H, *J* = 7.0 Hz), 3.42 (dd, 4H, *J* = 16.6 Hz, 7.0 Hz), 3.25 (dd, 4H, *J* = 16.6 Hz, 7.0 Hz); ^{13}C-NMR (67.8 MHz, $CDCl_3$) δ 198.4, 144.0, 137.0, 132.9, 128.8, 128.5, 128.1, 126.8, 125.7, 44.7, 37.2; IR (KBr) 3057 (m), 2895 (w), 1684 (s), 1596 (s), 1579 (m), 1489 (w), 1448 (s), 1406 (m), 1359 (m), 1270 (m), 1211 (s), 1180 (m), 1074 (w), 988 (m), 883 (w), 782 (w), 754 (s), 689 (s), 609 (w), 523 (w) cm^{-1}; Anal. Calcd for $C_{40}H_{34}O_4$: C, 83.02; H, 5.92. Found: C, 83.01; H, 5.89.

m-Bis(2,6-diphenylpyrylium-4-yl)benzene [$\mathbf{20}^{2+}$•2(BF_4^-)]

To a mixture of **19** (1.0 g, 1.8 mmol) and chalcone (0.77 g, 3.7 mmol) was added boron trifluoride etherate (2.8 ml) under nitrogen. The reaction mixture was heated at 110 °C for three hours with stirring. After cooling, ether (40 ml) was added to the reaction mixture and yellow precipitates appeared. Filtration and washing with dry ether gave of $\mathbf{20}^{2+}$•2(BF_4^-) (980 mg, 76%).

$\mathbf{20}^{2+}$•2(BF_4^-): yellow crystals; mp 210-211 °C (decomp.); FAB MS *m/z* 627 (M^+-BF_4), 540 [M^+-2(BF_4)]; ^{1}H-NMR (270 MHz, $CDCl_3$-CF_3CO_2D) δ 8.90 (t, 1H, *J* = 1.9 Hz), 8.74 (s, 4H), 8.43 (dd, 2H, *J* = 7.9 Hz, 1.9 Hz), 8.36 (d, 8H, *J* = 7.4 Hz), 8.06 (t, 1H, *J* = 7.9 Hz), 7.87 (t, 4H, *J* = 7.4 Hz), 7.77 (t, 8H, *J* = 7.4 Hz); ^{13}C-NMR (67.8 MHz, $CDCl_3$-CF_3CO_2D) δ 172.9, 166.5, 137.0, 136.0, 134.7, 132.6, 131.1, 130.1, 129.1, 128.8, 116.5; IR (KBr) 3057 (w), 1617 (s), 1506 (s),

1446 (m), 1278 (w), 1234 (m), 1192 (w), 1057 (bs), 996 (w), 780 (m), 684 (m), 604 (w), 521 (w) cm^{-1}; UV (CH_3CN) λ_{max} / nm (log ε) 409 (4.63), 356 (4.76), 277 (4.49)

m-Bis(1-methyl-2,6-diphenylpyridinium-4-yl)benzene [$\mathbf{1}^{2+}\cdot 2(BF_4^-)$]

A solution of $\mathbf{20}^{2+}\cdot 2(BF_4^-)$ (100 mg, 0.14 mmol) and methylamine (24.3% ethanol solution, 31 mg, 0.28 mmol) was stirred overnight in acetonitrile (2.5 ml) at room temperature. After concentration, the residue was dissolved with acetonitrile (0.5 ml). Pale yellow needles appeared by addition of ethanol (4 ml). Filtration and washing with ethanol gave $\mathbf{1}^{2+}\cdot 2(BF_4^-)$ (75 mg, 72%).

$\mathbf{1}^{2+}\cdot 2(BF_4^-)$: pale yellow needles (from CH_3CN-C_2H_5OH); mp 289-290 °C; FAB MS *m/z* 653 (M^+-BF4), 565 [M^+-2(BF4)]; ^{1}H-NMR (270 MHz, CD_3CN) δ 8.51 (t, 1H, *J* = 1.7 Hz), 8.34 (s, 4H), 8.26 (dd, 2H, *J* = 7.9 Hz, 1.7 Hz), 7.84 (t, 1H, *J* = 7.9 Hz), 7.75-7.66 (m, 20H), 3.78 (s, 6H); ^{13}C-NMR (67.8 MHz, CD_3CN) δ 158.2, 154.8, 136.2, 133.8, 132.6, 132.3, 132.0, 130.3, 130.1, 128.9, 127.1, 46.1; IR (KBr) 3059 (w), 1620 (s), 1566 (m), 1494 (w), 1442 (w), 1377 (w), 1256 (w), 1083 (bs), 882 (w), 779 (m), 704 (m), 591 (w), 522 (w) cm^{-1}; UV (CH_3CN) λ_{max} / nm (log ε) 298 (4.77); FAB HRMS *m/z* Calcd for $C_{42}H_{34}N_2BF_4$: 653.2751. Found: 653.2728.

1,3,5-Tris(2-benzoylethenyl)benzene (**21**)

A solution of 1,3,5-triformylbenzene (100 mg, 0.62 mmol) in DMSO (1 ml) was added to a solution of benzoylmethyltriphenylphosphonium bromide (910 mg, 2.0 mmol) and potassium *tert*-butoxide (220 mg, 2.0 mmol) in DMSO (5 ml) under nitrogen. The reaction mixture was stirred and heated at 80 °C for four hours. After cooling, water (50 ml) and 6 N hydrochloric acid (50 ml) were added, the reaction mixture was extracted with benzene-ethyl acetate (1:1 v/v). The extracts were combined, washed with water and brine, and dried over anhydrous magnesium sulfate. After concentration, the residue was purified by column chromatography on silica gel using benzene-ethyl acetate (10:1 v/v). Crystallization with benzene gave **21** (230 mg, 78%).

21: pale yellow needles (from C_6H_6); mp 194-195 °C; FAB MS *m/z* 469 (M^++1), 364 (M^++1-C_6H_5CO); ^{1}H-NMR (270 MHz, $CDCl_3$) δ 8.06 (dt, 6H, *J* = 6.5 Hz, 1.7 Hz), 7.91 (s, 3H), 7.86 (d, 3H, *J* = 15.5 Hz), 7.63 (d, 3H, *J* = 15.5 Hz), 7.65-7.51 (m, 9H); ^{13}C-NMR (67.8 MHz, $CDCl_3$) δ 190.0, 142.9, 137.9, 136.5, 133.1, 129.4, 128.8, 128.6, 123.9, IR (KBr) 3061 (w), 1662 (s), 1602

(s), 1447 (m), 1292 (s), 1214 (s), 1174 (m), 1038 (m), 1022 (s), 983 (m), 848 (m), 774 (m), 707 (m), 686 (m), 657 (m) cm^{-1}; Anal. Calcd for $C_{33}H_{24}O_3$: C, 84.59; H, 5.16. Found: C, 84.33; H, 5.13.

1,3,5-Tris(1,3-dibenzoyl-2-propyl)benzene (**22**)

Potassium *tert*-butoxide (53 mg, 0.47 mmol) was added to a solution of **21** (1.0 g, 2.1 mmol) and acetophenone (10 ml, 80 mmol) in THF (60 ml) and *tert*-butanol (40 ml). The reaction mixture was stirred at room temperature for two hours, then water (40 ml) was added to the brown solution, the aqueous layer was extracted with benzene-ethyl acetate (1:1 v/v). The organic layers were combined, washed with water and brine, and dried over anhydrous magnesium sulfate. After concentration, the residue was purified by column chromatography on silica gel using benzene-ethyl acetate (15:1 v/v). **22** (690 mg, 39%) was obtained as yellow oil. **22** was used the next reaction without further purification.

22: pale yellow oil; FAB MS *m/z* 830 (M^++1), 709 (M^++1-$C_6H_5COCH_2$); ^{1}H-NMR (300 MHz, $CDCl_3$) δ 7.84 (d, 12H, *J* = 7.3 Hz), 7.49 (t, 6H, *J* = 7.3 Hz), 7.38 (t, 12H, *J* = 7.3 Hz), 6.97 (s, 3H), 3.96 (quintet, 3H, *J* = 7.0 Hz), 3.34 (dd, 6H, *J* = 16.4 Hz, 7.0 Hz), 3.15 (dd, 6H, *J* = 16.4 Hz, 7.0 Hz); ^{13}C-NMR (67.8 MHz, $CDCl_3$) δ 198.6, 144.3, 137.1, 132.9, 128.5, 128.3, 125.1, 44.5, 37.3; IR (KBr) 3058 (w), 1683 (s), 1596 (s), 1579 (m), 1448 (s), 1360 (m), 1278 (s), 1212 (s), 988 (m), 754 (s), 690 (s) cm^{-1}

1,3,5-Tris(2,6-diphenylpyrylium-4-yl)benzene [**23**$^{3+}$•3(BF_4^-)]

A mixture of **22** (0.5 g, 0.60 mmol) and chalcone (380 mg, 1.8 mmol) in boron trifluoride etherate (2.1 ml) was heated at 100 °C for five hours under nitrogen. After cooling, deep yellow precipitates appeared by addition of ether (20 ml). Filtration and washing with ether under nitrogen gave **23**$^{3+}$•3(BF_4^-) (600 mg, 90%).

23^{3+}•3(BF_4^-): yellow precipitate; mp 155-156 °C (dec.); FAB MS 860 [M^+-2(BF_4)], 772 [M^+-3(BF_4)]; ^{1}H-NMR (270 MHz, $CDCl_3$-CF_3CO_2D) δ 9.13 (s, 3H), 8.87 (s, 6H), 8.41 (d, 12H, *J* = 7.9 Hz), 7.88 (t, 6H, *J* = 7.9 Hz), 7.78 (t, 12H, *J* = 7.9 Hz); ^{13}C-NMR (67.8 MHz, $CDCl_3$-CF_3CO_2D) δ 173.9, 165.7, 138.7, 137.6, 134.2, 131.4, 129.7, 129.2, 117.6; IR (KBr) 3055 (w),

1621 (s), 1565 (s), 1440 (w), 1258 (m), 1165 (m), 1061 (bs), 882 (w), 779 (m), 704 (m), 592 (w), 521 (w) cm^{-1}; UV (CH_3CN) λ_{max} / nm (log ε) 414 (4.69), 351 (4.84), 280 (4.61)

1,3,5-Tris(1-methyl-2,6-diphenylpyridinium-4-yl)benzene [$\mathbf{2}^{3+}$•3(BF_4^-)]

A solution of $\mathbf{2}^{3+}$•3(BF_4^-) (200 mg, 0.19 mmol) and methylamine (24.3% ethanol solution, 136 mg, 1.1 mmol) in acetonitrile (4 ml) was stirred overnight at room temperature. The solvent was evaporated and the residue was dissolved with acetonitrile (2 ml). 42% Hydrofluoroboric acid (2 ml) was added and the reaction mixture was stood for thirty minutes at room temperature. The black tar was removed by filtration through filter paper, yellow precipitate appeared by addition of water (8 ml) to the filtrate. Filtration and washing with water, ethanol, and ether gave $\mathbf{2}^{3+}$•3(BF_4^-) (71 mg, 34%). $\mathbf{2}^{3+}$•3(BF_4^-): yellow powder; mp 219-221 °C (decomp.); FAB MS *m/z* 986 (M^+-BF_4); ^{1}H-NMR (270 MHz, CD_3CN) δ 8.69 (s, 3H), 8.43 (s, 6H), 7.72-7.64 (m, 30H), 3.80 (s, 9H); ^{13}C-NMR (67.8 MHz, CD_3CN) δ 158.4, 153.7, 137.0, 133.8, 132.4, 132.0, 130.4, 130.1, 127.5, 127.5, 46.3; IR (KBr) 3055 (w), 1622 (s), 1566 (m), 1495 (w), 1445 (w), 1253 (w), 1083 (bs), 876 (w), 781 (m), 703 (m), 593 (w), 521 (w) cm^{-1}; UV (CH_3CN) λ_{max} / nm (log ε) 296 (4.91); Anal. Calcd for $C_{60}H_{48}N_3B_3F_{12}$: C, 67.26; H, 4.52; N, 3.92. Found: C, 67.17; H, 4.73; N, 3.58.

p- Bis(2-benzoylethenyl)benzene (**25**)

A solution of of terephthalaldehyde (2.0 g, 15 mmol) in DMSO (20 ml) was added to a solution of benzoylmethyltriphenylphosphonium bromide (15.2 g, 32 mmol) and potassium *tert*-butoxide (3.6 g, 32 mmol) in DMSO (100 ml) under nitrogen. The reaction mixture was stirred and heated at 80 °C for six hours. After cooling, water (200 ml) and 6 N hydrochloric acid (20 ml) were added, the reaction mixture was extracted with benzene. The extracts were combined, washed with water and brine, and dried over anhydrous sodium sulfate. After concentration, the residue was purified by column chromatography on silica gel using benzene-ethyl acetate (10:1 v/v). **26** (3.9 g, 78%) was obtained. **25**: pale yellow needles (from C_6H_6); mp 194-195 °C; EI MS *m/z* 338 (M^+), 233 (M^+-C_6H_5CO); ^{1}H-NMR (300 MHz, $CDCl_3$) δ 8.03 (d, 4H, *J* = 7.1 Hz), 7.81 (d, 2H, *J* = 15.7 Hz), 7.70 (s, 4H), 7.61 (t, 2H, *J* = 7.1 Hz), 7.58 (d, 2H, *J* = 15.7 Hz), 7.52 (t, 4H, *J* = 7.1 Hz); ^{13}C-NMR (67.8 MHz, $CDCl_3$) δ 190.2, 143.5, 138.1, 136.9, 132.9, 129.0, 128.7, 128.5, 123.1; IR (KBr) 1655 (s), 1606

(s), 1446 (w), 1418 (w), 1337 (m), 1293 (w), 1226 (m), 1038 (w), 1020 (m), 980 (m), 834 (m), 770 (m), 693 (m) cm^{-1}; Anal. Calcd for $C_{24}H_{18}O_2$: C, 85.18 ; H, 5.36. Found: C, 85.15 ; H, 5.34.

p-Bis(1,3-dibenzoyl-2-propyl)benzene (**26**)

Potassium *tert*-butoxide (280 mg, 2.5 mmol) was added to a solution of **25** (2.0 g, 6.0 mmol) and acetophenone (10 ml, 80 mmol) in THF (80 ml) and *tert*-butanol (32 ml). The reaction mixture was stirred at room temperature overnight. The colorless crystals was collected by filtration and washed with benzene. Recrystallization with chloroform gave **26** (720 mg, 85%) as colorless crystals.

26: colorless crystals (from $CHCl_3$); mp 208-209 °C; EI MS *m/z* 578 (M^+), 458 (M^+-C_6H_5 $COCH_2$), 338 [M^+-2($C_6H_5COCH_2$)]; ^{1}H-NMR (300 MHz, $CDCl_3$) δ 7.91 (d, 8H, *J* = 7.5 Hz), 7.52 (t, 4H, *J* = 7.5 Hz), 7.42 (t, 8H, *J* = 7.5 Hz), 7.19 (s, 8H), 4.02 (quintet, 2H, *J* = 7.0 Hz), 3.44 (dd, 4H, *J* = 16.7 Hz, 7.0 Hz), 3.31 (dd, 4H, *J* = 16.7 Hz, 7.0 Hz); ^{13}C-NMR (67.8 MHz, $CDCl_3$) δ 198.6, 142.2, 137.0, 133.0, 128.6, 128.1, 127.7, 44.8, 36.7; IR (KBr) 1684 (s), 1596 (m), 1448 (m), 1415 (m), 1361 (m), 1271 (s), 1211 (m), 992 (m), 838 (w), 765 (m), 703 (m) cm^{-1}

p-Bis(2,6-diphenylpyrylium-4-yl)benzene [$\mathbf{27}^{2+}$•2(BF_4^-)]

To a mixture of **26** (1.0 g, 1.8 mmol) and chalcone (0.77 g, 3.7 mmol) was added boron trifluoride etherate (3.0 ml) under nitrogen. The reaction mixture was heated at 110 °C for three hours with stirring. After cooling, ether (40 ml) was added to the reaction mixture and yellow precipitates appeared. Filtration and washing with dry ether gave of $\mathbf{27}^{2+}$•2(BF_4^-) (1.2 g, 99%).

$\mathbf{27}^{2+}$•2(BF_4^-): yellow crystals; mp > 300 °C; FAB MS *m/z* 627 (M^+-BF_4), 540 [M^+-2(BF_4)]; ^{1}H-NMR (270 MHz, $CDCl_3$-CF_3CO_2D) δ 8.76 (s, 4H), 8.52 (s, 4H), 8.40 (d, 8H, *J* = 7.4 Hz), 7.92 (t, 4H, *J* = 7.4 Hz), 7.81 (t, 8H, *J* = 7.4 Hz); ^{13}C-NMR (67.8 MHz, $CDCl_3$-CF_3CO_2D) δ 173.8, 166.6, 139.5, 137.9, 131.7, 131.7, 129.6, 129.3, 116.7

p-Bis(1-methyl-2,6-diphenylpyridinium-4-yl)benzene [$\mathbf{24}^{2+}$•2(BF_4^-)]

A solution of $\mathbf{28}^{2+}$•2(BF_4^-) (300 mg, 0.42 mmol) and methylamine (24.3% ethanol solution, 186 mg, 1.7 mmol) was stirred overnight in acetonitrile (10 ml) at room temperature. Colorless crystals

appeared by addition of ether (30 ml). Filtration and washing with ethanol gave $\mathbf{24}^{2+}\cdot 2(BF_4^-)$ (240 mg, 77%).

$\mathbf{24}^{2+}\cdot 2(BF_4^-)$: colorless crystals (from CH_3CN-C_2H_5OH); mp > 300 °C; FAB MS *m/z* 653 (M^+-BF_4), 566 [M^+-2(BF_4)]; ^{1}H-NMR (270 MHz, CD_3CN) δ 8.28 (s, 4H), 8.22 (s, 4H), 7.75-7.70 (m, 20H), 3.79 (s, 6H); ^{13}C-NMR (67.8 MHz, CD_3CN) δ 158.2, 154.6, 137.9, 133.7, 132.3, 130.4, 130.2, 130.0, 127.0, 46.3; FAB HRMS *m/z* Calcd for $C_{42}H_{34}N_2BF_4$: 653.2751. Found: 653.2769.

2,6-Bis(2-benzoylethenyl)toluene (**28**)

A solution of 2-methyl-1,3-benzenedicarboxaldehyde (200 mg, 1.4 mmol) in DMSO (10 ml) was added to a solution of benzoylmethyltriphenylphosphonium bromide (1.5 g, 3.2 mmol) and potassium *tert*-butoxide (360 mg, 3.2 mmol) in DMSO (15 ml) under nitrogen. The reaction mixture was stirred and heated at 80 °C for three hours. After cooling, water (40 ml) and 6 N hydrochloric acid (40 ml) were added, the reaction mixture was extracted with benzene. The extracts were combined, washed with water and brine, and dried over anhydrous sodium sulfate. After concentration, the residue was purified by column chromatography on silica gel using benzene. **28** (350 mg, 73%) was obtained.

28: pale yellow needles (from C_2H_5OH); mp 178-179 °C; EI MS *m/z* 352 (M^+), 337 (M^+-CH_3), 247 (M^+-C_6H_5CO); ^{1}H-NMR (300 MHz, $CDCl_3$) δ 8.19 (d, 2H, *J* = 15.5 Hz), 8.04 (d, 4H, *J* = 7.4 Hz), 7.71 (d, 2H, *J* = 7.8 Hz), 7.61 (t, 2H, *J* = 7.4 Hz), 7.52 (t, 4H, *J* = 7.4 Hz), 7.43 (d, 2H, *J* = 15.5 Hz), 7.32 (t, 1H, *J* = 7.8 Hz), 2.55 (s, 3H); ^{13}C-NMR (67.8 MHz, $CDCl_3$) δ 189.3, 142.3, 138.0, 137.5, 135.6, 132.6, 128.5, 128.4, 128.2, 126.2, 124.5, 15.7; IR (KBr) 3057 (w), 1695 (s), 1661 (s), 1603 (s), 1446 (m), 1321 (s), 1211 (m), 1015 (m), 772 (m), 689 (m), 638 (w) cm^{-1}; Anal. Calcd for $C_{25}H_{20}O_2$: C, 85.20 ; H, 5.72. Found: C, 85.11 ; H, 5.65.

2,6-Bis(1,3-dibenzoyl-2-propyl)toluene (**29**)

Potassium *tert*-butoxide (30 mg, 0.27 mmol) was added to a solution of **28** (200 mg, 0.57 mmol) and acetophenone (3 ml, 24 mmol) in THF (12 ml) and *tert*-butanol (8 ml). The reaction mixture was stirred overnight at room temperature. Water (20 ml) and 6 N hydrochloric acid (4 ml) were added, the aqueous layer was extracted with benzene. The organic layers were combined, washed with water and brine, and dried over anhydrous sodium sulfate. After concentration, the residue was purified by

column chromatography on silica gel using benzene (to remove acetophenone) and benzene-ethyl acetate (9:1 v/v). **29** (330 mg, 97%) was obtained as pale yellow needles.

29: colorless needles (from C_2H_5OH); mp 151-152 °C; FAB MS *m/z* 593 (M^++1); ^{1}H-NMR (270 MHz, $CDCl_3$) δ 7.90 (dt, 8H, *J* = 7.2 Hz, 1.6 Hz), 7.52 (tt, 4H, *J* = 7.2 Hz, 1.6 Hz), 7.41 (dt, 8H, *J* = 7.2 Hz, 1.6 Hz), 7.13-7.09 (m, 3H), 4.41 (quintet, 2H, *J* = 6.9 Hz), 3.43 (dd, 4H, *J* = 16.5 Hz, 6.9 Hz), 3.25 (dd, 4H, *J* = 16.5 Hz, 6.9 Hz), 2.28 (s, 3H); ^{13}C-NMR (67.8 MHz, $CDCl_3$) δ 198.9, 142.6, 137.1, 133.7, 133.0, 128.6, 128.1, 126.0, 124.2, 44.7, 32.7, 14.4; IR (KBr) 3058 (w), 2894 (w), 1686 (s), 1596 (m), 1579 (w), 1448 (m), 1346 (w), 1272 (m), 1209 (m), 1001 (w), 755 (m), 730 (w), 699 (m), 529 (w) cm^{-1}; Anal. Calcd for $C_{41}H_{36}O_4$: C, 83.08 ; H, 6.12. Found: C, 82.96 ; H, 6.07.

2-Methyl-1,3-Bis(2,6-diphenylpyrylium-4-yl)benzene [$\mathbf{3}^{2+}$•2(BF_4^-)]

A mixture of **29** (200 mg, 0.34 mmol) and chalcone (140 mg, 0.67 mmol) in boron trifluoride etherate (1 ml) was stirred and heated at 110 °C for four hours under nitrogen. After cooling, yellow precipitate appeared by the addition of ether (50 ml). Filtration and washing with ether gave $\mathbf{3}^{2+}$•2(BF_4^-) (170 mg, 68%).

$\mathbf{3}^{2+}$•2(BF_4^-): yellow crystals (from C_2H_5OH); mp 177-179 °C (dec.); FAB MS *m/z* 641.3 (M^+-BF_4), 554.3 [M^+-2(BF_4)]; ^{1}H-NMR (270 MHz, $CDCl_3$-CF_3CO_2D) δ 8.57 (s, 4H), 8.32 (d, 8H, *J* = 7.3 Hz), 8.25-8.20 (m, 2H), 7.85 (t, 4H, *J* = 7.3 Hz), 7.75 (t, 8H, *J* = 7.3 Hz), 7.18-7.15 (m, 1H); ^{13}C-NMR (67.8 MHz, $CDCl_3$-CF_3CO_2D) δ 172.0, 170.0, 137.6, 136.7, 132.8, 130.8, 129.9, 129.2, 128.9, 128.3, 119.5, 18.5; IR (KBr) 3419 (bm), 3058 (w), 1616 (s), 1576 (s), 1495 (s), 1470 (s), 1269 (m), 1241 (m), 1083 (bs), 782 (m), 686 (m), 620 (w), 606 (w), 522 (w) cm^{-1}; UV (CH_3CN) λ_{max} / nm (log ε) 402 (4.62), 358 (4.50), 279 (4.55); FAB HRMS *m/z* Calcd for $C_{41}H_{30}O_2BF_4$: 641.2275. Found: 641.2297.

2-Methyl-1,3-Bis(1-methyl-2,6-diphenylpyridinium-4-yl)benzene [$\mathbf{3}^{2+}$•2(BF_4^-)]

A solution of $\mathbf{3}^{2+}$•2(BF_4^-) (150 mg, 0.21 mmol) and methylamine (24.3% ethanol solution, 79 mg, 0.63 mmol) in acetonitrile (5 ml) was stirred overnight at room temperature. After concentration,

the residue was crystallized from ethanol (2 ml). Filtration and washing with ethanol and ether gave $\mathbf{3}^{2+}\bullet 2(BF_4^-)$ (120 mg, 75%).

$\mathbf{3}^{2+}\bullet 2(BF_4^-)$: orange crystals (from CH_3CN-C_2H_5OH); mp > 300 °C; FAB MS *m/z* 667 (M^+-BF_4), 565 [M^+-2(BF_4)-CH_3]; ^{1}H-NMR (270 MHz, CD_3CN) δ 7.97 (s, 4H), 7.75-7.60 (m, 23H), 3.83 (s, 6H), 2.44 (s, 3H); ^{13}C-NMR (67.8 MHz, CD_3CN) δ 158.0, 157.9, 138.8, 134.7, 133.8, 132.6, 132.4, 130.4, 130.3, 130.2, 128.2, 46.5, 19.2; IR (KBr) 3058 (w), 1625 (s), 1563 (m), 1495 (w), 1447 (w), 1249 (w), 1083 (bs), 893 (w), 779 (m), 704 (m), 522 (w) cm^{-1}; UV (CH_3CN) λ_{max} / nm (log ε) 300 (4.63); FAB HRMS *m/z* Calcd for $C_{43}H_{36}N_2BF_4$: 667.2908. Found: 667.2926.

2,4-Dibromo-1,5-dimethylbenzene

A three necked flask, which was wrapped with aluminum foil, was charged with of *m*-xylene (24.2 g, 0.23 mol), iron powder (1.2 g, 21 mmol), and carbon tetrachloride (150 ml). A solution of bromine (73.0 g, 0.46 mol) in carbon tetrachloride (50 ml) was added dropwise at 0 °C with stirring under a nitrogen stream. After the addition of bromine, the reaction mixture was allowed to room temperature and stirred overnight. Water (200 ml) was added and the aqueous layer was extracted with carbon tetrachloride. The organic layers were combined, washed with water, 5% sodium bisulfite, water, and brine, and dried over anhydrous sodium sulfate. After concentration, the residue was crystallized from ethanol and 2,4-dibromo-1,5-dimethylbenzene (18.6 g, 31%) was obtained.

2,4-Dibromo-1,5-dimethylbenzene: colorless needles (from C_2H_5OH); mp 70-71 °C; ^{1}H-NMR (400 MHz, $CDCl_3$) δ 7.68 (s, 1H), 7.10 (s, 1H)

2,4-Dimethyl-1,5-diformylbenzene

To a solution of 2,4-dibromo-1,5-dimethylbenzene (2.5 g, 9.5 mmol) in THF (25 ml) under nitrogen was added dropwise a 1.6 M solution of n-butyllithium in hexane (6 ml, 9.5mmol) at -30 °C. After stirring for ten minutes at -30 °C, DMF (0.73 ml, 9.5mmol) was added dropwise and the reaction mixture was stirred for ten minutes at 0 °C. This procedures repeated again. After the second addition of DMF, the reaction mixture was stirred at 0 °C for thirty minutes. 1 N Solution of hydrochloric acid (60 ml) was added, the reaction mixture was extracted with benzene. The benzene extracts were combined, washed with water, 10% sodium hydroxide, water, and brine, and dried over anhydrous

sodium sulfate. After concentration, the residue was purified by column chromatography on silica gel using benzene as a eluent. 2,4-Dimethyl-1,5-diformylbenzene (660 mg, 44%) was obtained.
2,4-Dimethyl-1,5-diformylbenzene: colorless needles (from C_6H_6); mp 103-104 °C (lit.[63] 104-106 °C); ^{1}H-NMR (270 MHz, $CDCl_3$) δ 10.26 (s, 2H), 8.22 (s, 1H), 7.19 (s, 1H), 2.71 (s, 6H)

2,4-Dimethyl-1,5-bis(2-benzoylethenyl)benzene (**31**)

A solution of 2,4-dimethyl-1,5-diformylbenzene (1.0 g, 6.2 mmol) in DMSO (20 ml) was added to a solution of benzoylmethyltriphenylphosphonium bromide (8.7 g, 19 mmol) and potassium *tert*-butoxide (1.8 g, 16 mmol) in DMSO (80 ml) at 80 °C. After addition, the reaction mixture was heated at 80 °C overnight. After cooling, 1 N hydrochloric acid (120 ml) was added, the reaction mixture was extracted with benzene. The benzene extracts were combined, washed with water and brine, and dried over anhydrous sodium sulfate. After concentration, the residue was purified by column chromatography on silica gel using benzene as a eluent. Crystallization from benzene gave **31** (1.2 g, 55%).
31: pale yellow needles (from C_2H_5OH); mp 158-159 °C; EI MS *m/z* 366 (M^+), 351 (M^+-CH_3), 261 (M^+-C_6H_5CO); ^{1}H-NMR (400 MHz, $CDCl_3$) δ 8.08 (d, 2H, J = 15.7 Hz), 8.05 (d, 4H, J = 7.5 Hz), 7.97 (s, 1H), 7.61 (t, 2H, J = 7.5 Hz), 7.53 (t, 4H, J = 7.5 Hz), 7.49 (d, 2H, J = 15.7 Hz), 7.13 (s, 1H), 2.48 (s, 6H); ^{13}C-NMR (67.8 MHz, $CDCl_3$) δ 190.2, 141.8, 140.4, 138.2, 133.5, 132.8, 132.3, 128.61, 128.55, 124.7, 123.3, 19.8; IR (KBr) 3055 (w), 1686 (m), 1651 (s), 1584 (s), 1494 (m), 1446 (m), 1316 (s), 1218 (s), 1180 (m), 1013 (s), 974 (m), 858 (m), 779 (m), 720 (m), 688 (s), 648 (m) cm^{-1}

2,4-Dimethyl-1,5-bis(1,3-dibenzoyl-2-propyl)benzene (**32**)

Potassium *tert*-butoxide (6 mg, 0.05 mmol) was added to a solution of **31** (100 mg, 0.27 mmol) and acetophenone (1.5 ml, 12 mmol) in THF (6 ml) and *tert*-butanol (4 ml). The reaction mixture was stirred for three hours at room temperature. Water (30 ml) and a small amount of 6 N hydrochloric acid were added, the reaction mixture was extracted with benzene. The benzene extracts were combined, washed with water and brine, and dried over anhydrous sodium sulfate. After concentration, the residue was purified by column chromatography on silica gel using benzene to remove acetophenone

and then benzene-ethyl acetate (9:1 v/v). **32** (170 mg, quant.) was obtained as yellow oil. **32** was used the next reaction without further purification.

32: yellow oil; ^{1}H-NMR (270 MHz, $CDCl_3$) δ 7.86 (d, 8H, *J* = 7.3 Hz), 7.48 (t, 4H, *J* = 7.3 Hz), 7.37 (t, 8H, *J* = 7.3 Hz), 7.15 (s, 1H), 6.83 (s, 1H), 4.23 (quintet, 2H, *J* = 7.0 Hz), 3.37 (dd, 4H, *J* = 16.7 Hz, 7.0 Hz), 3.23 (dd, 4H, *J* = 16.7 Hz, 7.0 Hz), 2.23 (s, 6H); ^{13}C-NMR (67.8 MHz, $CDCl_3$) δ 198.9, 139.5, 138.0, 133.6, 132.9, 128.5, 128.3, 128.1, 124.0, 44.0, 32.5, 19.0; IR (KBr) 3054 (m), 1664 (s), 1596 (s), 1505 (m), 1450 (s), 1236 (s), 984 (s), 876 (w), 756 (s), 700 (s), 590 (s), 516 (m) cm^{-1}

2,4-Dimethyl-1,5-bis(2,6-diphenylpyrylium-4-yl)benzene [**33**$^{2+}$•2(BF_4^-)]

A mixture of **32** (800 mg, 1.3 mmol) and chalcone (600 mg, 2.8 mmol) in boron trifluoride etherate (5 ml) was stirred and heated at 110 °C for four hours under nitrogen. After cooling, ether (50 ml) was added. Yellow precipitate was filtered and washed with ether. **33**$^{2+}$•2(BF_4^-) (580 mg, 60%) was obtained.

33^{2+}•2(BF_4^-): yellow powder; mp 190-192 °C (decomp.); FAB MS *m/z* 655.4 (M^+-BF4), 568.3 [M^+-2(BF4)]; ^{1}H-NMR (270 MHz, $CDCl_3$-CF_3CO_2D) δ 8.44 (s, 4H), 8.26 (d, 8H, *J* = 7.4 Hz), 7.90 (s, 1H), 7.82 (t, 4H, *J* = 7.4 Hz), 7.71 (t, 8H, *J* = 7.4 Hz), 7.58 (s, 1H), 2.63 (s, 6H); ^{13}C-NMR (67.8 MHz, $CDCl_3$-CF_3CO_2D) δ 171.9, 168.7, 141.6, 136.6, 136.1, 134.1, 131.7, 130.7, 128.8, 128.4, 118.9, 20.3; IR (KBr) 3059 (w), 1621 (s), 1578 (m), 1489 (s), 1431 (m), 1266 (w), 1083 (bs), 836 (w), 779 (m), 686 (m), 521 (w) cm^{-1}; UV (CH_3CN) λ_{max} / nm (log ε) 396 (4.67), 278 (4.52); FAB HRMS *m/z* Calcd for $C_{42}H_{32}O_2BF_4$: 655.2432. Found: 655.2459.

2,4-Dimethyl-1,5-bis(1-methyl-2,6-diphenylpyridinium-4-yl)benzene [**4**$^{2+}$•2(BF_4^-)]

A solution of **33**$^{2+}$•2(BF_4^-) (240 mg, 0.2 mmol) and methylamine (24.3% ethanol solution, 132 mg, 1.0 mmol) in acetonitrile (2.5 ml) was stirred overnight at room temperature. After concentration, ethanol (4 ml) was added to the residue and yellow precipitate appeared. Filtration and washing with ethanol gave **4**$^{2+}$•2(BF_4^-) (140 mg, 56%).

4^{2+}•2(BF_4^-): yellow crystals (from CH_3CN-C_2H_5OH); mp 271-272 °C, FAB MS *m/z* 681 (M^+-BF4), 580 [M^+-2(BF4)-CH_3]; ^{1}H-NMR (270 MHz, CD_3CN) δ 7.88 (s, 4H), 7.68-7.59 (m, 20H),

7.56 (s, 1H), 7.41 (s, 1H), 3.77 (s, 6H), 2.46 (s, 6H); ^{13}C-NMR (67.8 MHz, CD_3CN) δ 157.6, 157.2, 139.7, 135.4, 135.0, 133.8, 132.3, 131.9, 130.3, 130.1, 130.0, 46.2, 20.2; IR (KBr) 3059 (w), 1623 (s), 1567 (m), 1494 (w), 1445 (w), 1249 (w), 1083 (bs), 888 (w), 778 (m), 704 (m) cm^{-1}; UV (CH_3CN) λ_{max} / nm (log ε) 303 (4.61); FAB HRMS *m/z* Calcd for $C_{44}H_{38}N_2BF_4$: 681.3064. Found: 681.3082.

1,8-Bis(hydroxymethyl)anthracene

To a solution of 1,8-bis(methoxycarbonyl)anthracene (1.0 g, 3.4 mmol) in THF (15 ml) was added LAH (260 mg, 6,8 mmol) at 0 °C. The reaction mixture was stirred for 90 minutes at 0 °C. Ethyl acetate (20 ml) was added, and the reaction mixture was stirred for 15 minutes at room temperature. After concentration, 6 N hydrochloric acid (10 ml) was added and the yellow suspension was stirred overnight at room temperature. Pale yellow precipitate was collected and washed with water and hexane. 1,8-Bis(hydroxymethyl)anthracene (780 mg, 96%) was obtained.

1,8-Bis(hydroxymethyl)anthracene: pale yellow needles (from C_2H_5OH); mp 212-214 °C (lit.[64] 217-218 °C); ^{1}H-NMR (300 MHz, DMSO-d_6) δ 8.79 (s, 1H), 8.57 (s, 1H), 7.98 (d, 2H, *J* = 8.3 Hz), 7.59 (d, 2H, *J* = 6.8 Hz), 7.48 (dd, 2H, *J* = 8.3 Hz, 6.8 Hz), 5.37 (t, 2H, *J* = 5.5 Hz), 5.16 (d, 4H, *J* = 5.5 Hz)

1,8-diformylanthracene

To a solution of 1,8-bis(hydroxymethyl)anthracene (400 mg, 1.7 mmol) in methylene chloride (80 ml) was added PCC (1.5 g, 7.3 mmol). The reaction mixture was stirred for an hour at room temperature. After filtration and concentration of filtrate, the residue was purified by column chromatography on silica gel using methylene chloride as a eluent. 1,8-diformylanthracene (270 mg, 68%) was obtained as yellow needles.

1,8-diformylanthracene: orange needles (from C_6H_6); mp 183-185 °C (lit.[64] 189-191 °C); ^{1}H-NMR (270 MHz, $CDCl_3$) δ 11.14 (s, 1H), 10.61 (s, 2H), 8.56 (s, 1H), 8.27 (d, 2H, *J* = 8.6 Hz), 8.10 (d, 2H, *J* = 6.3 Hz), 7.71-7.65 (m, 2H)

1,8-Bis(2-benzoylethenyl)anthracene (**35**)

A solution of 1,8-diformylanthracene (400 mg, 1.7 mmol) in DMSO (20 ml) was added to a solution of benzoylmethyltriphenylphosphonium bromide (7.0 g, 15 mmol) and potassium *tert*-butoxide (825 mg, 7.4 mmol) in DMSO (40 ml) under nitrogen. The reaction mixture was heated at 80 °C overnight. After cooling, 6 N hydrochloric acid (20 ml) and water (100 ml) were added and the reaction mixture was extracted with benzene. The benzene extracts were combined, washed with water and brine, and dried over anhydrous sodium sulfate. After concentration, the residue was purified by column chromatography on silica gel using benzene as a eluent. **35** (680 mg, 91%) was obtained as yellow needles.

35: yellow needles (from C_6H_6); mp 189-190 °C; EI MS *m/z* 438 (M^+), 333 (M^+-C_6H_5CO); ^{1}H-NMR (270 MHz, $CDCl_3$) δ 9.07 (s, 1H), 8.70 (d, 2H, *J* = 15.7 Hz), 8.51 (s, 1H), 8.13-8.07 (m, 6H), 7.89 (d, 2H, *J* = 6.9 Hz), 7.65 (d, 2H, *J* = 15.7 Hz), 7.60-7.51 (m, 8H); ^{13}C-NMR (67.8 MHz, $CDCl_3$) δ 190.3, 141.8, 138.2, 133.4, 132.8, 131.8, 130.7, 130.1, 128.7, 128.64, 128.55, 126.1, 125.9, 125.4, 118.7; IR (KBr) 3057 (w), 1636 (s), 1598 (s), 1446 (m), 1387 (w), 1333 (m), 1286 (s), 1217 (s), 1171 (m), 1070 (w), 1018 (s), 964 (m), 880 (s), 767 (s), 743 (m), 692 (s), 599 (m) cm^{-1}; Anal. Calcd for $C_{32}H_{22}O_2$: C, 87.00; H, 5.06. Found: C, 87.00; H, 4.97.

1,8-Bis(1,3-dibenzoyl-2-propyl)anthracene (**36**)

A solution of **35** (200 mg, 0.46 mmol), acetophenone (2 ml, 16 mmol), and (20 mg) of potassium *tert*-butoxide (20 mg, 0.18 mmol) in THF (12 ml) and *tert*-butanol (8 ml) were stirred overnight at room temperature. 6 N Hydrochloric acid (5 ml) and water (30 ml) were added and the aqueous layer was extracted with ethyl acetate-benzene (2:1 v/v). The organic layers were combined, washed with water and brine, and dried over anhydrous sodium sulfate. After concentration, the residue was purified by column chromatography on silica gel using benzene to remove acetophenone and then benzene-ethyl acetate (9:1 v/v). **36** (170 mg, quant.) was obtained.

36: pale yellow crystals (from C_2H_5OH); mp 156-158 °C; EI MS *m/z* 678 (M^+), 559 (M^+-$C_6H_5COCH_2$), 439 [M^+-2($C_6H_5COCH_2$)]; ^{1}H-NMR (270 MHz, C_6D_5Br, 100 °C) δ 9.58 (s, 1H), 8.25 (s, 1H), 7.82 (d, 8H, *J* = 6.9 Hz), 7.71 (d, 2H, *J* = 8.3 Hz), 7.47 (d, 2H, *J* = 6.6 Hz), 7.29-7.10 (m, 14H), 5.36 (quintet, 2H, *J* = 6.6 Hz), 3.70 (d, 8H, *J* = 6.6 Hz); ^{13}C-NMR (67.8 MHz,

C_6D_5Br) δ 197.7, 141.1, 137.7, 132.3, 130.0, 128.2, 128.0, 127.2, 125.0, 96.3, 44.6; IR (KBr) 3056 (w), 1682 (s), 1596 (m), 1578 (m), 1448 (s), 1408 (w), 1352 (m), 1278 (s), 1213 (s), 977 (m), 875 (m), 788 (w), 758 (s), 688 (s), 602 (w) cm^{-1}

1,8-Bis(2,6-diphenylpyrylium-4-yl)anthracene [$\mathbf{37}^{2+}$•2(BF_4^-)]

A mixture of **36** (200 mg, 0.46 mmol) and chalcone (190 mg, 0.92 mmol) in boron trifluoride etherate (1.2 ml) was stirred and heated at 110 °C for four hours under nitrogen. After cooling, ether (15 ml) was added. Dark red precipitate was filtered and washed with ether. $\mathbf{37}^{2+}$•2(BF_4^-) (210 mg, 80%) was obtained.

$\mathbf{37}^{2+}$•2(BF_4^-): dark red crystals (from C_2H_5OH); mp 185-190 °C (dec.); FAB MS *m/z* 727 (M^+-BF4), 641 [M^+-2(BF4)]; ^{1}H-NMR (270 MHz, $CDCl_3$-CF_3CO_2D) δ 8.80 (s, 1H), 8.70 (s, 1H), 8.47 (s, 4H), 8.38 (d, 2H, *J* = 7.6 Hz), 8.02 (d, 8H, *J* = 7.6 Hz), 7.75-7.72 (m, 4H), 7.65 (t, 4H, *J* = 7.6 Hz), 7.50 (t, 8H, *J* = 7.6 Hz); ^{13}C-NMR (67.8 MHz, $CDCl_3$-CF_3CO_2D) δ 171.4, 169.3, 135.8, 134.4, 133.9, 132.2, 131.0, 130.3, 130.2, 129.0, 128.6, 128.43, 128.35, 125.7, 120.3, 118.9; IR (KBr) 3060 (w), 1620 (s), 1578 (m), 1488 (s), 1262 (m), 1217 (m), 1083 (bs), 777 (m), 685 (m), 521 (w) cm^{-1}; UV (CH_3CN) λ_{max} / nm (log ε) 512 (3.95), 404 (4.58), 322 (4.36), 251 (4.95)

1,8-Bis(1-methyl-2,6-diphenylpyridinium-4-yl)anthracene [$\mathbf{5}^{2+}$•2(BF_4^-)]

A solution of $\mathbf{37}^{2+}$•2(BF_4^-) (40 mg, 0.05 mmol) and methylamine (24.3% ethanol solution, 20 mg, 0.15 mmol) in acetonitrile (2 ml) was stirred overnight at room temperature. After concentration, ethanol (10 ml) was added to the residue and brown precipitate appeared. Filtration and washing with ethanol gave $\mathbf{5}^{2+}$•2(BF_4^-) (25 mg, 60%).

$\mathbf{5}^{2+}$•2(BF_4^-): brown crystals (from CH_3CN-C_2H_5OH); mp 200-205 °C (dec.); FAB MS *m/z* 753 (M^+-BF4); ^{1}H-NMR (270 MHz, CD_3CN) δ 8.85 (s, 1H), 8.59 (s, 1H), 8.33 (d, 2H, *J* = 7.6 Hz), 8.07 (s, 4H), 7.74-7.54 (m, 24H), 3.89 (s, 6H); ^{13}C-NMR (67.8 MHz, CD_3CN) δ 158.0, 135.2, 133.6, 132.9, 132.4, 32.3, 130.9, 130.3, 130.2, 129.9, 129.8, 126.5, 121.8, 46.8; IR (KBr) 3059 (w), 1623 (s), 1563 (m), 1494 (w), 1446 (m), 1246 (m), 1083 (bs), 775 (m), 701 (m), 499 (w) cm^{-1}; UV (CH_3CN) λ_{max} / nm (log ε) 411 (3.91), 249 (4.79); FAB HRMS *m/z* Calcd for $C_{50}H_{38}N_2BF_4$: 753.3064. Found: 753.3056.

Procedure of the measurement of the UV-vis spectra of pyridinyl radicals

An apparatus shown in Figure 2-2 (p. 22) was used for the measurement of the UV-vis spectra. About 1.5 mg of pyridinium salt was charged in the vessel B and about 300 mg of 3% Na-Hg was placed in the vessel C. The system was degassed after the point D was sealed. About 5 ml of a well degassed solvent [acetonitrile or 2-methyltetrahydrofuran (MTHF)-acetonitrile (1:1 v/v)] was transferred into the B from the vessel K, and the point F was sealed. A solution of pyridinium salt in the B was transferred into the UV cell A (d=1 mm) and UV-vis spectrum of the solution of pyridinium salt was measured. The solution was transferred into the C. After shaking with 3% Na-Hg for a suitable time, the solution was filtered through the glass filter E. The UV-vis spectrum of this partially reduced solution was measured. The UV-vis spectral change was measured by the repetition of this procedure. The solution was separated from 3% Na-Hg during the measurement of UV-vis spectrum. Each spectrum was recorded as a function of the time contact.

Procedure of the measurement of ESR spectra of pyridinyl radicals

An apparatus shown in Figure 2-14 (p. 32) was used for the measurement of the ESR spectra. Reduction of pyridinium salt and the measurement of the UV-vis spectra of pyridinyl radical were already described above [MTHF-acetonitrile (1:1 v/v) was used as solvent]. When the intensity of the absorption (ca. 350 nm and 550~580 nm) of pyridinyl radical started to decrease, the reduction was stopped. The reduced solution was transferred to the ESR tube L up to 2-3 cm height and the tube was sealed at the point M.

2-8. References

[46] R. N. Carde, P. C. Hayes, G. Jones, and C. J. Cliff, *J. Chem. Soc., Perkin Trans. 1*, **1981**, 1132.

[47] S. Hünig, B. J. Garner, G. Ruider, and W. Schenk, *Liebigs Ann. Chem.*, **1973**, 1036.

[48] 1,8-Bis(2,6-diphenylpyridine-4-yl)naphtalene could not be converted into bispyridinium salt but mono-pyridinium salt by reaction with methyl iodide (40 equiv.) in acetonitrile in sealed tube at 120 °C for 7 days.

[49] a) A. R. Katritzky, J. M. Lloyd, and R. C. Patel, *J. Chem. Soc., Perkin Trans. 1*, **1982**, 117.

b) A. R. Katritzky, U. Gruntz, D. H. Kenny, M. C. Rezende, and H. Sheikh, *J. Chem. Soc., Perkin Trans. 1*, **1979**, 430.

c) A. R. Katritzky, N. F. Eweiss, and P-L. Nie, *J. Chem. Soc., Perkin Trans. 1*, **1979**, 433.

d) A. R. Katritzky and S. S. Thind, *J. Chem. Soc., Perkin Trans. 1*, **1980**, 1895.

[50] V. A. Yampol'skii, A. I. Mitichkin, E. P. Nikolova, Yu. K. Khudenskii, and V. G. Tishchenko, *Zh. Obsh. Khim.*, **43** (9), 2004 (1973).

[51] a) *Org. Synth. Coll. Vol.* **1**, 78.

b) St. V. Kostanecki and G. Rossbach, *Chem. Ber.*, **29**, 1488 (1896).

c) J. A. VanAllan and G. A. Reynolds, *J. Org. Chem.*, **33**, 1102 (1963).

[52] K. Akiyama, S. Kubota, and Y. Ikegami, *Chem. Lett.*, **1981**, 469.

[53] F. Pragst, A. Henrion,W. Abraham, and G. Miceal, *J. Prakt. Chem.*, **329**, 1071 (1987).

[54] a) M. S. Newman, *Organic Synthesis, Collect. Vol. 3*, 631 (1955).

b) R. H. Mitchell and V. Boekelheide, *J. Am. Chem. Soc.*, **96**, 1547 (1974).

[55] Kagaku Jiten, pp 821.

[56] H. O. House, D. Koepsell, and W. Jaeger, *J. Org. Chem.*, **38**, 1167 (1973).

[57] a) D. E. Seeger and J. A. Berson, *J. Am. Chem. Soc.*, **105**, 5144 (1983).

b) D. E. Seeger and J. A. Berson, *J. Am. Chem. Soc.*, **105**, 5146 (1983).

c) D. E. Seeger, P. M. Lahti, A. R. Rossi, and J. A. Berson, *J. Am. Chem. Soc.*, **108**, 1251 (1986).

[58] M. E. Rogers and B. A. Averill, *J. Org. Chem.*, **51**, 3308 (1986).

[59] MOPAC 6, J. J. P. Stewart, QCPE # 455.

[60] F. Ramirez and S. Dershowitz, *J. Org. Chem.*, **22**, 41 (1957).

[61] L. F. Fieser, M. Fieser, "*Reagents for Organic Synthesis*", Vol. 1, Wiley, New York, **1967**, 1030.

[62] E. J. Corey and J. W. Suggs, *Tetrahedron Lett.*, **1975**, 2647.

[63] A. P. Yakubov, D. V. Tsyganov, L. I. Belen'kii, and M. M. Krayushkin, *Tetrahedron*, **49**, 3397 (1993).

[64] S. Akiyama, S Misumi, and M. Nakagawa, *Bull. Chem. Soc. Jpn.*, **35**, 1829 (1962).

Chapter 3. Preparations and properties of 1,3- and 1,4-bis(2,4,6-triphenylpyridinyl-1-yl)benzene and 1,5-bis(2,4,6-triphenylpyridinyl-1-yl) naphthalene

3-1. Introduction

In the previous chapter, the bis-pyridinyl radicals linked by π-spacers at 4-positions of the pyridinyl ring were studied. In this chapter, the bis-pyridinyl radicals **6**-**8** linked at the nitrogen position are studied. The main purpose of this chapter is to compare the exchange interactions between the nitrogen-substituted bis-pyridinyl radicals **6**,**7** and the carbon-substituted ones **1**, **24**.

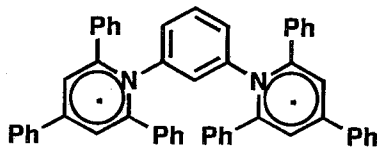

6

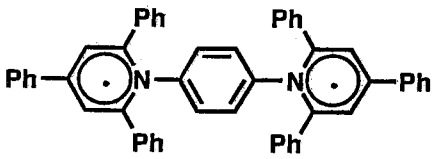

7

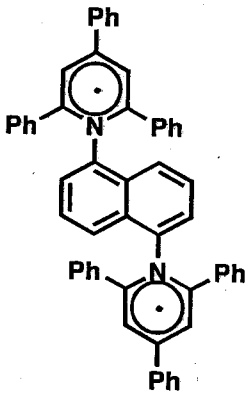

8

The unique features of **6** and **7** will become clear in the following consideration.

3-1-1. Bis-pyridinyl radicals 1 and 6

The diradical **1** was shown to have a triplet ground state or a singlet ground state with $\Delta E_{S\text{-}T} \approx 0$ in section 2-3. This result is compatible with the VB structures **1m**-1~**1m**-3 (section 1-4-2). The **1m**-1 structure has electron spins at the C-4 and C-4'-positions and lone pair electrons on the nitrogen atom. We may consider similar VB structures **6m**-1~**6m**-3 for **6**. In **6m**-1, two electron spins are separated by the two nitrogen atoms which do not have a net electron spin. Therefore, the spin-spin interaction may be small and the singlet and triplet energies may not be so different for **6m**.

The above argument is valid for the spin structure **6m**-1. Obviously, lone pair electrons on the nitrogen atoms delocalize in the whole molecule. Since many delocalization manners are possible, there are many VB structures. Furthermore, each VB canonical structure has a different contribution factor and a different energy. This is a big difference between heteroatomic systems and alternant hydrocarbon systems where a single spin-alternating non-ionic structure is the most stable. Such analysis allows to draw both singlet-stabilizing and triplet-stabilizing structures. For instance, **6m**-2 favors the triplet state and **6m**-3 favors the singlet state. Therefore, the spin prediction of the ground state is not easy.

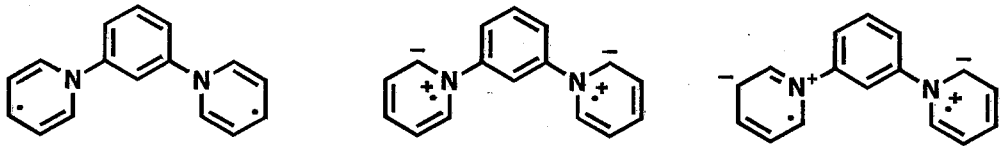

6m-1 **6m**-2 **6m**-3

3-1-2. Bis-pyridinyl radicals 24 and 7

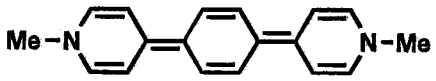

24m-1

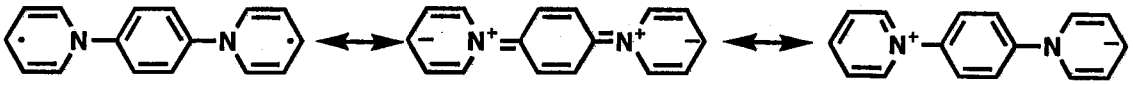

7m-1 **7m**-2 **7m**-3

The diradical **24** was shown to be a singlet ground state in section 2-4. This result can be easily explained by the ionic quinoid structure **24m**-1. However, similar quinoid-type non-ionic structures are difficult to draw for **7m**. Instead, a diradical structure **7m**-1 and an intramolecular electron transfer type ionic structure **7m**-2 (bis-ylide type) or **7m**-3 can be drawn. However, such ionic structures may have higher energies than the structure **7m**-1. In accordance with this qualitative consideration, the orbital energy gap (ΔE by Hückel MO)[45] between the two SOMOs is calculated to be small; **7m** (ΔE

= 0.16 β) compared to *p*-xylylene (ΔE = 0.62 β) and Thiele's hydrocarbon (ΔE = 0.31 β). This value 0.16 β is comparable to 10,10'-(*p*-phenylene)dithiadine dication (ΔE = 0.14 β) which was shown to have a stable triplet state.[42] The non-planar geometry with a large torsion angle between the pyridinyl radical and the *p*-phenylene spacer would further decrease the energy gap. Therefore, **7** may have a stable triplet state.

3-2. Syntheses of 1,3- and 1,4-bis(2,4,6-triphenylpyridinium-1-yl)benzene bis (tetrafluoroborate) [6^{2+}•2(BF_4^-) and 7^{2+}•2(BF_4^-)] and 1,5-bis(2,4,6-triphenyl-pyridinium-1-yl)naphthalene bis(tetrafluoroborate) [8^{2+}•2(BF_4^-)]

In order to synthesize the bispyridinium ions 6^{2+}, 7^{2+}, and 8^{2+}, the method of Katritzky et al.[49] was applied. This method is very useful compared to the procedure of N-alkylation of pyridines. The Katritzky method can be applied not only to secondary alkylamines but also to arylamines under mild conditions. For example, 1-*sec*-butyl-2,4,6-triphenylpyridinium tetrafluoro-borate was prepared from *sec*-butylamine and 2,4,6-triphenylpyrylium tetrafluoroborate in 81% yield at room temperature. In the case of the reaction of arylamines, for example aniline, 2.0 equivalents of triethylamine should be added to catalyze the nucleophilic attack of arylamine. 1,2,4,6-Tetraphenyl-pyridinium tetrafluoroborate can be prepared by this method in 77% yield at room temperature. Similarly, the bispyridinium ions 6^{2+}, 7^{2+}, and 8^{2+} were prepared from the corresponding diamines and 2.0 equivalents of 2,4,6-triphenylpyrylium in the presence of 4.0 equivalents of triethylamine in moderate yields (Scheme 3-1).

Scheme 3-1

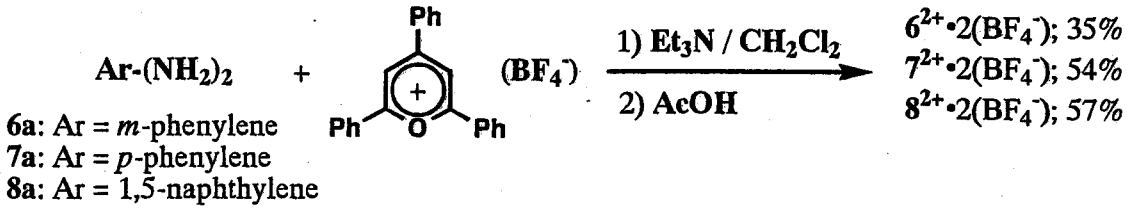

3-3. ^{1}H and ^{13}C chemical shifts of bispyridinium salts $6^{2+}\cdot 2(BF_4^-)$ and $7^{2+}\cdot 2(BF_4^-)$

Figure 3-1 shows an assignment of the ^{1}H and ^{13}C NMR chemical shifts for the bispyridinium ions 6^{2+} and 7^{2+}. These assignments are based on the C-H cosy and long range C-H cosy spectra of 6^{2+} and 7^{2+}. Bold letters show ^{13}C chemical shifts and plain letters show ^{1}H chemical shifts. As observed in the previous pyridinium ions, the signals of the C-4 and C-2(6) carbon of pyridinium rings appear at lower field than that of the C-3(5) carbon in the pyridinium ions. Because of the congested structure (overlapped phenyl rings) of these pyridinium ions, the ortho-protons of 2(6)-phenyl group appear at higher magnetic field region (7.01-6.99 for 6^{2+} and 7.24 for 7^{2+}). However, the signal of the ortho-protons of 4-phenyl group appears in the lower field (8.34 for 6^{2+} and 8.28 for 7^{2+}). Among the carbons of the central benzene ring, the N-substituted carbon appears at relatively low field (139.1 for 6^{2+} and 140.1 for 7^{2+}).

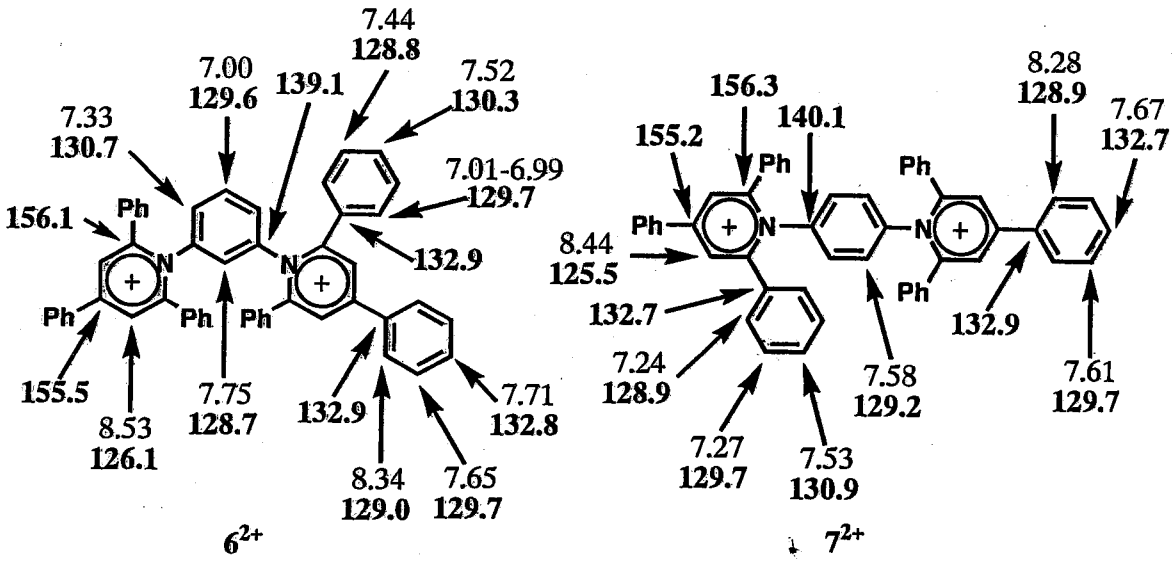

Figure 3-1. ^{1}H and ^{13}C chemical shifts of 6^{2+} and 7^{2+} (in DMSO-d_6).

3-4. Reduction potentials and absorption maximum in electronic spectra of bispyridinium salts $6^{2+}\cdot 2(BF_4^-)$, $7^{2+}\cdot 2(BF_4^-)$, and $8^{2+}\cdot 2(BF_4^-)$

Table 3-1 summarizes the reduction potentials and absorption maximum in the electronic spectra of the bispyridinium ions $\mathbf{6}^{2+}$, $\mathbf{7}^{2+}$, and $\mathbf{8}^{2+}$, along with those of 1,2,4,6-tetraphenylpyridinium ion $\mathbf{38}^{+}$. Because of their poor solubility, DMF was used as a solvent for the measurement of the reduction potentials. Cation $\mathbf{38}^{+}$ showed two reversible reduction potentials at -0.99 V and -1.16 V corresponding to cation ↔ radical and radical ↔ anion processes, respectively. These values are more positive than the reduction potentials of 1-methyl-2,4,6-triphenylpyridinium ion $\mathbf{16}^{+}$ (-1.20 V and -1.65 V). The ease of reduction for $\mathbf{38}^{+}$ indicates that the N-phenyl groups would stabilize the radical and anion species. Moreover, the difference between E_1 and E_3 for $\mathbf{38}^{+}$ (0.17 V) is much smaller than that for $\mathbf{16}^{+}$ (0.45 V). This may suggest that the pyridinyl radical **38** might not be cleanly prepared because of the further reduction.

Table 3-1. Reduction potentials [a, b] and absorption maxima of pyridinium salts.[c]

	E_1 / V	E_2 / V	E_3 / V	E_4 / V	λ_{max} / nm (ε x 10^{-4})
$\mathbf{38}^{+}\cdot(BF_4^-)$	-0.99		-1.16		307 (3.47)
$\mathbf{6}^{2+}\cdot 2(BF_4^-)$	-0.82	-0.99	-1.13	-1.36	316 (7.08)
$\mathbf{7}^{2+}\cdot 2(BF_4^-)$	-0.87	-1.00	-1.12	-1.33	315 (6.61)
$\mathbf{8}^{2+}\cdot 2(BF_4^-)$	-1.00		-1.47	-1.62	316 (7.33) ca. 220 (sh)

a) supporting electrolyte, 0.1 M tetrabutylammonium tetrafluoroborate; indicating electrode, glassy carbon; reference electrode, S. C. E.; scan rate, 100 mV / sec
b) in DMF c) in acetonitrile

The *m*-bispyridinium ion $\mathbf{6}^{2+}$ showed four reversible reduction waves at -0.82 V, -0.99 V, -1.13 V, and -1.36 V which correspond to dication ↔ cation radical, cation radical ↔ diradical, diradical ↔ anion radical, and anion radical ↔ dianion, respectively. The reversibility of the reduction indicates that the radical and anionic species are stable at least in CV time scale. The difference between E_2 and E_3 was again small (0.14 V). The *p*-bispyridinium ion $\mathbf{7}^{2+}$ also showed four reversible reduction potentials. If there were a stable quinoid structure in the diradical **7**, the difference between E_1 and E_2 of $\mathbf{7}^{2+}$ would be smaller than that of $\mathbf{6}^{2+}$. The similarity of the reduction potentials between $\mathbf{6}^{2+}$ and

7^{2+} indicates that the electronic structure of the diradical **7** resembles that of 6^{2+}. The 1,5-naphthalenediyl-linked bispyridinium ion 8^{2+} showed three reversible reduction potentials at -1.00 V, -1.47 V, and -1.62 V. The E_1 process of 8^{2+} is considered to involve a two-electron transfer corresponding to dication ↔ diradical because the integration of E_1 is about two times as large as that of E_3 and E_4.

The absorption maximum in the electronic spectrum of 38^+ is 307 nm and the molar absorptivity is 3.47 x 10^4 $cm^{-1}mol^{-1}L$. Compared with 16^+ (302 nm, 3.16 x 10^4 $cm^{-1}mol^{-1}L$), a small red shift and a hyperchromic effect are observed. This suggests that N-phenyl group of 38^+ participates in the electron delocalization. The absorption maximum of 6^{2+} is 316 nm, which is a little longer than 307 nm of 38^+. The molar absorptivity of 6^{2+} is about two times as large as that of 38^+. Dication 7^{2+} has a similar absorption and molar absorptivity to 6^{2+}. Dication 8^{2+} shows the absorption maximum at 316 nm. The molar absorptivity of 8^{2+} is a little larger than that of 6^{2+} and 7^{2+}. This may be partly due to the overlap of the pyridinium absorption with the naphthalene absorption (naphthalene: 220 nm (5.05), 272 nm (3.75), and 314 nm (2.15) in ethanol).

3-5. Electronic spectrum of 1,2,4,6-tetraphenylpyridinyl radical (38)

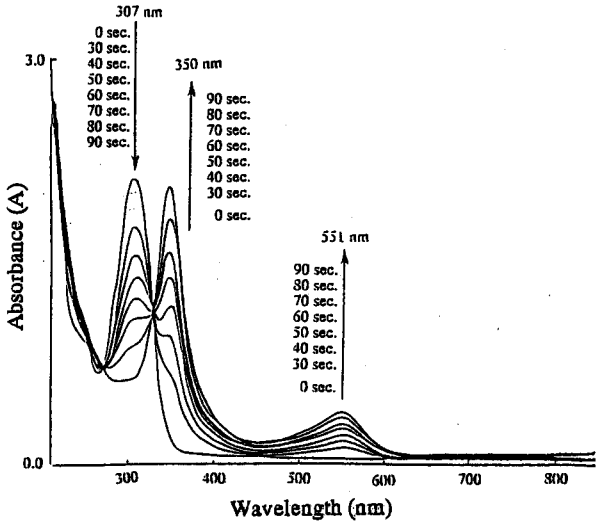

Figure 3-2. UV-vis spectral change upon reduction of $38^+ \cdot (BF_4^-)$ to form radical **38**.

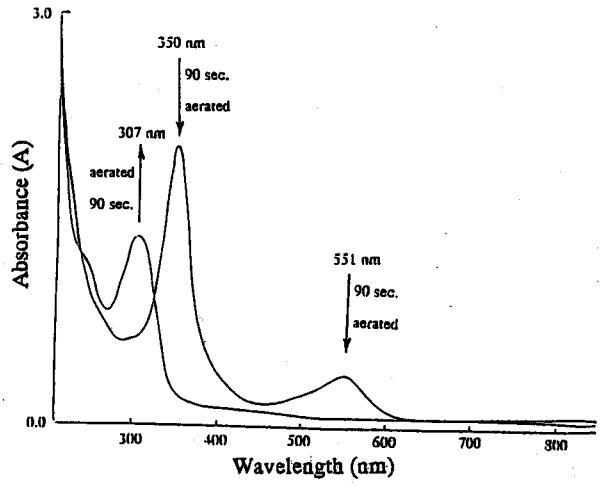

Figure 3-3. UV-vis spectral change when the solution of **38** was aerated.

Before the chemical reduction of the bispyridinium ions $\mathbf{6}^{2+}$, $\mathbf{7}^{2+}$, and $\mathbf{8}^{2+}$, 1,2,4,6-tetraphenylpyridinium $\mathbf{38}^{+}$ was reduced by 3% Na-Hg in acetonitrile at room temperature in order to know whether the pyridinyl radical **38** is cleanly prepared or not. Figure 3-2 shows the UV-vis spectral change upon the reduction of $\mathbf{38}^{+}$ in acetonitrile at room temperature. The colorless solution turned reddish purple and the absorptions at 350 nm and 551 nm increased as the reduction proceeded. This reddish purple species was assigned as the pyridinyl radical **38**. Two isosbestic points at about 275 nm and 340 nm suggests a clean conversion to radical **38**. When this reddish purple solution was aerated, the absorption due to the starting $\mathbf{38}^{+}$ was recovered by 67% of the original intensity (Figure 3-3).

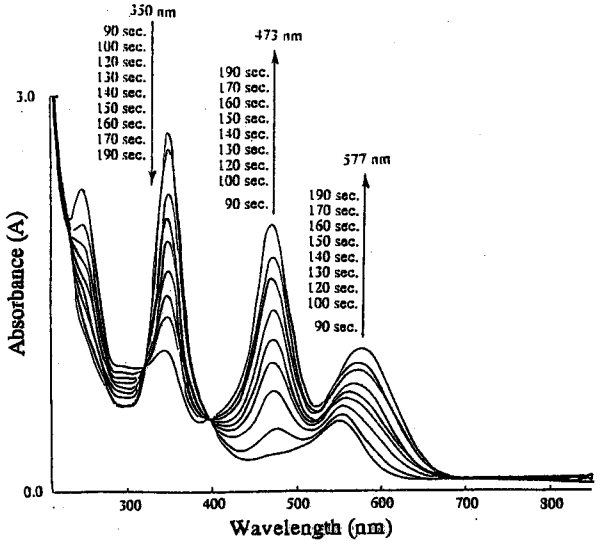

Figure 3-4. UV-vis spectral change when the solution of **38** was further reduced.

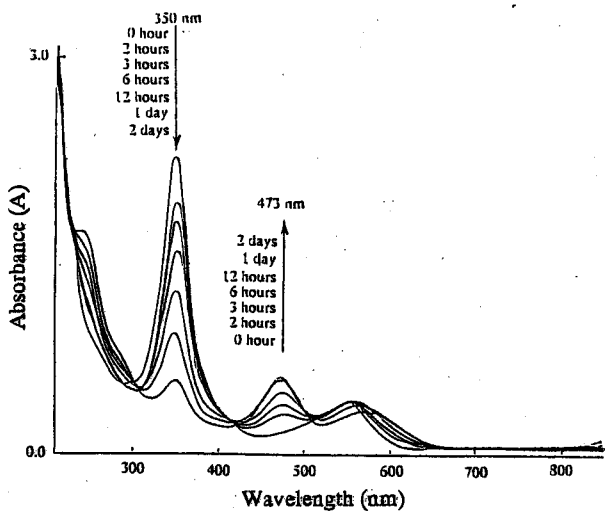

Figure 3-5. UV-vis spectral change when the solution of pyridinyl radical **38** was stood at room temperature.

Further reduction of the reddish purple solution gave a dark red solution. This color change accompanies the increase of the absorptions at 473 nm and 577 nm and the decrease of the 350 nm absorption (Figure 3-4). This reduction also cleanly proceeded as judged by the observation of the isosbestic points at about 320 nm and 390 nm. This dark red species would be anion $\mathbf{38}^{-}$. The formation of pyridinyl anion is characteristic for the reduction of N-phenylpyridinium compounds, since the anions were not observed for the previous N-methylpyridinium compounds. The radical **38** should be observable if the reduction is stopped when the absorption due to $\mathbf{38}^{+}$ almost disappear. This dark red solution did not reproduce $\mathbf{38}^{+}$ upon air oxidation. Surprisingly, when the solution of pyridinyl radical **38** was stood without contact with a bulk of Na-Hg under inert atmosphere at room

temperature, the absorption at 473 nm gradually increased while the intensity of the absorption at 350 nm decreased slowly (Figure 3-5). Although the reason for such a spectral change is not clear at present, the presence of a small amount of reductant impurity (small amount of sodium) in the filtered solution may account for the observation.

3-6. Electronic spectra of bis-pyridinyl radicals 6, 7, and 8

3-6-1. Electronic spectra for the reduction of bispyridinium salt 6^{2+}•2(BF_4^-)

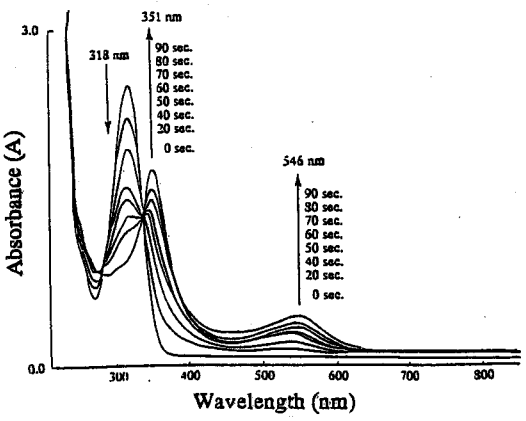

Figure 3-6. UV-vis spectral change upon reduction of 6^{2+}•2(BF_4^-) to form diradical **6**.

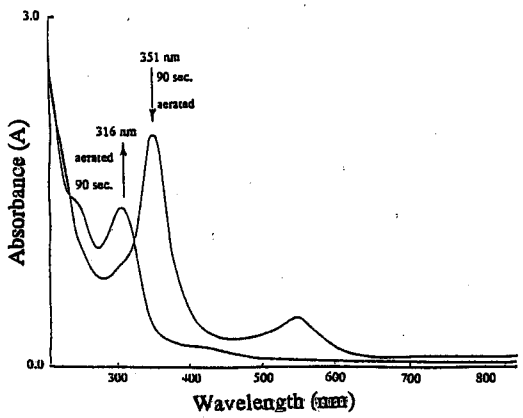

Figure 3-7. UV-vis spectral change when the solution of **6** was aerated.

The UV-vis spectral change upon the reduction of 6^{2+} in MTHF-acetonitrile (1:1 v/v) at room temperature is shown in Figure 3-6. The colorless solution of 6^{2+} turned reddish purple and the intensity of the absorptions at 351 nm and 546 nm increased as the reduction proceeded. The two isosbestic points at about 275 nm and 340 nm were also observed. The reduction was stopped when the absorption due to 6^{2+} at 318 nm almost disappeared. The resulted species (351, 546 nm) was assigned as diradical **6** and was subjected to the ESR measurement (section 3-7-1). Upon exposure of this solution to air, the starting absorption was recovered by 53% of the original intensity (Figure 3-7). When this solution was further reduced, the solution turned dark red with increase of the absorptions at 476 nm and 575 nm (Figure 3-8). These absorptions are assignable to the bis-pyridinyl anion 6^{2-}. Slow conversion of **6** to 6^{2-} or 6^{-} without contact with a bulk of Na-Hg was again observed.

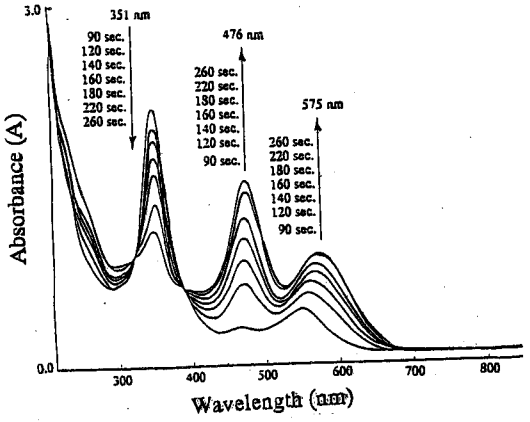

Figure 3-8. UV-vis spectral change when the solution of **6** was further reduced.

3-6-2. Electronic spectra for the reduction of bispyridinium salt $7^{2+}\cdot 2(BF_4^-)$

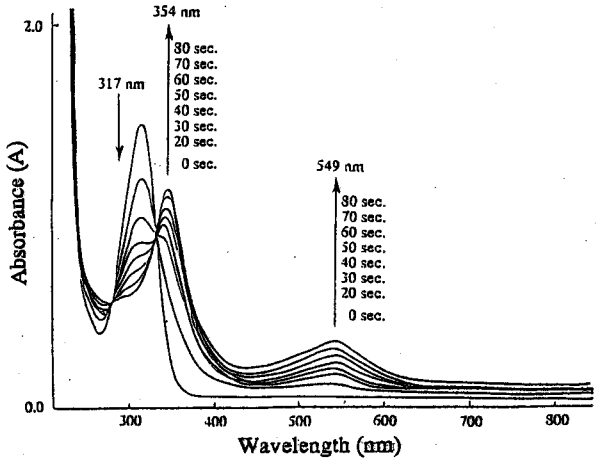

Figure 3-9. UV-vis spectral change upon reduction of $7^{2+}\cdot 2(BF_4^-)$ to form diradical **7**.

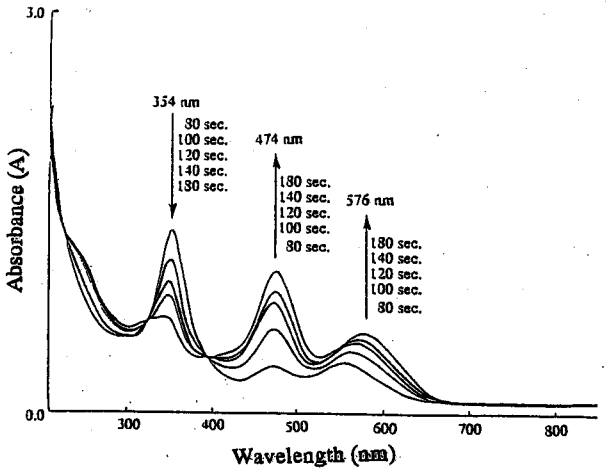

Figure 3-10. UV-vis spectral change when the solution of **7** was further reduced.

Interestingly, the similar behaviors were observed in the reduction of *p*-isomer 7^{2+}. Figure 3-9 shows UV-vis spectral change upon the reduction of 7^{2+} in MTHF-acetonitrile (1:1 v/v) at room temperature. The colorless solution of 7^{2+} turned reddish purple with increase of the absorptions at 354 nm and 549 nm which is assignable to **7**. The similarity of the diradical absorptions between **6** and **7** strongly indicates that **7** is in a diradical form and not in a quinoid form. When this reddish purple species was exposed to air, the absorption of the starting material was recovered by 47% of the original intensity. On the other hand, when this reddish purple solution was further reduced with 3% Na-Hg, the solution turned dark red with increase of the absorptions at 474 nm and 576 nm, which is assignable

to 7^{2-} (Figure 3-10). When the filtered solution containing diradical **7** was stood at room temperature, the absorptions due to the anionic species again appeared.

3-6-3. Electronic spectra for reduction of bispyridinium salt $8^{2+}\cdot 2(BF_4^-)$

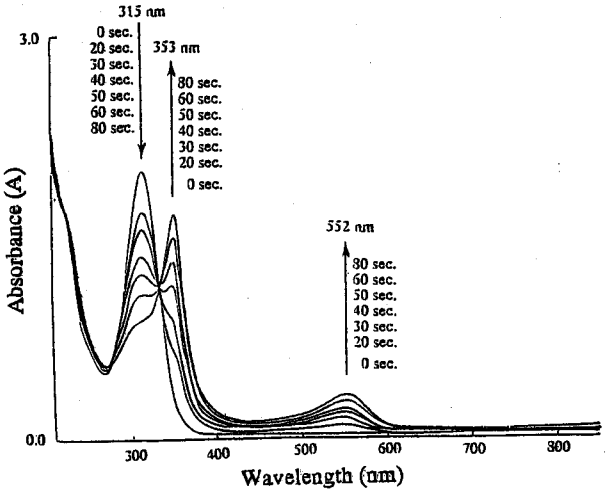

Figure 3-11. UV-vis spectral change upon reduction of $8^{2+}\cdot 2(BF_4^-)$ to form diradical **8**.

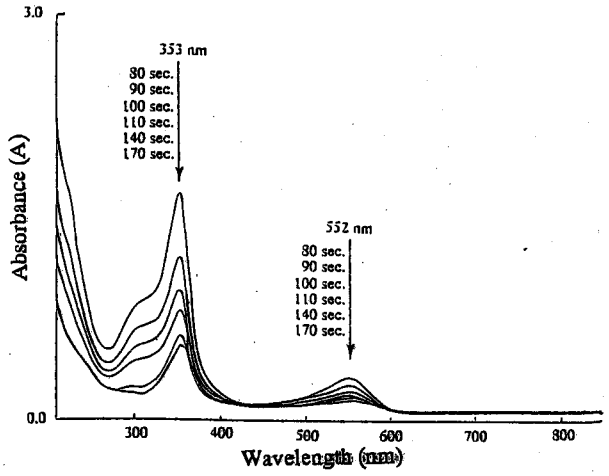

Figure 3-12. UV-vis spectral change when the solution of **8** was further reduced.

Figure 3-11 shows UV-vis spectral change upon the reduction of bispyridinium ion 8^{2+} in acetonitrile at room temperature. The colorless solution of 8^{2+} also turned reddish purple and the absorptions appeared at 353 nm and 552 nm which were assigned to the diradical **8**. When the diradical solution was exposed to air, the absorption due to the starting 8^{2+} was recovered by 74% of the original intensity. This diradical solution was very stable in the sealed tube. After seven days, the diradical absorptions remained with the 71% intensity, somehow accompanying the increase of the absorption of the starting pyridinium ion. In addition, further reduction of the diradical **8** did not produce longer absorptions due to the anionic species (Figure 3-12). The latter result may be in accordance with the instability of the pyridinyl anions 8^{2-} as indicated by the reduction potentials (3-4); the reduction potentials for the formation of anion (38^-) or anion radicals (6^-, 7^-, and 8^-) are -1.16, -1.13, -1.12, and -1.47 V *vs.* SCE, respectively. The formation of anion 8^- requires an extra negative potential by 0.35 V in comparison with that for 6^- and 7^-. The observation of cationic species from **8** is in sharp contrast to the formation of anionic species for **38**, **6**, and **7**. Since the spectral change for **8**

leading to 8^{+} or 8^{2+} is considerably slower (day ~ a weak) than that for **38**, **6**, and **7** (hours), the reason of these phenomena may not be identical and not clear at present.

3-7. ESR spectra of 1,3- and 1,4-bis(2,4,6-triphenylpyridinyl-1-yl)benzene (6 and 7) and 1,5-bis(2,4,6-triphenylpyridinium-1-yl)naphthalene (8)

3-7-1. ESR spectrum of diradical 6

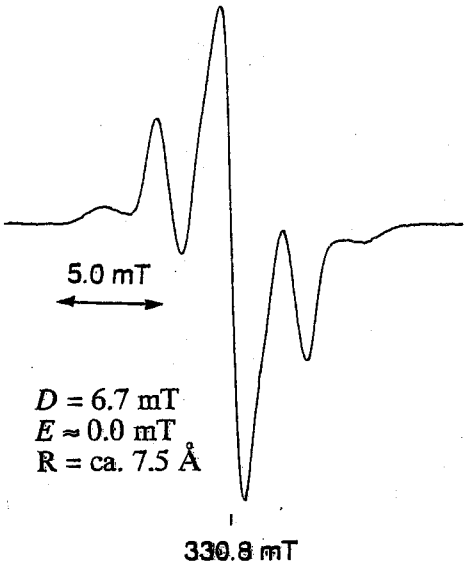

Figure 3-13. ESR spectrum of diradical **6** in MTHF-acetonitrile at 77 K.

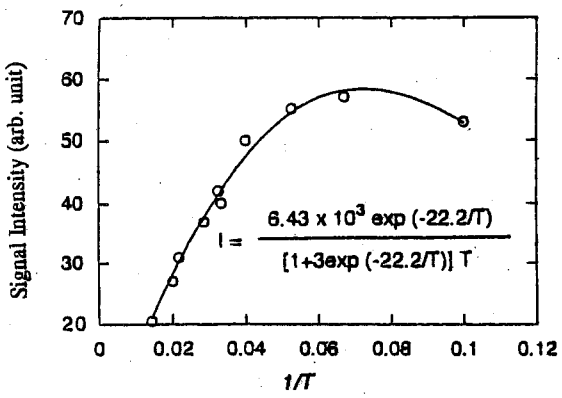

Figure 3-14. Temperature dependence of signal intensity of the axial z-components of **6**.

The ESR spectrum of diradical **6** in MTHF-acetonitrile (1:1 v/v) at 77 K is shown in Figure 3-13. A typical pattern for randomly oriented triplet species was observed. The zero-field splitting parameters *D* and *E* were 6.7 mT and 0.0 mT, respectively. A signal due to $\Delta M_S = \pm 2$ transition was observed at the lower temperature (ca. 5 K) in the half magnetic field region. The averaged distance between the radical centers was estimated to be 7.5 Å by the point dipole approximation. This distance suggests that the radical centers of **6** locate near the centers of the pyridinyl rings; the distance between the two nitrogen atoms is ca. 5 Å and the distance between the 4-positions of the two 4-pyridinyl rings is ca. 10 Å.

Temperature dependence of the signal intensity of the axial z-components of **6** is shown in Figure 3-14. The plots for the diradical **6** gave a convex curve which indicates that diradical **6** has a singlet ground state. The energy difference between the singlet and triplet states was estimated to be 44 cal/mol. The singlet nature of **6** can be explained mainly by the following two reasons.

a) electronic effect

As considered in the introduction of this chapter (3-1-1), the diradical **6** has VB canonical model-structures **6m**-1~3, which would place both triplet **6m**-T and singlet **6m**-S1 states in nearly degenerate level. Furthermore, the singlet state would be stabilized by the mixing of ionic structure (**6m**-S4). These model analyses do not take into consideration whether **6m** has a large dihedral angle between the spin sources and the central benzene ring or not. Since the triplet state is destabilized by the large dihedral angle, the same analysis can be expanded for 2,4,6-triphenylsubstituted **6**. Furthermore, as noted in the UV-vis spectrum of **6**, the pyridinyl anion $\mathbf{6}^{2-}$ is stable species, which suggests that stabilization in the singlet state by the mixing of the ionic structure **6m**-S2 is likely.

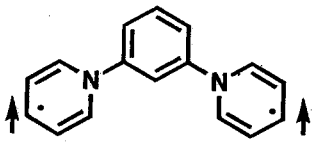

6m-T

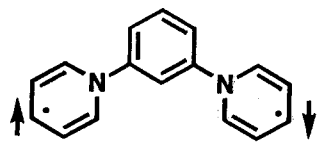

6m-S1

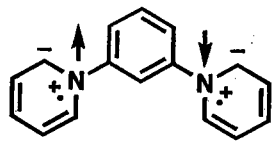

6m-S2

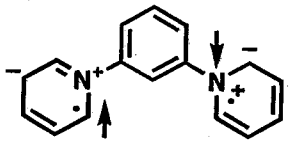

6m-S3

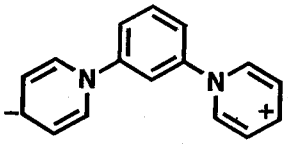

6m-S4

b) dihedral angle effect

Application of the idea described in section 1-3-4 to the present bis-pyridinyl radical **6** seems to be reasonable since **6** has relatively large dihedral angles (58° and 69° for singlet **6**, two 55° for triplet **6** by AM1-CI calculation[59]). Therefore, the singlet nature of **6** is also accountable by the dihedral angle effect.

The differentiation between the electronic and the dihedral angle effects is difficult at present.

3-7-2. ESR spectrum of diradical 7

As expected from the diradical formation in the UV-vis spectrum, **7** showed a typical triplet pattern (Figure 3-15). The zero-field splitting parameters were D = 5.5 mT and E = 0.3 mT. In addition, a weak signal due to ΔMs = ± 2 transition was also observed at low temperature (ca. 5 K).

Temperature dependence of the signal intensity of the axial z-components was shown in Figure 3-16. The convex curve in the figure indicates that **7** has a singlet ground state. ΔE_{S-T} is calculated to be 51 cal/mol.

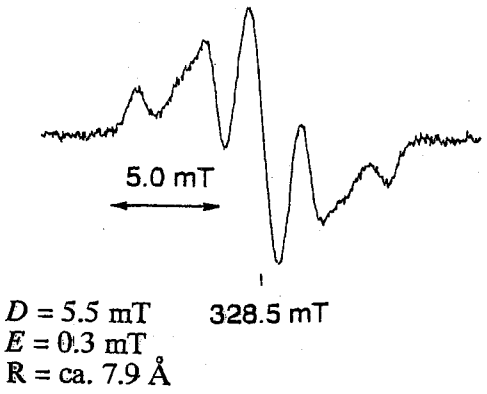

Figure 3-15. ESR spectrum of diradical **7** in MTHF-acetonitrile at 77 K.

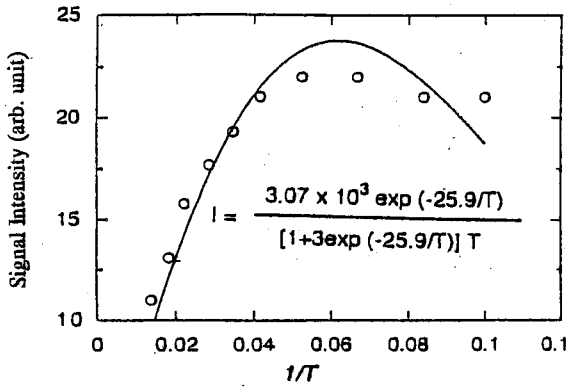

Figure 3-16. Temperature dependence of signal intensity of the axial z-components of **7**.

As discussed in the previous section, two explanations are possible.

a) <u>electronic effect</u>

As considered in the section 3-1-2, the model diradical has a main VB structure of **7m**-1 where two spins are separated by the non-spin-carrying nitrogen atoms. In this electronic configuration, the triplet (**7m**-T) and the singlet (**7m**-S1) would have similar energies. The mixing of ionic spin structures **7m**-S2 and **7m**-S3 would stabilize the singlet state. The stability of the pyridinyl anionic species was experimentally shown in the previous sections. These considerations accord with the observations; 1) **7** has a stable triplet state, but 2) the ground state of **7** is a singlet state.

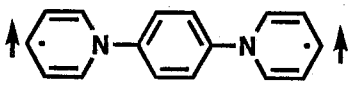

7m-T

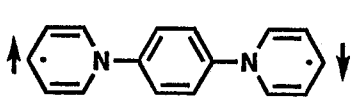

7m-S1

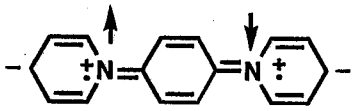

7m-S2

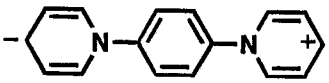

7m-S3

b) dihedral angle effect

If the dihedral angle between *p*-phenylene plane and pyridinyl plane is almost 90°, the singlet and triplet states are almost degenerate in *p*-orbital interaction sense (This idea does not relate to whether the nitrogen atom has a net spin or not.). The orbital interaction through σ-bond may favor the singlet state, although the orbital interaction through σ-bond of *p*-phenylene spacer might be smaller than that through σ-bond of *m*-phenylene spacer. In this context, bis(phenothiazine cation) linked by *p*-phenylene spacer **39**, which has almost perpendicular geometry, has been reported to have a triplet ground state or a singlet ground state with $\Delta E_{S-T} < 10$ cal/mol.[42]

The diradical **7** would have a large torsion angle (two 59° for the singlet, 55° and 70° for the triplet state by AM1-UHF calculation[59]). These intermediate dihedral angles indicate several mode of orbital interactions. Since the orbital interaction through σ-bond of *p*-phenylene spacer is considered to be small as judged from the results of **39**, the low-spin nature of **7** would be ascribable to the π-face interaction through *p*-topology.

3-7-3. ESR spectrum of the diradical 8

The ESR spectrum of diradical **8** in MTHF-acetonitrile (1:1 v/v) at 77 K are shown in Figure 3-17. A typical triplet pattern was observed and the zero-field splitting parameters *D* and *E* were determined as 4.4 mT and 0.0 mT, respectively. The averaged distance between the two radical centers was estimated

to be 8.5 Å by the point dipole approximation. This distance was a little longer than that of diradical **6** and would be reasonable. The determination of the ground state was not pursued.

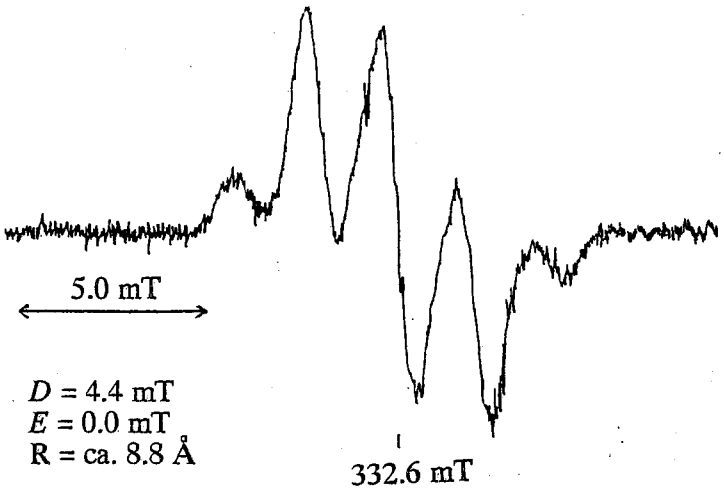

Figure 3-17. ESR spectrum of diradical **8** in MTHF-acetonitrile at 77 K.

3-8. Summary

1) The nitrogen substituted *m*-phenylene- and *p*-phenylene-linked bispyridinium ions ($\mathbf{6}^{2+}$ and $\mathbf{7}^{2+}$) and 1,5-bis(2,4,6-triphenylpyridinium-1-yl)naphthalene ($\mathbf{8}^{2+}$) were synthesized. They had reversible reduction potentials. Particularly, dications $\mathbf{6}^{2+}$ and $\mathbf{7}^{2+}$ had more positive reduction potentials corresponding to the formation of dianionic species than $\mathbf{8}^{2+}$ or N-methylpyridinium cations, suggesting that $\mathbf{6}^{2-}$ and $\mathbf{7}^{2-}$ is stable.

2) 1,2,4,6-Tetraphenylpyridinium ion $\mathbf{3}^{+}$, bispyridinium ions $\mathbf{6}^{2+}$, and $\mathbf{7}^{2+}$ afforded the corresponding radical and diradical by the reduction with 3% Na-Hg. Moreover, the corresponding anionic or dianionic species were observed by further reduction in their electronic spectra. Dication $\mathbf{8}^{2+}$ could be reduced to the corresponding diradical, but the corresponding anionic or dianionic species could not be observed in the electronic spectrum.

3) The triplet states of the bis-pyridinyl radicals **6**, **7**, and **8** were all observed in MTHF-acetonitrile (1:1 v/v) at 77 K by ESR spectroscopy. The zero-field splitting parameters D and E were; D = 6.7 mT, $E \approx 0.0$ mT for **6**, D = 5.5 mT, E = 0.3 mT for **7**, and D = 4.4 mT, $E \approx 0.0$ mT for **8**.

4) The diradicals **6** and **7** had singlet ground states and the energy differences between the singlet and triplet ground states were 44 cal/mol and 51 cal/mol, respectively. The singlet nature of the *m*-phenylene-linked diradical **6** and the low lying triplet state of the *p*-isomer **7** reveals the unique character of these pyridinyl radicals. Two explanations based on electronic effect and/or dihedral angle effect were presented.

3-9. Experimental section

Materials and Solvents:

Diamines **6a~8a** and acetic acid were commercially available and used without further purification. Methylene chloride and triethylamine were distilled from calcium hydride. 1,2,4,6-Tetraphenylpyridinium tetrafluoroborate[49a] were prepared as described in the literature.

General procedure for the synthesis of dipyridinium salts $6^{2+}\cdot 2(BF_4^-)$~$8^{2+}\cdot 2(BF_4^-)$

A solution of the corresponding diamine, 2.0 equivalents of 2,4,6-triphenylpyrylium tetrafluoroborate and 4.0 equivalents of triethylamine in methylene chloride was stirred overnight at room temperature. 8.0 Equivalents of acetic acid was added to the reaction mixture and the reaction mixture was stirred for an hour at room temperature. After concentration, ethanol was added to deposit the target bispyridinium salts in moderate yields (Scheme 5-1).

$6^{2+}\cdot 2(BF_4^-)$: colorless needles (from C_2H_5OH); mp 209-211 °C; FAB MS *m/z* 777 (M^+-BF_4), 690 [M^+-2(BF_4)], 383 [M^+-2(BF_4)-triphenylpyridine]; ^{1}H-NMR (500 MHz, DMSO-d_6) δ 8.53 (s, 4H), 8.34 (d, 4H, *J* = 7.6 Hz), 7.75 (t, 1H, *J* = 2.0 Hz), 7.71 (t, 2H, *J* = 7.6 Hz), 7.65 (t, 4H, *J* = 7.6 Hz), 7.52 (t, 4H, *J* = 7.8 Hz), 7.44 (t, 8H, *J* = 7.8 Hz), 7.33 (dd, 2H, *J* = 8.2 Hz, 2.0 Hz), 7.00 (d, 8H, *J* = 7.8 Hz), 7.00 (t, 1H, *J* = 8.2 Hz); ^{13}C-NMR (125 MHz, DMSO-d_6) δ 156.1, 155.5, 139.1, 132.89, 132.87, 132.8, 130.7, 130.3, 129.7, 129.6, 129.0, 128.8, 128.7, 126.1; IR (KBr) 3056 (m), 1619 (s), 1594 (s), 1556 (s), 1494 (m), 1458 (w), 1414 (m), 1359 (w), 1243 (w), 1062 (bs), 889 (w), 767 (s), 701 (s), 533 (w) cm^{-1}; UV (CH_3CN) λ_{max} / nm (log ε) 316 (4.85); FAB HRMS *m/z* Calcd for $C_{52}H_{38}N_2BF_4$: 777.3064. Found: 777.3074.

$7^{2+}\cdot 2(BF_4^-)$: colorless prisms (from CH_3CN); mp > 300 °C; FAB MS *m/z* 777 (M^+-BF_4), 690 [M^+-2(BF_4)], 383 [M^+-2(BF_4)-triphenylpyridine]; ^{1}H-NMR (500 MHz, DMSO-d_6) δ 8.44 (s, 4H), 8.28 (d, 4H, *J* = 7.5 Hz), 7.67 (tt, 2H, *J* = 7.5 Hz, 1.5 Hz), 7.61 (t, 4H, *J* = 7.5 Hz), 7.58 (s, 4H), 7.53 (tt, 4H, *J* = 7.7 Hz, 1.5 Hz), 7.27 (t, 8H, *J* = 7.7 Hz), 7.24 (dd, 8H, *J* = 7.7 Hz, 1.5 Hz); ^{13}C-NMR (125 MHz, DMSO-d_6) δ 156.3, 155.2, 140.1, 132.9, 132.7, 132.2, 130.9, 129.7, 129.2, 128.9,

128.4, 125.5; IR (KBr) 3056 (m), 1626 (s), 1560 (s), 1497 (s), 1459 (w), 1412 (m), 1362 (m), 1228 (m), 1040 (bs), 888 (w), 763 (s), 699 (s), 612 (w), 561 (w), 522 (w) cm^{-1}; UV (CH_3CN) λ_{max} / nm (log ε) 315 (4.82); FAB HRMS *m/z* Calcd for $C_{52}H_{38}N_2BF_4$: 777.3064. Found: 729.3085.

8^{2+}•2(BF_4^-): colorless crystals (from C_2H_5OH); mp > 300 °C; FAB MS *m/z* 827 (M^+-BF_4), 740 [M^+-2(BF_4)], 433 [M^+-2(BF_4)-triphenylpyridine]; ^{1}H-NMR (270 MHz, CD_3CN) δ 8.36 (s, 4H), 8.10 (dt, 4H, *J* = 6.4 Hz, 1.8 Hz), 7.84 (dd, 2H, *J* = 6.1 Hz, 2.5 Hz), 7.72-7.63 (m, 6H), 7.41-7.39 (m, 6H), 7.35 (t, 2H, *J* = 4.3 Hz), 7.11-7.09 (m, 16H); ^{13}C-NMR (67.8 MHz, CD_3CN) δ 158.7, 158.2, 136.0, 134.6, 133.9, 132.9, 131.8, 131.3, 130.9, 129.8, 129.7, 129.2, 127.8, 127.5, 126.1; IR (KBr) 3056 (w), 1621 (s), 1598 (s), 1556 (s), 1495 (m), 1447 (w), 1416 (m), 1359 (m), 1243 (m), 1185 (m), 1061 (bs), 887 (w), 806 (w), 765 (s), 701 (s), 533 (w) cm^{-1}; UV (CH_3CN) λ_{max} / nm (log ε) 316 (4.87); FAB HRMS *m/z* Calcd for $C_{56}H_{40}N_2BF_4$: 827.3221. Found: 827.3265.

Chapter 4. Preparation and exchange interaction of bis(2,4,6-triphenylpyridinyl-1-yl)diradicals linked with polymethylene and 1,4-*trans*-cyclohexanediyl spacer

4-1. Introduction

In the previous chapters, several bis-pyridinyl radicals linked by π-spacers were investigated. This chapter focuses on the exchange interaction between the pyridinyl radicals linked by σ-frames. Although some bis-pyridinyl radicals linked by σ-spacer have been prepared and their ESR studies have been reported, the study on their exchange interaction including the determination of the ground state has never been reported. For other radicals, relatively little study for σ-linked diradicals has been carried out.

Ullman et al. reported on the dimethylene- and trimethylenebis(nitronyl nitroxide) diradicals **40** and **41**.[65] The ESR spectrum of **40** or **41** in a mixture of toluene and methylcyclohexane frozen in a

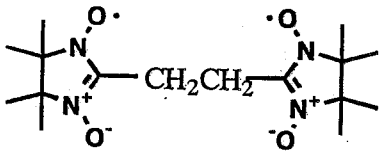

40

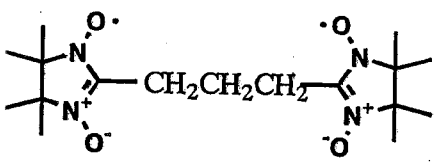

41

rigid glass showed a normal six-line pattern which was expected for diradicals with nonvanishing E values. Half-field resonances were also observed. The zero-field splitting parameters were D = 22.3 mT and E = 2.5 mT for **40** and D = 21.2 mT and E = 1.2 mT for **41**. The large D values indicate that the two heterocyclic rings must be relatively close to one another. A plot of susceptibility shifts *vs.* its concentration (Figure 4-1) indicates that the diradical **40** has a singlet ground state with a thermally accessible triplet state. The energy difference of the singlet and triplet states was estimated to be at least 340 cal/mol from the temperature dependence of the NMR contact shift (Figure 4-2). Diradical **41** was also shown to be in a singlet state with $\Delta E_{S\text{-}T} \approx 200$ cal/mol.

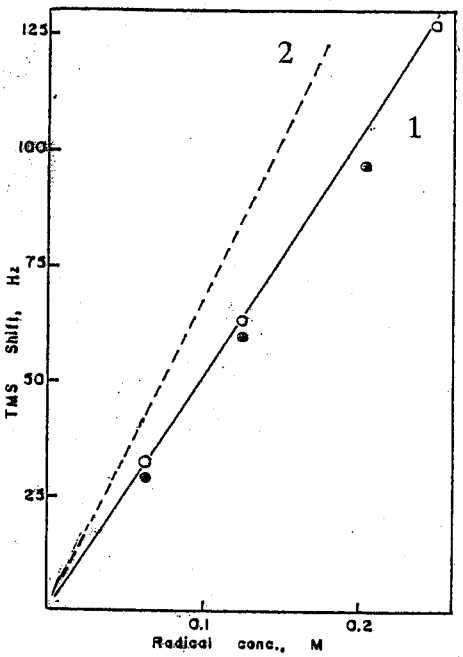

Figure 4-1. Susceptibility shifts for diradicals at 297 K: (1) theoretical line for diradical with RT > ΔE, (2) theoretical line for triplet; ○, diradical **40**; ●, diradical **41**.

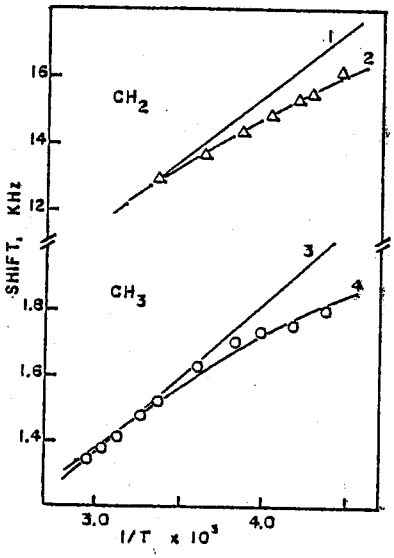

Fig. 4-2. Contact NMR shift temperature dependence for diradical **40**: △, methylene protons; ○, methyl protons; (1) and (3) predicted behavior when RT >> ΔE; (2) line predicted when a (CH_2) = -0.956 G, ΔE = 340 cal/mol, and ΔS = 2.62 eu; (4) line predicted when a (CH_3) = -0.112 G, ΔE = 409 cal/mol, and ΔS = 2.84 eu.

In our laboratory, the trimethylenebisphenoxide radical **43** was generated by photodissociation of the corresponding cyclomer **42**.[66] The zero-field splitting parameters *D* and *E* were 9.9 mT and 0.0 mT, respectively.

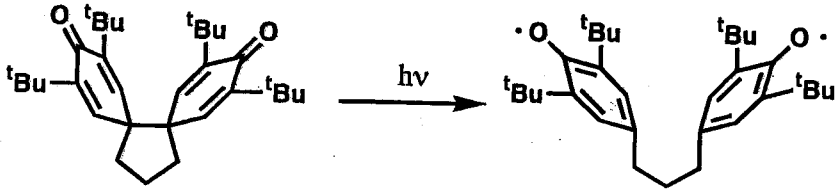

42 **43**

As to the pyridinyl radicals, Kosower and Ikegami reported an ESR spectrum of a dimethylene-linked bis-pyridinyl radical in 1967.[30] Later, Ikegami and co-workers generated dimethylene- and trimethylene-linked bis-pyridinyl radicals from photolysis of their cyclomers.[32] These studies focussed on the identification of these diradicals, including the monomer-dimer equilibrium and the reactivity of the cyclomers. The exchange interaction of these diradicals has not been reported. However, it is expected that the exchange interaction is dependent on the σ-frame structure. In

connection with the previous studies of the bis-pyridinyl radicals incorporated in π-frames, the exchange interaction of σ-framed bis-pyridinyl radicals are studied in this chapter.

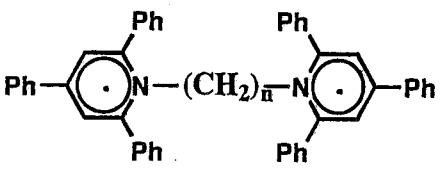

9: n = 2
10: n = 3
11: n = 4
12: n = 5
13: n = 6
14: n = 8

4-2. Preparations of 1,1'-(1,n-alkanediyl)bis(2,4,6-triphenylpyridinium-1-yl)bis (tetrafluoroborate) [9^{2+}•2(BF_4^-) to 14^{2+}•2(BF_4^-)]

As shown in Scheme 4-1, the bispyridinium ions 9^{2+}-14^{2+} were synthesized from the corresponding diamines and 2,4,6-triphenylpyrylium by applying the method described in section 3-2. A mixture of diamines and 2,4,6-triphenylpyrylium (2.0 equiv.) in the presence of triethylamine (4.0 equiv.) in chloroform was refluxed overnight. After the solution was cooled, acetic acid (8.0 equiv.) were added and the reaction mixture was stirred for an hour at room temperature. After evaporation of the solvent, ethanol was added to the residue to crystallize the desired bispyridinium salts. The isolated yields are given in Scheme 4-1. Lower yield with decreasing the carbon number of the methylene chain is ascribed to the difficulty of the crystallization.

Scheme 4-1

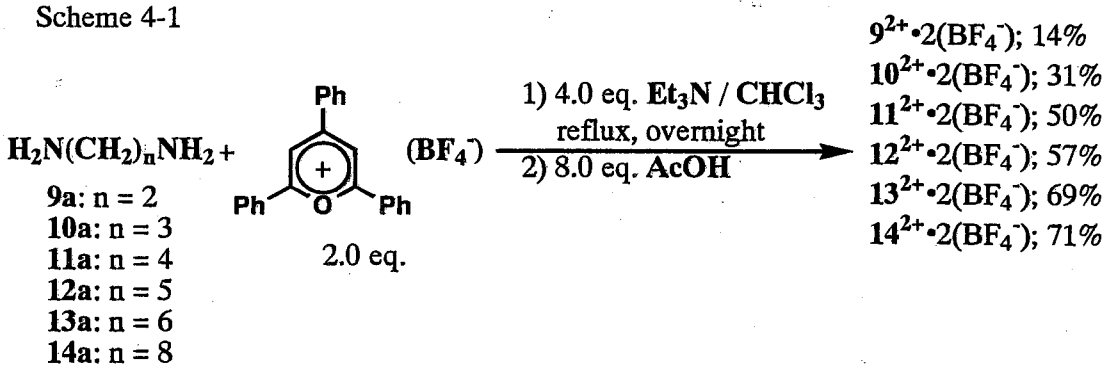

4-3. ^1H and ^{13}C chemical shifts of bispyridinium salts 9^{2+}•2(BF_4^-)-14^{2+}•2(BF_4^-)

Table 4-1. ^{1}H chemical shifts (δ ppm) of bispyridinium ions $\mathbf{9}^{2+}$ to $\mathbf{14}^{2+}$ in CD_3CN.

	H-3 (pyridinium)	N-CH_2	N-CH_2CH_2	N-$(CH_2)_2CH_2$	N-$(CH_2)_3CH_2$	H_o, H_m, H_p (2, 6-phenyl group)	H_o, H_m, H_p (4-phenyl group)
$\mathbf{9}^{2+}$	8.01 (s)	4.73 (s)				7.13 (d), 7.56 (t), 7.74-7.62 (m)	8.04 (d), 7.74-7.62 (m), 7.74-7.62 (m)
$\mathbf{10}^{2+}$	8.06 (s)	3.78-3.74 (m)	1.68-1.66 (m)			7.38-7.36 (m), 7.62-7.56 (m), 7.70-7.64 (m)	7.95 (dt), 7.62-7.56 (m), 7.70-7.64 (m)
$\mathbf{11}^{2+}$	8.09 (s)	3.74-3.72 (m)	0.86-0.84 (m)			7.49-7.46 (m), 7.65-7.59 (m), 7.75-7.71 (m)	7.95 (dt), 7.65-7.59 (m), 7.65-7.59 (m)
$\mathbf{12}^{2+}$	8.14 (s)	3.99 (t)	0.92 (quintet)	0.10 (t)		7.58-7.56 (m), 7.67-7.61 (m), 7.67-7.61 (m)	7.98 (dt), 7.67-7.61 (m), 7.67-7.61 (m)
$\mathbf{13}^{2+}$	8.14 (s)	4.07-4.01 (m)	1.14-1.09 (m)	0.17-0.15 (m)		7.68-7.59 (m), 7.68-7.59 (m), 7.68-7.59 (m)	7.97 (dt), 7.68-7.59 (m), 7.68-7.59 (m)
$\mathbf{14}^{2+}$	8.17 (s)	4.24-4.18 (m)	1.32-1.24 (m)	0.54-0.46 (m)	0.43-0.36 (m)	7.70-7.63 (m), 7.70-7.63 (m), 7.70-7.63 (m)	7.98 (dt), 7.70-7.63 (m), 7.70-7.63 (m)
$\mathbf{16}^{+}$	8.20 (s)	3.76 (s)				7.74-7.60 (m), 7.74-7.60 (m), 7.74-7.60 (m)	8.01 (dt), 7.74-7.60 (m), 7.74-7.60 (m)

Table 4-1 and 4-2 show the ^{1}H and ^{13}C chemical shifts of the bispyridinium ions $\mathbf{9}^{2+}$-$\mathbf{14}^{2+}$ with a reference ion $\mathbf{16}^{+}$. As shown in Table 4-1 (^{1}H-NMR), a lower magnetic field shift of H-3(5) proton of the pyridinium ring was observed with increasing the carbon number of the spacer though the shift is small. A similar lower magnetic field shift of *o*-protons of 2,6-phenyl groups was also observed. These observations may suggest that there are some intramolecular overlap between 2(6)-phenyl group in one pyridinium ring and 2'(6')-phenyl group in the other pyridinium ring in the shorter methylene compounds.

As shown in Table 4-2 (^{13}C-NMR), the chemical shift of the C-4 carbon in the pyridinium ring slightly shifts to higher field as the number of methylene carbon increases. On the other hand, the signal of the N-$\underline{C}H_2$ carbon moves to lower field with increase of n for $3 \leq n \leq 8$. This chemical shift difference suggests that a longer methylene chain behaves as a better electron donor to dilute the cationic charge of the two pyridinium rings; the longer the methylene chain, the more the cationic charge at the C-4 carbon is diluted and the N-$\underline{C}H_2$ carbon becomes cationic. The chemical shift of N-$\underline{C}H_2$ carbon of $\mathbf{9}^{2+}$ (n = 2) deviates from this relation probably because the inductive effect of the two pyridinium ring directly influences the electron density of this carbon.

Table 4-2. ^{13}C chemical shifts (δ ppm) of bispyridinium ions $\mathbf{9}^{2+}$ to $\mathbf{14}^{2+}$ in CD_3CN.

	C-2(6) (pyridinium)	C-4 (pyridinium)	N-$\underline{C}H_2$	N-$CH_2\underline{C}$	N-$(CH_2)_2\underline{C}$	N-$(CH_2)_3\underline{C}$
$\mathbf{9}^{2+}$	157.1	157.6	53.6			
$\mathbf{10}^{2+}$	156.6	156.2	51.3	29.7		
$\mathbf{11}^{2+}$	156.7	155.9	53.3	25.9		
$\mathbf{12}^{2+}$	156.8	155.8	54.5	28.6	22.9	
$\mathbf{13}^{2+}$	156.8	155.7	54.7	29.4	24.7	
$\mathbf{14}^{2+}$	156.8	155.7	55.0	29.4	27.4	25.7
$\mathbf{16}^{+}$	158.0	156.3	46.1			

4-4. Reduction potentials and absorption maximum in electronic spectra of bispyridinium salts $9^{2+}\cdot 2(BF_4^-)$-$14^{2+}\cdot 2(BF_4^-)$

Table 4-3 shows the reduction potentials and absorption maximum in the electronic spectra of the bispyridinium ions 9^{2+}-14^{2+} along with 16^+. All reduction potentials were reversible. As methylene chain becomes longer, E_1 becomes more negative and approaches to the E_1 value of 16^+. This shows that the electron withdrawing through bond interaction between pyridinium rings becomes smaller as methylene chain becomes longer. In the case of 9^{2+} and 10^{2+}, E_1 and E_2 reduction waves were separately observed. However, for the longer methylene chain compound 11^{2+}-14^{2+}, E_1 and E_2 are observed as a single wave, indicating that the through-bond interaction between the pyridinium rings is outstanding for 9^{2+} and 10^{2+}.

Table 4-3. Reduction potentials [a, b] and absorption maximum of pyridinium salts [b]

	E_1 / V	E_2 / V	E_3 / V	λ_{max} / nm (ε x 10^{-4})
$9^{2+}\cdot 2(BF_4^-)$	-0.88	-1.02	-1.73	317 (5.51)
$10^{2+}\cdot 2(BF_4^-)$	-1.02	-1.13	-1.69	307 (5.64)
$11^{2+}\cdot 2(BF_4^-)$	-1.10		-1.68	305 (5.89)
$12^{2+}\cdot 2(BF_4^-)$	-1.09		-1.67	304 (5.71)
$13^{2+}\cdot 2(BF_4^-)$	-1.12		-1.70	302 (5.96)
$14^{2+}\cdot 2(BF_4^-)$	-1.14		-1.70	302 (6.03)
$16^{+}\cdot (BF_4^-)$	-1.20		-1.65	302 (3.16)

a) supporting electrolyte, 0.1 M tetrabutylammonium tetrafluoroborate; indicating electrode, glassy carbon; reference electrode, S. C. E.; scan rate, 100 mV / sec
b) in acetonitrile

The absorption maximum of the bispyridinium ions shifts to shorter wavelength with increase of n and approaches to that of 16^+. This blue shift accompanied the hyperchromic effect. This observation might also be explicable by the through bond interaction between the pyridinium rings.

4-5. Electronic spectra obtained by reduction of bispyridinium salts $9^{2+}\cdot 2(BF_4^-)$-$14^{2+}\cdot 2(BF_4^-)$

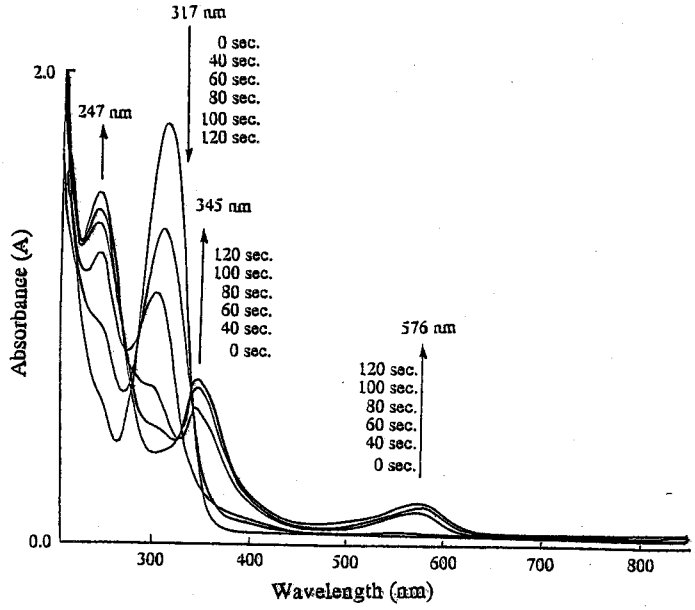

Figure 4-3. UV-vis spectral change upon reduction of $9^{2+}\cdot 2(BF_4^-)$ to form diradical **9**.

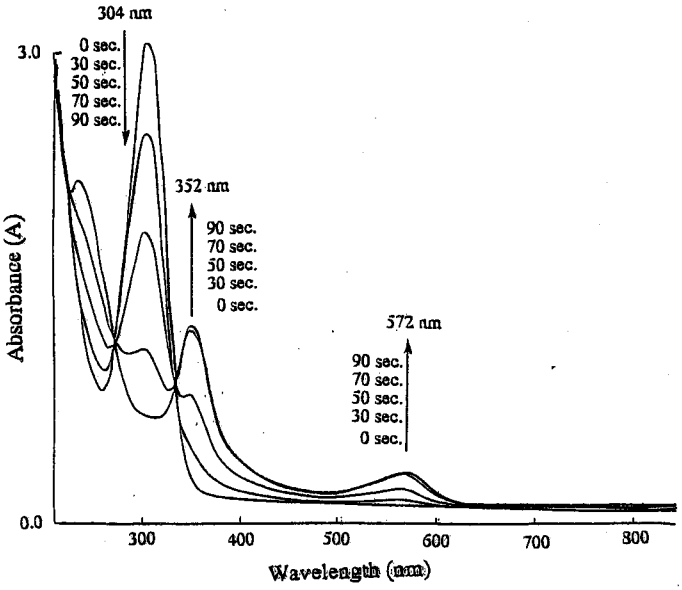

Figure 4-4. UV-vis spectral change upon reduction of $10^{2+}\cdot 2(BF_4^-)$ to form diradical **10**.

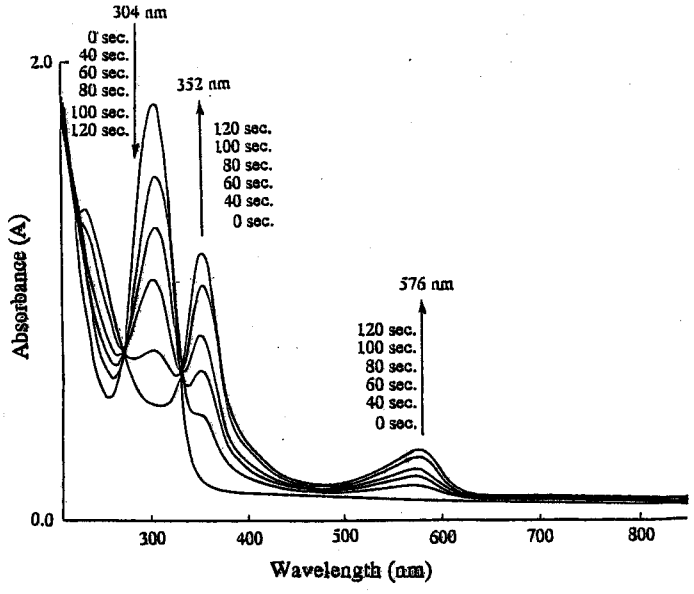

Figure 4-5. UV-vis spectral change upon reduction of $11^{2+}\cdot 2(BF_4^-)$ to form diradical **11**.

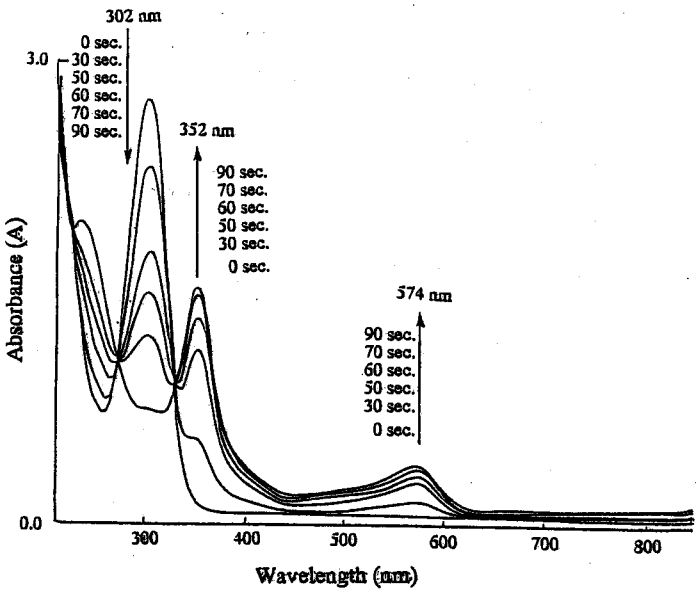

Figure 4-6. UV-vis spectral change upon reduction of $12^{2+}\cdot 2(BF_4^-)$ to form diradical **12**.

Figure 4-3 shows UV-vis spectral change upon the reduction of bispyridinium ion $\mathbf{9}^{2+}$ with 3% Na-Hg in acetonitrile at room temperature. Although the reduction potentials of $\mathbf{9}^{2+}$ were reversible, the reduction did not proceed cleanly and no isosbestic point was observed. However, the absorptions appeared at 345 nm and 576 nm which is assignable to the radical species. These absorptions did not change by temperature in the range of -30 °C to 25 °C, which suggests that the cyclization does not occur in contrast to the studies of Ikegami et al. The reduction of $\mathbf{10}^{2+}$-$\mathbf{14}^{2+}$ proceeded cleanly with two isosbestic points as shown in Figure 4-4 to 4-8. The colorless solution of pyridinium salts all turned reddish purple as the reduction proceeded. All these radicals showed the absorption maxima at the similar wavelength which is characteristic for 2,4,6-triphenylpyridinyl radicals. These radical species were also decolored by further reduction or by standing for several hours at room temperature.

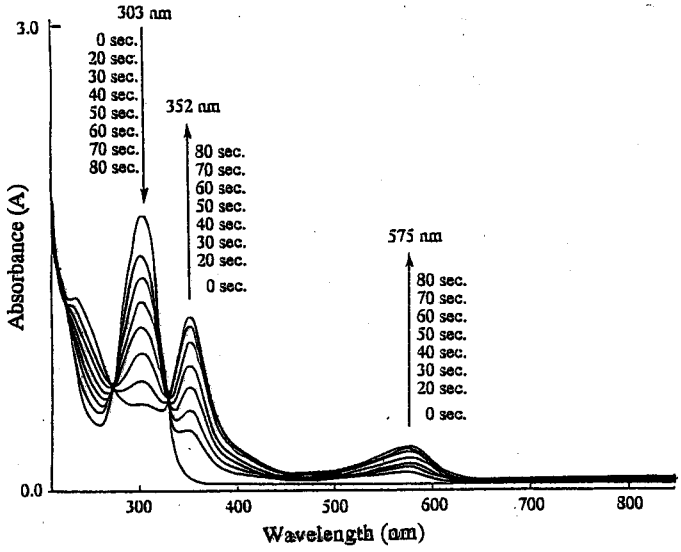

Figure 4-7. UV-vis spectral change upon reduction of $\mathbf{13}^{2+}\cdot 2(BF_4^-)$ to form diradical **13**.

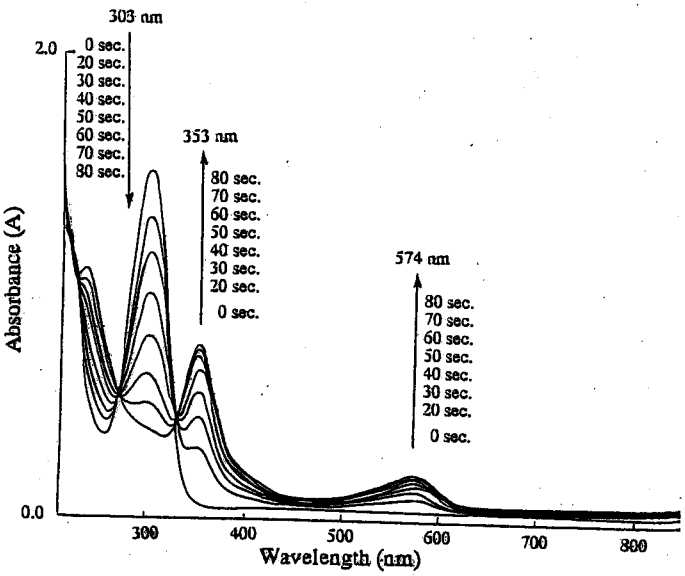

Figure 4-8. UV-vis spectral change upon reduction of $\mathbf{14}^{2+}\cdot 2(BF_4^-)$ to form diradical **14**.

4-6. ESR spectra of diradicals 9-14

In the preceding section, all the bispyridinium ions $\mathbf{9}^{2+}$-$\mathbf{14}^{2+}$ were converted into the diradicals **9-14** by the reduction with 3% Na-Hg. The detection by ESR spectroscopy is described in this section.

Although clean spectral change into **9** was not observed in the electronic spectral, the ESR spectrum of the diradical **9** in MTHF-acetonitrile (1:1 v/v) at -150 °C gave a typical triplet pattern with the intense central signal due to a monoradical (Figure 4-9). The zero-field splitting parameters were D = 16.0 mT and E = 1.1 mT. The averaged distance between the radical centers was estimated to be 5.6 Å by point dipole approximation.

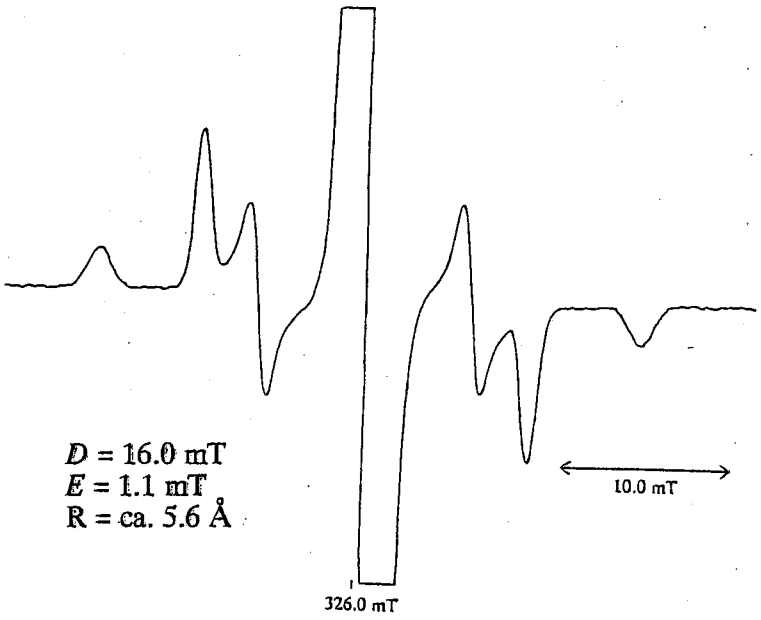

Figure 4-9. ESR spectrum of diradical **9** in MTHF-acetonitrile at -150 °C.

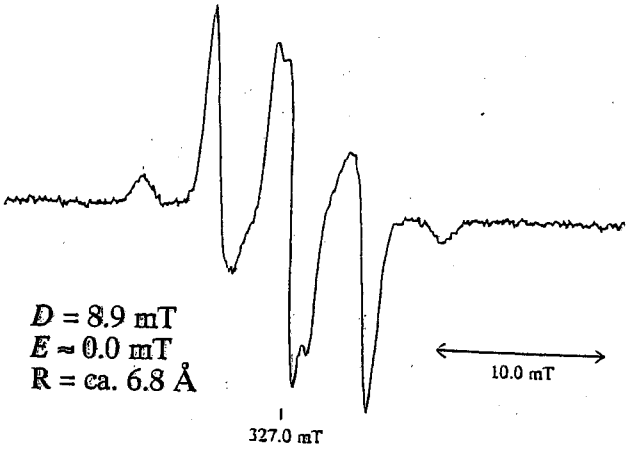

Figure 4-10. ESR spectrum of diradical **10** in MTHF-acetonitrile at -150 °C.

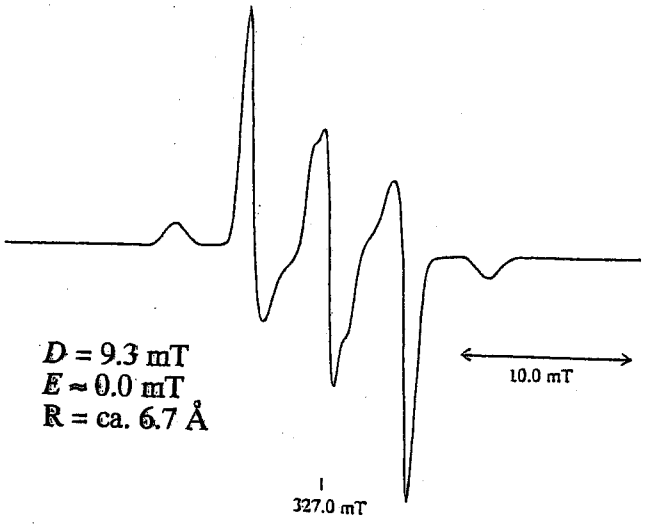

Figure 4-11. ESR spectrum of diradical **11** in MTHF-acetonitrile at -150 °C.

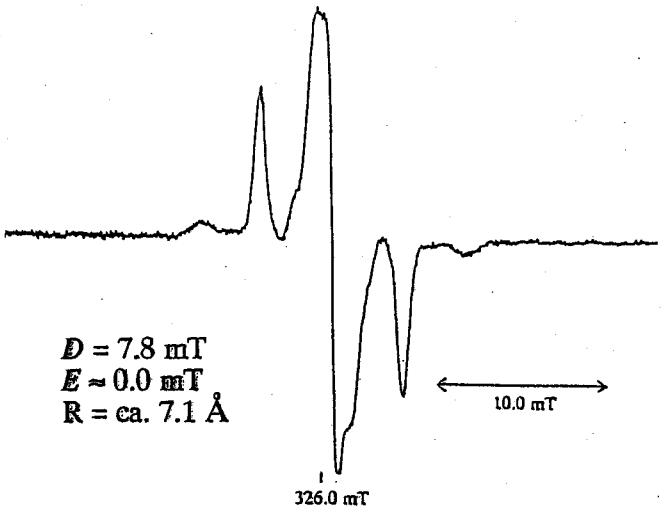

Figure 4-12. ESR spectrum of diradical **12** in MTHF-acetonitrile at -150 °C.

Similarly, the diradical **10**, **11**, and **12** were observed as triplet species as shown in Figure 4-10, Figure 4-11, and Figure 4-12, respectively. The zero-field splitting parameter *D* were 8.9 mT, 9.3 mT, and 7.8 mT, respectively. *E* was zero in all cases. The ESR spectrum of diradical **13** was not a typical triplet pattern as shown Figure 4-13. The assignment of triplet spectrum is shown in the figure. The zero-field splitting parameter *D* of the diradical **13** was ca. 4.2 mT. In the diradical **14**, any signal due to the triplet species could not be observed (Figure 4-14). If Z signals of diradical **14** were involved in the central signal, *D* value must be less than 2.0 mT.

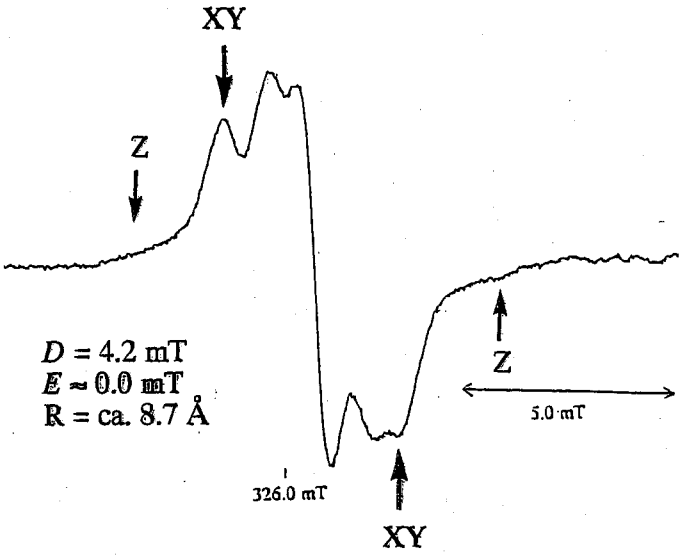

Figure 4-13. ESR spectrum of diradical **13** in MTHF-acetonitrile at -150 °C.

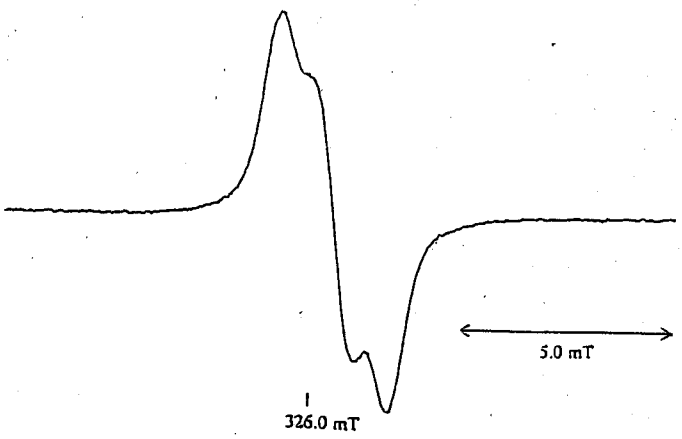

Figure 4-14. ESR spectrum of diradical **14** in MTHF-acetonitrile at -150 °C.

Table 4-4 summarizes the zero-field splitting parameters *D* and *E*, and the averaged distance (R) between the radical centers in diradical **9-14**. These diradicals would have many conformations. However, the most stable conformation would have a zigzag methylene chain conformation. In order to estimate rough distance between the radical centers, 1,n-diphenylalkanes were used as model compounds and their zigzag conformations were optimized by MM2 method. The distance between radical centers was estimated by assuming that a radical center was located on a center of the phenyl ring in the zigzag 1,n-diphenylalkanes. These estimated distances are summarized as a "R-model" in Table 4-4.

Interestingly, the distance (R) between the radical centers of diradical **10**, **11**, and **12** are similar. Moreover, these distances are shorter than the zigzag model values (R-model). These results suggest

that these diradicals have a conformation that has almost constant distance (R = ca. 7 Å) between two pyridinyl rings. A weakly coupled intramolecular dimer model (Figure 4-15) may account for these observations. This model predicts that diradicals **10-12** have singlet ground states because of the through-space interaction.

Table 4-4. Zero-field splitting parameters and the distance between the average radical centers of diradical **9-14**.

	D / mT	E / mT	R / Å[a)]	R-model / Å[b)]
9	16.0	1.1	5.6	6.5
10	8.9	0	6.8	7.5
11	9.3	0	6.7	9.0
12	7.8	0	7.1	9.9
13	4.2	0	8.7	11.5
14	< 2.0	c	> 11.6	14.0

a) estimated by $-(3/2)g^2b^2/r^3$. b) estimated from molecular model assuming that unpaired electrons are located around the center of the pyridinyl ring in the zigzag conformation. c) could not be determined.

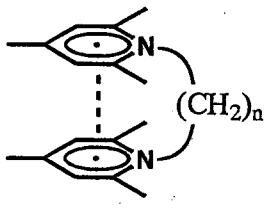

Fig. 4-15. Proposed conformation of diradical **10-12**.

The temperature dependence of the signal intensity was studied for the diradicals **9**, **10**, and **11**. The Curie plots using $\Delta M_S = \pm 2$ transition of diradical **9**, **10**, and **11** are shown in Figure 4-16, Figure 4-17, and Figure 4-18, respectively. In the case of diradical **9**, the signal intensity of $\Delta M_S = \pm 2$ transition decreases as temperature decreases from 120 K to 77 K. This shows that diradical **9** has a singlet ground state. The ΔE_{S-T} value cannot be precisely determined. The monotonous decrease of the signal intensity in this temperature range places the lower limit of ΔE_{S-T} value as > 400 cal/mol. The singlet nature of **9** would be due to strong through-bond (or through-space) interaction between the pyridinyl rings.

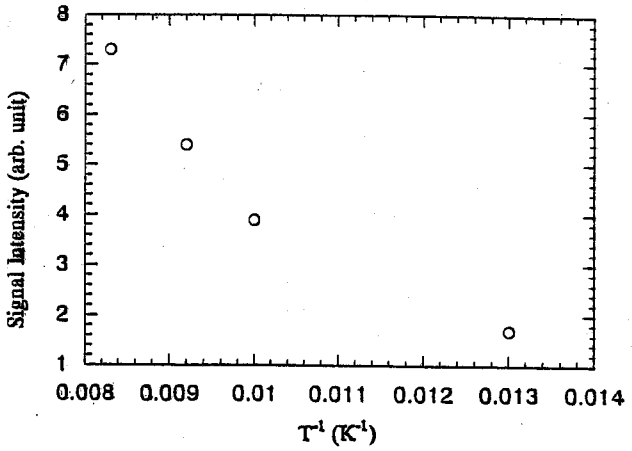

Figure 4-16. Temperature dependence of the signal intensity of $\Delta M_S = \pm 2$ transition of diradical **9**.

The diradical **10** showed considerably different temperature dependence. The signal intensity increased as temperature decreased (59 - 20 K). However, curiously, the intensity becomes almost constant in the lower temperature range (20 - 5 K). This is not due to the saturated transition in ESR absorption, because the signal intensity proportionally increased to the square root of microwave power under the measurement conditions. The plateau region is probably ascribed to the presence of several conformational isomers whose triplet states have different temperature dependence. The observed curve is difficult to simulate using the theoretical S-T model. In such a case, the simulated curve (solid line in Figure 4-17) would provide $\Delta E_{S\text{-}T}$ = ca. 55 cal/mol for a conformer which has the highest $\Delta E_{S\text{-}T}$ value. Quite similar temperature dependence was observed for **11** ($\Delta E_{S\text{-}T}$ < 55 cal/mol).

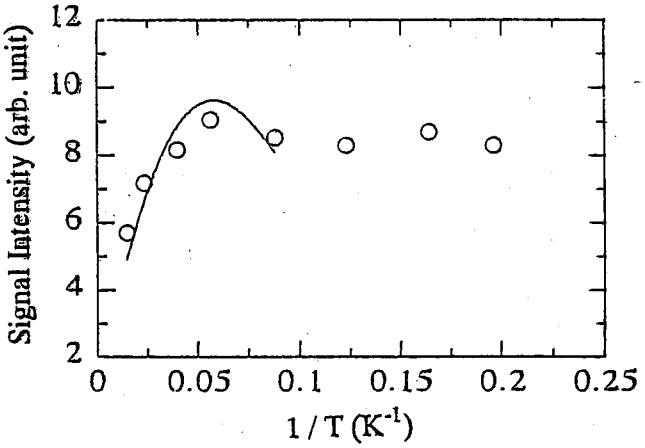

Figure 4-17. Temperature dependence of the signal intensity of $\Delta Ms = \pm 2$ transition of diradical **10**.

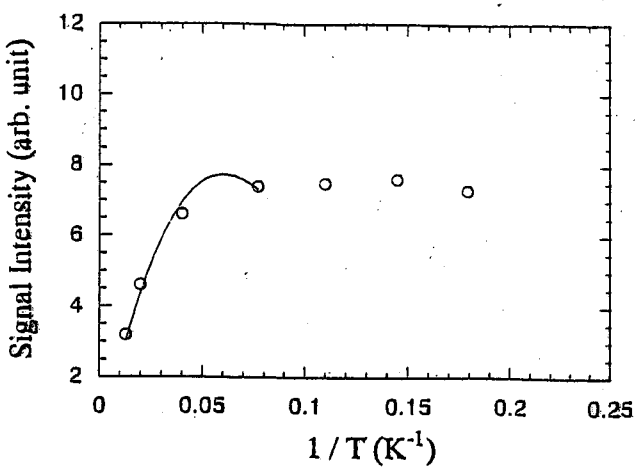

Figure 4-18. Temperature dependence of the signal intensity of $\Delta Ms = \pm 2$ transition of diradical **11**.

The results obtained in this section can be summarized as follows. 1) Diradical **9** (n = 2) has a singlet ground state. 2) Diradicals **10-12** (n = 3-5) have similar *D* values (7.8-8.3 mT). These diradicals would have a intramolecular dimer conformations. The ground states of **10-12** are predicted to be singlet states. The Curie plots for **10** and **11** accord with this prediction. 3) The diradical **13** (n = 6) has a small *D*. The triplet state of **14** (n = 8) could not be observed.

4-7. Preparation and characterization of 1,4-*trans*-bis(2,4,6-triphenyl-pyridinyl-1-yl)cyclohexane (15)

1,1'-(1,n-Alkanediyl)bis(2,4,6-triphenylpyridinyl) (n = 3, 4, 5) were shown to have a singlet ground state. The singlet nature is due to the intramolecular dimer formation. The intramolecular dimer formation is based on the flexible nature of the spacer. In order to get more insight on the conformation effect on the ground state spin multiplicity, 1,4-*trans*-bis(2,4,6-triphenylpyridinyl-1-yl)cyclohexane (**15**) was prepared. Diradical **15** has a considerably rigid spacer and the formation of intramolecular π-π singlet dimer is impossible. Since 1,4-cyclohexanediyl is a four carbon spacer, the result of **15** is comparable with that of **11** with tetramethylene spacer.

1,4-*trans*-Bis(2,4,6-triphenylpyridinium-1-yl)cyclohexane $\mathbf{15}^{2+}$, the precursor of diradical **15**, was prepared from 1,4-*trans*-diaminocyclohexane and 2,4,6-triphenylpyrylium in 47% yield according to the procedure described in section 4-2. In ^{1}H-NMR, the protons of pyridinium ring and of 2(6)-phenyl groups appeared as broad signals, which indicates slow rotation of C(spacer carbon)-N bond. The reduction potentials of $\mathbf{15}^{2+}$ appeared at -1.11 V, -1.50 V, and -1.61 V. The reduction wave at -1.11 V was reversible. By comparison of these potentials with those of $\mathbf{9}^{2+}$-$\mathbf{14}^{2+}$, this wave at -1.11 V involves two-electron reduction, dication ↔ diradical. The reduction waves at -1.50 V and -1.61 V were irreversible. These results suggest that diradical **15** is prepared by the reduction of $\mathbf{15}^{2+}$. Dication $\mathbf{15}^{2+}$ has an absorption maximum (molar absorptivity) at 307 nm (5.69×10^4 cm^{-1}mol^{-1}L). This value is in a normal range in comparison with those of $\mathbf{9}^{2+}$-$\mathbf{14}^{2+}$ (section 4-4).

The reduction of $\mathbf{15}^{2+}$ with 3% Na-Hg in acetonitrile at room temperature under degassed condition gave a red color which immediately disappeared. The diradical **15** could not be generated at room temperature. However, the reduction at -30 °C gave a clean change to the diradical **15** which has an absorption maxima at 355 nm and 553 nm (Figure 4-19). The 553 nm absorption is rather shorter than the absorption (572-576 nm) of **9**-**14**. The blue shift may be due to the steric effect which prevents the conjugation between pyridinyl ring and 2(6)-phenyl groups (see 2-5-4 and 2-6-2).

To clarify the instability of **15** at room temperature, the product analysis for the reduction of **15** was carried out. One of the products of the reduction of $\mathbf{15}^{2+}$ was 2,4,6-triphenylpyridine. Moreover, in the reduction of $\mathbf{15}^{2+}$, precipitates, which would be a polymer showing a complex NMR spectrum,

appeared. Homolytic carbon-nitrogen bond cleavage would occur to give triphenylpyridine and the corresponding cyclohexanyl radical or cyclohexanediyl diradical which would porimerize. In order to clarify this mechanism, the reduction of $\mathbf{15}^{2+}$ was performed in the presence of 2.0 equivalents of diphenyldiselenide at room temperature, 1,4-bis(phenylselenyl)cyclohexane (*cis/trans* = ca. 1.9 determined from NMR spectrum[67]) and 2,4,6-triphenyl-pyridine were obtained in 35% and 85% yield, respectively (Scheme 4-2).

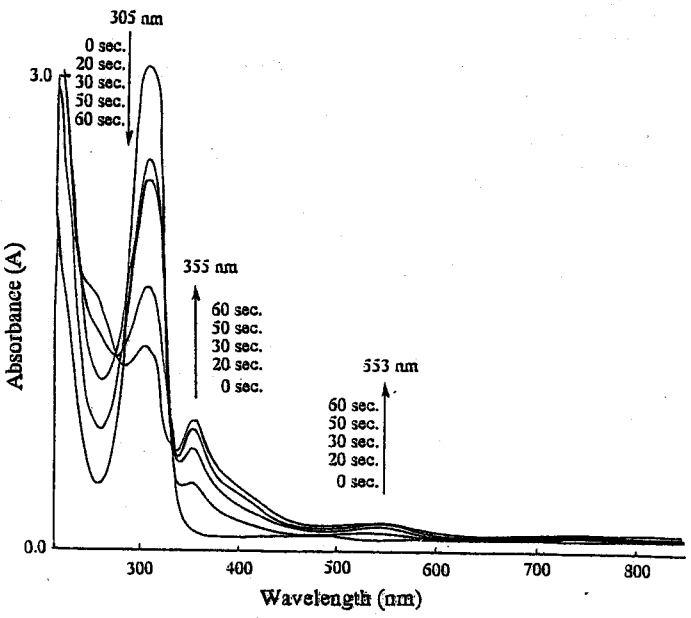

Figure 4-19. UV-vis spectral change upon reduction of $\mathbf{15}^{2+}\cdot 2(BF_4^-)$ to form diradical **15**.

Scheme 4-2

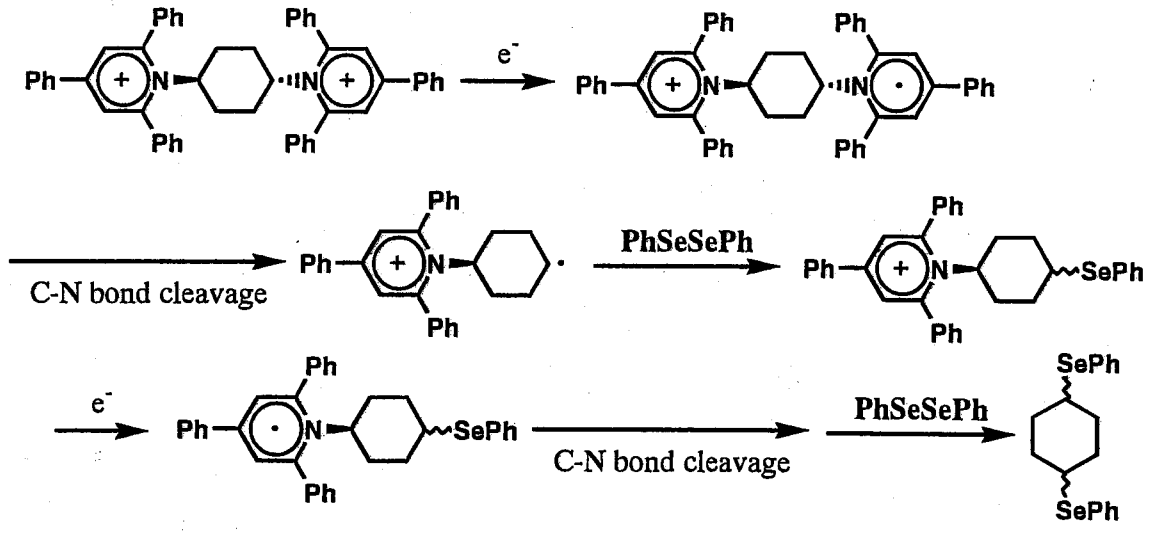

The same instability was observed in 1-*sec*-butyl-2,4,6-triphenylpyridinium and 1-benzyl-2,4,6-triphenylpyridinium. In the latter case, no absorption was observed even at -30 °C. These results show that the stability of 1-alkyl-2,4,6-triphenylpyridinyl radical decreases as the stability of alkyl radical was increases.

The ESR spectrum of the reddish purple species obtained by the reduction of $\mathbf{15}^{2+}$ in MTHF-acetonitrile at -150 °C was shown in Figure 4-20. A typical triplet pattern which is assignable to bis-

pyridinyl radical **15** was observed. The zero-field splitting parameters D and E were determined to be 4.8 mT and 0 mT, respectively. The distance between the radical centers was estimated to 8.3 Å by point dipole approximation. This distance is longer than that for **11** which has a four carbon spacer.

Temperature dependence of the signal intensity of $\Delta M_S = \pm 2$ transition was shown in Figure 4-21. The signal intensity increased proportionally to the reciprocal temperature, which shows a triplet ground state or a singlet ground state with $\Delta E_{S-T} \approx 0$. The high-spin or the stable triplet nature of **15** is a sharp contrast to the result of **11**. This result clearly suggests that suitable rigid σ-spacer may generally be used for the construction of high-spin molecules.

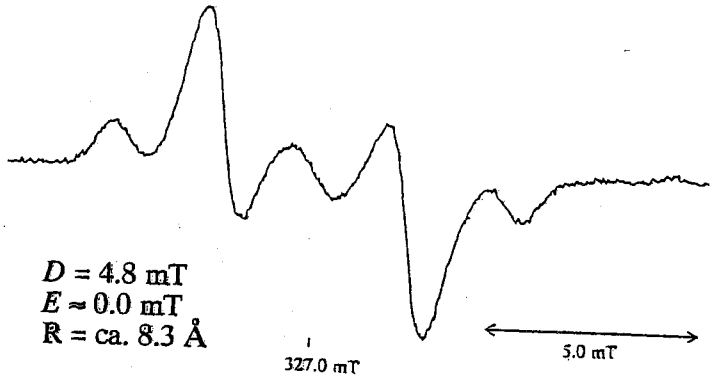

Figure 4-20. ESR spectrum of diradical **15** in MTHF-acetonitrile at -150 °C.

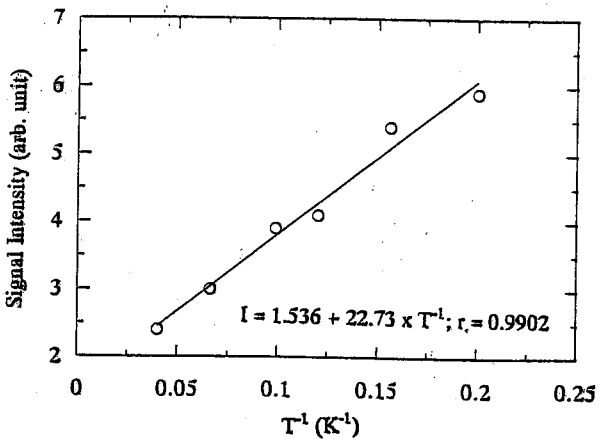

Figure 4-21. Temperature dependence of the signal intensity of $\Delta Ms = \pm 2$ transition of diradical **15**.

4-8. Summary

1) The bispyridinium ions $\mathbf{9}^{2+}$-$\mathbf{14}^{2+}$, with polymethylene spacers were prepared from 2,4,6-triphenylpyrylium and the corresponding diamines. The reduction potentials of these bispyridinium ions were all reversible. Reduction of these dications gives the bis-pyridinyl radicals **9**-**14** which have absorptions at about 350 nm and 575 nm.

2) The triplet states of bis-pyridinyl radicals **9**-**12** were detected by ESR spectroscopy. Their zero-field splitting parameters were determined (D = 16.0 mT and E = 1.1 mT for **9**, D = 8.9 mT and $E \approx$

0.0 mT for **10**, D = 9.3 mT and $E \approx$ 0.0 mT for **11**, and D = 7.8 mT and $E \approx$ 0.0 mT for **12**). The similarity of D values indicates that these diradicals have an intramolecular dimer conformation. The bis-pyridinyl radical **13** has a smaller D value (4.2 mT). In the case of **14**, no triplet signal could not observed.

3) 1,4-*trans*-Bis(2,4,6-triphenylpyridinyl-1-yl)cyclohexane **15** could not be prepared at room temperature but prepared by the reduction at low temperature (-30 °C). The triplet state was observed by ESR spectroscopy. The instability of the radical species was deduced to be a homolytic C-N bond cleavage. The intermediate, cyclohexyl radical or cyclohexanediyl diradical, was successfully trapped by diphenyldiselenide.

4) Temperature dependence of the signal intensity of $\Delta M_S = \pm 2$ transition was investigated for the bis-pyridinyl radicals **9**, **10**, **11**, and **15**. Diradical **9**, **10**, and **11** were shown to have a singlet ground state whereas diradical **15** has a triplet ground state or a singlet ground state with $\Delta E_{S\text{-}T} \approx 0$. The energy difference of the singlet and triplet states is estimated to be > 400 cal/mol for **9**, < 55 cal/mol for **10** and **11**. The singlet nature of **9** would be explained by the large through-bond or through-space interaction between the pyridinyl rings. For diradicals **10** and **11**, the formation of intramolecular dimer may be an origin of the singlet ground state. Prevention of the formation of such intramolecular dimer by using a rigid 1,4-cyclohexanediyl spacer gave a stable triplet species **15**.

4-9. Experimental section

Materials and Solvents:

Diamines **9a~14a**, 1,4-*trans*-diaminocyclohexane, and diphenyldiselenide were commercially available and used without further purification. 1-*sec*-butyl-2,4,6-triphenylpyridinium tetrafluoroborate[49a] and 1-benzyl-2,4,6-triphenylpyridinium tetrafluoroborate[49b] were prepared as described in the literature. Chloroform was distilled from calcium hydride.

General procedure for the synthesis of dipyridinium salts $9^{2+}\cdot 2(BF_4^-)$~$15^{2+}\cdot 2(BF_4^-)$

A mixture of the corresponding diamine, 2.0 equivalents of 2,4,6-triphenylpyrylium tetrafluoroborate and 4.0 equivalents of triethylamine in chloroform was heated to reflux overnight. After cooling, acetic acid (8.0 equivalents) was added, the reaction mixture was stirred for an hour at room temperature. The solvent was evaporated, ethanol was added to the residue to crystallize bispyridinium salts.

$\mathbf{9}^{2+}\cdot 2(BF_4^-)$: orange crystals (from C_2H_5OH); mp 178-179 °C; FAB MS *m/z* 729 (M^+-BF_4), 642 [M^+-2(BF_4)], 334 [M^+-2(BF_4)-triphenylpyridine]; ^{1}H-NMR (400 MHz, CD_3CN) δ 8.04 (d, 4H, *J* = 7.1 Hz), 8.01 (s, 4H), 7.74-7.62 (m, 10H), 7.56 (t, 8H, *J* = 7.6 Hz), 7.13 (d, 8H, *J* = 7.6 Hz), 4.73 (s, 4H); ^{13}C-NMR (75 MHz, CD_3CN) δ 157.6, 157.1, 133.8, 133.4, 132.5, 132.1, 130.51, 130.48, 129.6, 129.3, 127.9, 53.6; IR (KBr) 3060 (m), 1618 (s), 1557 (s), 1494 (m), 1459 (w), 1415 (m), 1335 (w), 1166 (m), 1083 (bs), 891 (w), 767 (s), 701 (s), 522 (w) cm^{-1}; UV (CH_3CN) λ_{max} / nm (log ε) 317 (4.74); FAB HRMS *m/z* Calcd for $C_{48}H_{38}N_2BF_4$: 729.3064. Found: 729.3072.

$\mathbf{10}^{2+}\cdot 2(BF_4^-)$: orange crystals (from C_2H_5OH); mp 174-175 °C; FAB MS *m/z* 743 (M^+-BF_4), 656 [M^+-2(BF_4)], 348 [M^+-2(BF_4)-triphenylpyridine]; ^{1}H-NMR (400 MHz, CD_3CN) δ 8.06 (s, 4H), 7.95 (dt, 4H, *J* = 7.1 Hz, 1.5 Hz), 7.70-7.64 (m, 6H), 7.62-7.56 (m, 12H), 7.38-7.36 (m, 8H), 3.78-3.74 (m, 4H), 1.68-1.66 (m, 2H); ^{13}C-NMR (75 MHz, CD_3CN) δ 156.6, 156.2, 133.9, 133.1, 132.8, 131.8, 130.3, 130.0, 129.2, 128.9, 127.3, 51.3, 29.7; IR (KBr) 3058 (w), 1619 (s), 1561

(m), 1493 (w), 1412 (w), 1083 (bs), 891 (w), 764 (m), 701 (m), 522 (w) cm^{-1}; UV (CH_3CN) λ_{max} / nm (log ε) 307 (4.75); FAB HRMS *m/z* Calcd for $C_{49}H_{40}N_2BF_4$: 743.3221. Found: 743.3229.

11^{2+}•2(BF_4^-): orange crystals (from CH_3CN-C_2H_5OH); mp >300 °C; FAB MS *m/z* 757 (M^+-BF_4), 670 [M^+-2(BF_4)], 362 [M^+-2(BF_4)-triphenylpyridine]; ^{1}H-NMR (400 MHz, CD_3CN) δ 8.09 (s, 4H), 7.95 (dt, 4H, *J* = 7.2 Hz, 1.5 Hz), 7,73 (t, 4H, *J* = 7.2 Hz), 7.65-7.59 (m, 14H), 7.49-7.46 (m, 8H), 3.74-3.72 (m, 4H), 0.86-0.84 (m, 4H); ^{13}C-NMR (75 MHz, CD_3CN) δ 156.7, 155.9, 134.0, 133.0, 132.9, 131.8, 130.3, 129.8, 129.2, 128.9, 127.1, 53.3, 25.9; IR (KBr) 3059 (w), 1625 (s), 1567 (m), 1495 (w), 1469 (w), 1446 (w), 1416 (w), 1354 (w), 1167 (w), 1083 (bs), 886 (w), 770 (m), 706 (m), 520 (w) cm^{-1}; UV (CH_3CN) λ_{max} / nm (log ε) 304 (4.76); FAB HRMS *m/z* Calcd for $C_{50}H_{42}N_2BF_4$: 757.3377. Found: 757.3386.

12^{2+}•2(BF_4^-): orange crystals (from CH_3CN-C_2H_5OH); mp 142-143 °C; FAB MS *m/z* 771 (M^+-BF_4), 682 [M^+-2(BF_4)], 376 [M^+-2(BF_4)-triphenylpyridine]; ^{1}H-NMR (400 MHz, CD_3CN) δ 8.14 (s, 4H), 7.98 (dt, 4H, *J* = 6.8 Hz, 1.8 Hz), 7.67-7.61 (m, 18H), 7.58-7.56 (m, 8H), 3.99 (t, 4H, *J* = 7.9 Hz), 0.92 (quintet, 4H, *J* = 7.8 Hz), 0.10 (quintet, 2H *J* = 7.6 Hz); ^{13}C-NMR (75 MHz, CD_3CN) δ 156.8, 155.8, 134.1, 133.2, 133.0, 131.6, 130.3, 129.8, 129.4, 128.9, 127.2, 54.5, 28.6, 22.9; IR (KBr) 3058 (w), 1622 (s), 1564 (m), 1495 (w), 1445 (w), 1415 (w), 1163 (w), 1054 (bs), 889 (w), 767 (m), 704 (m), 521 (w) cm^{-1}; UV (CH_3CN) λ_{max} / nm (log ε) 305 (4.77); FAB HRMS *m/z* Calcd for $C_{51}H_{44}N_2BF_4$: 771.3522. Found: 771.3517.

13^{2+}•2(BF_4^-): orange crystals (from CH_3CN-C_2H_5OH); mp 284-285 °C; FAB MS *m/z* 785 (M^+-BF_4), 698 [M^+-2(BF_4)], 390 [M^+-2(BF_4)-triphenylpyridine]; ^{1}H-NMR (300 MHz, CD_3CN) δ 8.14 (s, 4H), 7.97 (dt, 4H, *J* = 6.6 Hz, 1.8 Hz), 7.68-7.59 (m, 26H), 4.07-4.01 (m, 4H), 1.14-1.09 (m, 4H), 0.17-0.15 (m, 4H); ^{13}C-NMR (75 MHz, CD_3CN) δ 156.8, 155.7, 134.1, 133.3, 132.9, 131.6, 130.3, 129.7, 129.4, 128.8, 127.2, 54.7, 29.4, 24.7; IR (KBr) 3059 (w), 1624 (s), 1565 (m), 1496 (w), 1469 (w), 1414 (w), 1083 (bs), 886 (w), 766 (m), 702 (m), 534 (w) cm^{-1}; UV (CH_3CN) λ_{max} / nm (log ε) 302 (4.78); FAB HRMS *m/z* Calcd for $C_{52}H_{46}N_2BF_4$: 785.3690. Found: 785.3699.

14^{2+}•2(BF_4^-): orange crystals (from CH_3CN-C_2H_5OH); mp >300 °C; FAB MS *m/z* 813 (M^+-BF_4), 726 [M^+-2(BF_4)], 418 [M^+-2(BF_4)-triphenylpyridine]; ^{1}H-NMR (300 MHz, CD_3CN) δ 8.17 (s, 4H), 7.98 (dt, 4H, *J* = 6.6 Hz, 1.8 Hz), 7.70-7.63 (m, 26H), 4.24-4.18 (m, 4H), 1.32-1.24 (m, 4H), 0.54-0.46 (m, 4H), 0.43-0.36 (m, 4H); ^{13}C-NMR (75 MHz, CD_3CN) δ 156.8, 155.7, 134.2, 133.4, 132.9, 131.5, 130.3, 129.7, 129.5, 128.8, 127.2, 55.0, 29.4, 27.4, 25.7; IR (KBr) 3057 (w), 2926 (m), 2856 (w), 1626 (s), 1565 (m), 1496 (m), 1445 (w), 1416 (w), 1162 (m), 1043 (bs), 891 (w), 768 (m), 706 (m), 521 (w) cm^{-1}; UV (CH_3CN) λ_{max} / nm (log ε) 302 (4.78); FAB HRMS *m/z* Calcd for $C_{54}H_{50}N_2BF_4$: 813.4003. Found: 813.4012.

15^{2+}•2(BF_4^-): colorless prisms (from CH_3CN-C_2H_5OH); mp >300 °C; FAB MS *m/z* 783 (M^+-BF_4), 697 [M^+-2(BF_4)], 388 [M^+-2(BF_4)-triphenylpyridine]; ^{1}H-NMR (400 MHz, CD_3CN) δ 8.02 (br, 4H), 7.90 (dt, 4H, *J* = 7.1 Hz, 1.4 Hz), 7.74 (br, 4H), 7.64-7.60 (m, 2H), 7.58-7.54 (m, 12H), 7.42-7.40 (m, 8H), 3.96-3.92 (m, 2H), 1.87-1.85 (m, 4H), 1.02-0.97 (m, 4H); ^{13}C-NMR (75 MHz, CD_3CN) δ 157.6 (br), 155.1, 133.7, 133.5, 133.1, 132.1, 130.2, 129.2 (br), 128.8, 68.9, 32.4; IR (KBr) 3059 (w), 1621 (s), 1563 (m), 1495 (m), 1445 (w), 1414 (m), 1356 (w), 1083 (bs), 889 (w), 775 (m), 754 (m), 707 (m), 547 (w) cm^{-1}; UV (CH_3CN) λ_{max} / nm (log ε) 307 (4.76); FAB HRMS *m/z* Calcd for $C_{52}H_{44}N_2BF_4$: 783.3534. Found: 783.3543.

Reduction of **15**$^{2+}$•2(BF_4^-) in the presence of diphenyldiselenide

An apparatus shown in Figure 2-2 was used. Bispyridinium salt **15**$^{2+}$•2(BF_4^-) (87 mg, 0.01 mmol) and diphenyldiselenide (62 mg, 0.02 mmol) were charged in B and 3% Na-Hg (383 mg, 0.5 mmol) was charged in C. Acetonitrile (8 ml) was added to B, degassed three times, and D and F were sealed. The solution in B was transferred into C to reduce with 3% Na-Hg. The yellow solution turned dark yellow, dark brown, and then pale yellow. The reaction mixture was transferred into B, aerated, and the solvent was evaporated. The residue was purified by column chromatography on silica gel using hexane (to remove unreacted diphenyldiselenide) and then hexane-ethyl acetate (50:1 v/v). 1,4-Bis(phenylselenyl)cyclohexane (*cis/trans* = ca. 1.9, 15 mg, 35%) and 2,4,6-triphenylpyridine (52 mg, 85%) were obtained.

1,4-Bis(phenylselenyl)cyclohexane: FAB MS *m/z* 396 (M^++1), 239 (M^++1-SeC_6H_5); ^{1}H-NMR (400 MHz, $CDCl_3$) δ 7.55-7.51 (m, 4H), 7.27-7.25 (m, 6H), 3.46-3.44 (m, 1.3H), 3.14-3.12 (m, 0.7H), 2.11-1.86 (m, 6H), 1.54-1.51 (m, 1.7H)

4-10. References

[65] a) P. W. Kopf, R. Kreilick, D. G. B. Boocock, and E. F. Ullman, *J. Am. Chem. Soc.*, **92**, 4531 (1970).

b) E. F. Ullman, J. H. Osiecki, D. G. B. Boocock, and R. Darcy, *J. Am. Chem. Soc.*, **94**, 7049 (1972).

[66] K. Okada, K. Nakatsuji, and M. Oda, *Chem. Lett.*, in press.

[67] H. Duddeck, P. Wagner, and A. Biallaβ, *Magn. Reson. Chem.*, **29**, 248 (1991).

Conclusion

In the introductory part of this thesis, some unique characters (small energy gap between the singlet and triplet state for **1m**, stable triplet for **7m**) of bis-pyridinyl radicals were considered by the valence bond approach. The analysis shows that their unique characters are originated by the delocalization of the lone pair electrons on the nitrogen atoms. The analysis also indicates that the application of the spin-predicting models (Chapter 1) in alternant hydrocarbon high-spin molecules is not valid for **1m** and **7m** because the spin predicting models are based on the assumption that each π orbital is occupied by exactly one electron.

The purpose of this thesis is to characterize the nature of these types of bis-pyridinyl radicals. Especially, the clarification of the exchange interactions for the above types of bis-pyridinyl radicals is a key in this thesis. In Chapter 2, the bis-pyridinyl radical **1** was prepared and its ground state was experimentally determined to be a triplet state or a singlet state with $\Delta E_{S\text{-}T} \approx 0$ cal/mol. This result is compatible with the consideration of small energy gap for **1m**. In Chapter 3, diradical **7** was studied. The ground state was determined to be a singlet state with $\Delta E_{S\text{-}T} \approx 51$ cal/mol. This result is also compatible with the valence bond pictures of stable triplet for **7m**. The related *m*-phenylene type diradical **6** was studied in the same chapter. The observed singlet ground state with $\Delta E_{S\text{-}T} \approx 44$ cal/mol also accords with the valence bond consideration. As a result, these observations are roughly accountable by the above valence bond pictures. However, the valence bond method would not be suitable for the arguments of small differences in energies because of its qualitative methodology. The singlet ground state with small energy gap for **6** and **7** is also explained by the large dihedral angle effect (Chapter 1). The differentiation between the electronic (VB consideration) and geometrical factors (dihedral angle consideration) is difficult at present.

This thesis also clarified some other important aspects on the pyridinyl-based polyradicals. The ESR spectra of the bis-pyridinyl radicals **1**, **3**, and **4** established their small D values for the *m*-phenylene-linked diradicals at the C4-position. Compound **24** with *p*-phenylene linkage at the C4-position was shown to have a quinoid form. In addition, an antiferromagnetic interaction was experimentally demonstrated for the anthracene-1,8-diyl-linked diradical **5**.

Furthermore, the last Chapter 4 provided a precious information on the exchange interaction of bis-pyridinyl radicals linked by σ-frames. The ground states of the bis-pyridinyl radicals linked by flexible methylene chains (**9**-**11**) were shown to be singlet. The singlet nature of **9**-**11** was rationalized by the formation of the intramolecular dimers. In contrast to these results, **15** with a rigid cyclohexane-1,4-diyl spacer was shown to have a triplet ground state or a singlet ground state with $\Delta E_{S\text{-}T} \approx 0$ cal/mol. This result strongly suggests a new and general methodology for the construction of high-spin species using conformationally tight σ-spacers.

List of publication

1. Preparations and Spin-Spin Interactions of 4,4'-(*m*-Phenylene)bis(1-methyl-2,6-diphenylpyridinyl) and Its Analogue

Keiji Okada, Kouzou Matsumoto, Masaji Oda, Hisao Murai, Kimio Akiyama, and Yusaku Ikegami

Tetrahedron Lett., **36**, 6689 (1995).

2. Preparation and Spin-Spin Interaction of 4,4'-(Anthracene-1,8-diyl)bis(1-methyl-2,6-diphenyl-pyridinyl)

Keiji Okada, Kouzou Matsumoto, Masaji Oda, Hisao Murai, Kimio Akiyama, and Yusaku Ikegami

Tetrahedron Lett., **36**, 6693 (1995).

3. 1,1'-(*p*- Or *m*-Phenylene)bis(2,4,6-triphenylpyridinyl) Diradicals: Ground State in a Heteroatom-Containing System in Relation to the Topology Rule

Keiji Okada, Kouzou Matsumoto, Masaji Oda, Kimio Akiyama, and Yusaku Ikegami

Tetrahedron Lett., **38**, 6007 (1997).

4. Exchange Interaction of Bispyridinyl Diradicals Linked by σ-Frames

Kouzou Matsumoto, Masaji Oda, Masatoshi Kozaki, Kazunobu Sato, Takeji Takui, and Keiji Okada

Tetrahedron Lett., **39**, 6307 (1998).

Acknowledgement

The studies presented in this thesis have been carried out under the direction of Professor Masaji Oda at the Department of Chemistry, Graduate School of Science, Osaka University.

I wish to express my grateful gratitude to Professor Masaji Oda for his continuous guidance, helpful suggestion and encouragement throughout the work. I am also deeply grateful to Professor Keiji Okada at the Department of Chemistry, Graduate School of Science, Osaka City University, for his valuable advice and stimulating discussions during the cource of the work. I wish to thank Associate Professor Takeshi Kawase for his helpful advice and encouragement. I also wish to thank Dr. Hiroyuki Kurata and Dr. Masatoshi Kozaki for their helpful advice and encouragement.

I am greatly indebted to Professor Takeji Takui, Department of Chemistry, Graduate School of Science, Osaka City University, for his continuing interest and encouragement in the work. I also wish to thank Dr. Kazunobu Sato for his helpful advice and encouragement.

I am grateful to Dr. Ken-ichi Lee, Mr. Mitsugu Doi, and Mr. Seiji Adachi, Faculty of Science, Osaka University, and Mrs. Matsumi Doe, Department of Chemistry, Graduate School of Science, Osaka City University, for NMR measurements. I am also grateful to Mr. Hiroshi Adachi, Faculty of Science, Osaka University, and Mr. Tetsuya Shimada and Mrs. Rika Miyake, Department of Chemistry, Graduate School of Science, Osaka City University, for measurement of mass spectra, and to Mrs. Kazuyo Hayashi and Miss Tomomi Ikeuchi, Faculty of Science, Osaka University, and Mrs. Tamaki Nagasawa, Department of Chemistry, Graduate School of Science, Osaka City University, for elemental analyses. I wish to thank Mrs. Takako Abe for her kind assistance, and all members of Oda laboratory and Okada laboratory for their helpful discussions and kind friendship.

Finally, I am deeply indebted to my parents, Mr. Minoru Matsumoto and Mrs. Yayomi Matsumoto, for their helpful advice and encouragement throughout the study.

松本幸三